Compressible Turbulent Boundary Layers with Combined Air Injection and Pressure Gradient

By G. D. Thomas

Cambridge University, Engineering Department

Compressible Turbulent Boundary Layers with Combined Air Injection and Pressure Gradient

By G. D. THOMAS

Cambridge University, Engineering Department*

Summary

The purpose of the work described in this report was to study the effect of longitudinal pressure gradients upon compressible turbulent boundary layers on a flat plate, with and without air injection. A brief survey of some of the more recent work on pressure gradient flows with and without injection is given. Emphasis is placed upon the effects of the pressure gradients on the velocity and temperature profiles although theoretically predicted developments are indicated on the figures. The use of the razor-blade technique for measuring skin-friction in pressure gradient flows is also shown to be very satisfactory.

LIST OF CONTENTS

1. Introduction

This report gives the results of a series of experiments to study compressible turbulent boundary layers over porous surfaces with air injection, in the presence of both favourable and adverse pressure gradients. The tests were made in the same tunnel as used by Jeromin,[1] Squire[2] and Dunbar[3] and were made in parallel with work by Marriott[4] who studied the compressible turbulent boundary layer over a flat plate with discontinuous changes in injection rate.

The present results were obtained on a flat surface with the pressure gradient obtained by modifying the downstream end of a $M_1 = 2\cdot5$ liner, so that a linear increase or decrease in Mach number was produced over the test plate. In each case the region of linear Mach-number gradient was about 150 mm and the initial boundary-layer thickness without injection was about 6 mm. Two favourable gradients where the Mach number increased from about $M_1 = 2\cdot55$ to $M_1 = 3\cdot0$ and $3\cdot2$ respectively and an adverse gradient where the Mach number decreased from $M_1 = 2\cdot5$ to $2\cdot2$, were obtained. The actual gradients obtained varied slightly when the injection rate changed.

For each gradient, velocity and temperature profiles were measured at 25 mm steps along the test plate for various injection rates. These profiles are tabulated at the end of the report. In addition skin friction, in the absence of injection, was measured by the razor-blade technique.

The purpose of the programme was twofold; firstly to study the effects of pressure gradients on layers with injection and secondly to use the results as test cases for two prediction methods. One was the method of Verma[5] which used a finite difference scheme to solve the momentum and enthalpy equations using an eddy-viscosity model and a constant turbulent Prandtl number. The other was a direct modification of the Bradshaw–Ferriss[6,7] method by the present author. This method solves the turbulence energy equation and since it assumes that the temperature profile is related to the velocity profile by a Crocco relation, a supplementary purpose of the work was to check the accuracy of this relationship for the complex flows studied here.

In this report the emphasis will be placed on the effects of the pressure gradients and the velocity–temperature relation. A full comparison with the two prediction methods will be presented in a joint report with P. G. Marriott, where the performance of both methods will be assessed in relation to the non-equilibrium flows studied here and those studied by Marriott. However, many of the experimental results presented here are compared with the two prediction methods in the figures.

2. A Review of Earlier Work

There is very little profile data for boundary layers with fluid injection measured in strong pressure gradients in incompressible flow and to the author's knowledge no previous data for compressible boundary layers, although some boundary layers which have been studied have been influenced by upstream pressure gradients. There are now several reviews available for fluid injection into constant pressure flows and the present review will therefore consider pressure gradient flows without air injection briefly and pressure gradient flows with injection in more detail. A very full review of constant–pressure flows with air injection and pressure-gradient flows with or without injection is given by Thomas.[8]

2.1. Pressure Gradient Flows Without Injection

Many of the pressure gradient data along flat surfaces at low speeds have been analysed by Coles and Hirst[9] who found that most of the data were well represented by the law of the wall, $u/U_\tau = 1/k \log y^+ + B + (\pi/k)w(y/\delta_c)$ and a velocity defect law, $(U_1 - u)/U_\tau = f(y/\delta)$. Clauser[10] formed a dimensionless-pressure-gradient parameter $\beta = (\delta_i^*/\tau_w)(dp/dx)$ which was nearly constant along his equilibrium adverse-pressure-gradient flows. The wake parameter π appeared to be closely connected with β.

A method which predicts the velocity defect family throughout the boundary layer for $\beta \geqslant -0\cdot5$ is that of Mellor and Gibson.[11] They also use $U_p = U_\tau \beta^{\frac{1}{2}}$ instead of U_τ to non-dimensionalise the velocity defect since this gave a better collapse for large β. The predicted velocity defect and shear-stress distributions agree exceptionally well with the profiles of Clauser for $\beta = 1\cdot8$ and $8\cdot0$ and those of Herring and Norbury[12] for $\beta = -0\cdot35$ and $-0\cdot53$.

The zero skin-friction flow of Stratford[13] did not follow the trend of general agreement with the inner law and velocity-defect law, when analysed by Coles and Hirst. However, when compared with the theory of

Mellor and Gibson the velocity defect is predicted very well when non-dimensionalised by U_p instead of U_τ.

Investigations of pressure gradients in compressible flows are often incomplete in their collection of data such as temperature and static-pressure variations through the boundary layers. Pressure gradients produced on ramp models are subject to large static-pressure variations through the boundary layers. Three-dimensional influences such as end effects in two-dimensional flows or convergence and divergence along cylindrical flows are often neglected when they should not be.

An investigation of adverse and favourable pressure gradients, where complete measurements were made, was performed by Lewis, Gran and Kubota.[14] The boundary layer grows on the inside of a large radius cylindrical shell with a centre body producing the pressure gradient. The static pressure was constant through the boundary layer to within ± 10 per cent and the Crocco[15] temperature relation was verified to within experimental accuracy. It would appear that except where the boundary layer changes rapidly from $\beta = 1 \cdot 5$ to $-0 \cdot 8$ the velocity profiles are in near equilibrium conditions. The profiles in the adverse gradient show reasonable agreement with the wake function of Coles.[16] The velocity defects for the adverse gradient collapse for the same values of β with the incompressible curves of Coles and Hirst.

Boundary layers under the influence of imposed pressure gradients along flat plates have been studied by Michel, Quemard and Elena;[17] Sivasegaram,[18] and Voisinet, Lee and Yanta.[19]

Michel et al. produced their favourable pressure gradient with the least magnitude by modifying the rear of a linear in a smooth curve, while the two stronger gradients were caused by a single expansion corner on the liner. The profiles seem to show some signs of relaminarisation and the logarithmic velocity profiles do not bear linear characteristics. There is a large overshoot of velocity in the inner region and negligible wake component if indeed it is not negative.

Both Sivasegaram and Voisinet et al. have used flexible tunnel walls to produce their pressure gradients. Sivasegaram's three pressure gradients commence with strong favourable pressure gradients and it was thought that the boundary layers were not fully turbulent at the start of the gradients. The velocity profiles predicted by both the Patankar–Spalding[20] and Bradshaw–Ferriss methods do not agree well with the experimental profiles, even in the fully turbulent flow, until the gradient has been reduced almost to zero after 600 mm.

Voisinet et al. have taken comprehensive measurements in an adverse-pressure-gradient flow. Static-pressure and total-temperature measurements are taken through the layer. The static pressure variation is less than 5 per cent and often nearly constant. The temperature variation agreed better with that of Walz[21] than that of Crocco[15] but a noticeable discrepancy with Walz was the inflection at the edge of the sublayer. There was no observed overshoot in the stagnation temperature at the edge of the boundary layer.

The boundary layers measured were between 40 mm and 80 mm thick, consequently the traverses went well into the sublayer where viscous-flow interaction and probe-wall interference were encountered and allowed for. A velocity-profile family using the sublayer law, $u^+ = y^+$ and inner law with Coles' wake function $u^+ = 1/k \log y^+ + B + (\pi/k)w(y/\delta_c)$, agreed exceptionally well with experiment.

Three theoretical prediction methods which solve the boundary-layer partial-difference equations directly are those of Bradshaw and Ferriss; Patankar and Spalding, and Cebeci and Smith.[22]

The theory of Bradshaw and Ferriss has been comprehensively compared with pressure-gradient flows for zero heat transfer by Bradshaw and Ferriss[6,7] and Sivasegaram and Whitelaw.[23] The theory of Patankar and Spalding has also been compared with experiment in the last reference.

Cebeci[24] has published a comparison with the data of Pasiuk, Hastings and Chatham[25] for pressure-gradient flow and the overall agreement for velocity and temperature profiles, δ^* and θ is quite reasonable. The predictions of the other two methods mentioned, for this data, are very similar to that of Cebeci and Smith.

From the previous comparisons it is clear that there is very little data in pressure-gradient flows which is suitable for a comprehensive comparison with two-dimensional theories. The majority of experimental flows at the present time is subject to:

(1) A lack of complete experimental measurement; noticeably the static pressure and temperature traverses through the boundary layer, and unreliable skin-friction coefficients.

(2) Considerable three-dimensional effects, such as end effects, longitudinal curvature or lateral convergence and often a combination of two or more.

(3) The presence of laminar characteristics or influence of upstream pressure gradients persisting along the measured development.

For boundary layers not subject to the above, or only mildly so, the theories in general predict developments which agree very well with experiment.

4

2.2. Pressure Gradient Flows with Air Injection

The first thorough investigation was performed by McQuaid[26] who measured boundary-layer velocity profiles in both favourable and adverse pressure gradients, for incompressible flow. He also showed that a velocity defect law could be formed to include both injection and pressure gradient.

Similar work has been repeated by Julien[27] and Loyd[28] for stronger favourable pressure gradients. Whereas the injection rates of McQuaid varied along the pressure gradients, those of the above two studies were supposed to be constant. In practice the blowing rates were not kept constant and asymptotic flows with constant R_θ and C_f could not be achieved. Neither of the two investigations measured enough profiles to calculate the corrections to C_f. The boundary layers of Julien tended towards full development at the end of the pressure gradient whereas those of Loyd were at no time close to developed conditions. In practice the best estimates of C_f, for all the flows, were obtained by either fitting velocity profiles to sublayer laws which depends upon the smoothness of data near the wall, or by using a logarithmic region method. Neither of these methods provided values of C_f better than ± 20 per cent.

The comparison between the theoretical predictions using the Patankar–Spalding method, and the experiments of Julien shows that although there is considerable scatter in C_f the probable discrepancy is on the whole not as large as ± 20 per cent in the pressure gradient region. In the developing flow to and from the pressure gradient larger discrepancies occur. For the relaxing flow after the strongest pressure gradient, the θ development is consistently over-predicted by the order of 25 per cent, whereas the H development is reasonably predicted. It is therefore probable that, for the experimental values of R_θ given, the theory would predict considerably lower values of C_f in the relaxation development. It also implies that the velocity profiles are poorly predicted in this flow.

For the predictions of the data of Loyd, a constant value of F is assumed and in the pressure-gradient region departures up to 10 per cent occur between the assumed and experimental value. The clear emphasis has been upon predicting H correctly for all the flows. Again the R_θ development is over-predicted for all the flows by as much as 20 per cent and since the C_f predictions for three of the four developments shown under-predicted by as much as 15 per cent, there is clear evidence of the profiles not reaching a state of full development under local conditions.

The skin friction is clearly increased for all blowing rates in the pressure gradients of Julien over the upstream constant-pressure level. However, for the much stronger gradients of Loyd there is no increase in C_f in the pressure-gradient region within experimental accuracy for all blowing rates. It is also significant that in the constant-pressure region, upstream of the pressure gradients, for the same conditions of f, H and R_θ, Loyd consistently calculates values of C_f higher than Julien by as much as 10 per cent.

Baker[29] has also studied the effects of both favourable and adverse pressure gradients upon the transpired low-speed boundary layer. Density variations through the layer have also been considered by using Freon injection as well as air injection. The transition from constant-pressure flow to pressure-gradient flow was not measured as measurements were started downstream of the start of the pressure gradient.

For the largest blowing rates in the adverse pressure gradient the downstream stations were susceptible to three-dimensional effects and were on the point of separation. The pitot pressure close to the wall, for these stations, was equal to the static pressure. Baker also calibrated Preston tubes in channel flow with differing pressure gradients and mass-flow rates. For zero blowing the calibration was within 5 per cent of that of Patel.[30]

Baker has used the Prandtl mixing length with a constant value in the outer layer. The Van Driest damping function has been modified for blowing in a similar manner as that of Julien and Loyd. For air injection, the prediction of velocity profiles, H and R_θ is very good for all three pressure-gradient flows. The proposed model for the eddy-viscosity distribution was successful for the favourable pressure gradients and for moderate adverse pressure gradients with moderate blowing rates. The model became inadequate for severe blowing rates and adverse pressure gradient and it was necessary to adjust the constant value of $L_{\max}$ in the outer layer from $0 \cdot 09\delta_{995}$ down to between $0 \cdot 065\delta_{995}$ and $0 \cdot 07\delta_{995}$ to correct the shape factor developments. When density variation is introduced through the boundary layer the discrepancies are magnified.

Using this model, Baker has also predicted the pressure gradient transpired boundary-layer flows of McQuaid, Julien and Loyd. The agreement with the results of McQuaid, other than the C_f distribution which is not shown, is very good. The agreement with the results of Julien are overall better than that of the methods of Julien himself since R_θ is correctly predicted and the same scatter observed for C_f. Similarly, for the results of Loyd, R_θ is correctly predicted with the result that Baker's model predicts an increase in C_f in the pressure-gradient region which was neither calculated by Loyd nor predicted by the eddy-viscosity model which was adopted.

5

It would seem that prediction methods can be used successfully in favourable pressure gradients and in mild adverse pressure gradients with moderate blowing rates, for low-speed incompressible flow.

3. Experimental Equipment and Test Procedure

The experimental equipment used was basically the same as that of Jeromin,[1] Squire[2] and Dunbar[3] since the present work and theirs has all been concerned with the development of injection into the compressible boundary layer along a flat porous plate. Changes in the nature of the experiments so far have needed little adjustment, if any, to the test equipment. Since the present experiments involved the production of pressure-gradient flows along the test section, which is the lower surface of the wind-tunnel cross-section, it was easiest to modify the roof of the tunnel to produce the pressure gradients. Therefore the experimental description will be concentrated upon the production of the pressure gradient arfd will contain only the important features of the injection apparatus and design of the wind tunnel (*See* Fig. 1).

3.1. Wind Tunnel

The tunnel in the Cambridge University Engineering Department is an intermittent blow-down tunnel using air stored at 7×10^6 N/m^2. The air pressure is then reduced to provide a maximum running stagnation pressure, P_0, in the tunnel of about 10^6 N/m^2. There is no temperature control over the tunnel stagnation temperature; however, during a run the stagnation temperature, T_0, varies by only 2 K whilst the mean stagnation temperature for any one particular run may vary from 290 K to 300 K depending upon the amount of use of the tunnel and the external room temperature. The tunnel cannot be run in steady-state conditions due to the short running time and there will be small variable heat-transfer rates present.

3.2. The Design of the Pressure Gradients

Since it was possible to extend the traverse-gear platform so as to traverse the rear 250 mm of the test plate (*see* Fig. 1) it seemed reasonable to commence the pressure gradients about 200 mm upstream of the traverse gear. It was hoped that this would give a length of about 150 mm which was subjected to the pressure gradient and which could be traversed before the traverse gear affected the flow.

The three pressure gradients which were produced will be referred to as Gradients A, B and C. Gradients A and C are favourable gradients; C being the stronger; and Gradient B is an adverse gradient.

The pressure gradients were produced by modifying the rear section of an Araldite, $M = 2 \cdot 5$, wind-tunnel liner which was cast specifically for the purpose.

Gradient A was designed by the method of characteristics to increase the Mach number from $2 \cdot 5$ to $3 \cdot 0$ over the required range of 150 mm on the test plate. The rear of the wind-tunnel liner was machined to a smooth curve producing an expansion fan of 5 degrees on the tunnel liner, so that as near as possible a linear variation of Mach number was produced over the test section (*see* Fig. 2).

Gradient C was formed in an attempt to increase the favourable gradient so that a final Mach number of the order of $3 \cdot 5$ could be obtained with a linear change of Mach number. This could have been achieved by an expansion fan of 10 degrees on the linear surface. In practice, the effect of the last part of the expansion fan was downstream of the test section and a final Mach number of $3 \cdot 25$ was reached on the test section. It was not thought advisable to produce the gradient by a single turn of 10 degrees as used by Michel *et al.*,[17] since the lack of agreement between these results and prediction methods was explained by a possible relaminarisation of the boundary layers due to the large magnitude of the pressure gradients.

The severity of the Gradients A and C was determined to a large extent by the small dimension of the tunnel cross-section, since it was impossible to turn the flow back gradually enough after the initial 10 degree expansion to avoid forming a compression shock. It was therefore important to remove this compression far enough downstream so that the reflected compression shock off the test section did not occur over the test region. The design of the compression corner proved very difficult since the tunnel could not be started if the corner was too gradual and the cross-sectional area became too large. For Gradient A, a tunnel wall shape was eventually achieved which matched with the diffuser throat and removed the compression downstream from the test section. The tunnel could then be started at a stagnation pressure of $3 \cdot 7 \times 10^5$ N/m^2 instead of 3×10^5 N/m^2 as for a constant pressure flow at a Mach number of $2 \cdot 5$. When the flow was tested with injection through a porous test plate it was found necessary to increase the running stagnation pressure to 5×10^5 N/m^2 to maintain the compression shock system behind the test section in a stable condition. It was extremely important to operate the tunnel at a stagnation pressure as low as possible so that a sufficiently long run could be obtained to complete the temperature traverses, since the temperature probe has a small time lag.

6

A similar tunnel-wall shape was used for Gradient C downstream of the expansion fan but a stagnation pressure of 5.8×10^5 N/m^2 was needed to obtain the required injection rate with a stable shock system behind the test section.

Gradient B was produced by fitting a dural plate to the rear of the liner. The plate was rolled to an approximate shape and machined underneath at various positions to reduce its thickness so that it could be wedged to produce a sufficiently flexible wall. The upstream shape of the wall was then adjusted to produce the start of a linear variation of Mach number reducing from 2·5 to 2·2 over the test section. The plate was systematically adjusted further downstream until the Mach number variation was achieved. The tunnel-wall shape after the compression was a gradual expansion to match to the diffuser throat and caused no problems since no shocks were formed and the influence fell behind the test section. The presence of injection modified the pressure gradient so that the Mach number fell to 2·1 for the downstream stations. This is caused by the boundary layer being under the influence of more of the compression fan due to the thicker boundary layer. The tunnel could be operated at a stagnation pressure of 3×10^5 N/m^2 for all injection rates in this pressure gradient.

3.3. Probes

Four boundary-layer probes were used; the design of which can be seen in Fig. 3. Two pitot tubes were used for the calculation of the local Mach number profile; a temperature probe for the calculation of the static temperature through the boundary layer; and a static-pressure probe which was used to check that there was negligible transverse pressure gradients through the boundary layer and that the static pressure correlated with the free-stream Mach number determined by the pitot. The reason two pitot probes were used was that the initial probe was damaged during a tunnel run.

The pitot probes were made from hypodermic tubing of outside diameter 1 mm which was flattened and filed to give half heights from the wall to the centre line of the mouths of 0·053 mm and 0·061 mm. The probes were not symmetrical above and below the mouth due to the manufacture and also due to wear upon the lower surface of the initial probe which had been used for several years.

The temperature probe was made from a stainless steel cone of 5 degrees half angle and maximum diameter 1·65 mm which had a copper-constantan thermocouple hard-soldered inside. The cone was fitted to a piece of ceramic tubing 2·5 mm in length which in turn was fitted to hypodermic tubing which carried the insulated wires away to a switching device to which all the other wall thermocouples were connected. Previous temperature probes have used as much as 25 mm of ceramic tubing as insulation and have been strengthened by wedges of brass, but it is impossible to strengthen the ceramic tubing without adding too much to its outside diameter. This length of ceramic proved too fragile for the most upstream traverses during the large loads experienced in the tunnel starting process. Reducing the length of ceramic made no difference to the temperature profile recorded and consequently the stronger type with very little ceramic was adopted.

The static pressure probe was made with a 5 degree whole angle cone which was soldered into a hypodermic tube of outside diameter 1 mm. Two holes of diameter 0·4 mm were drilled through the top and lower sides of the tube at a position 20 mm from the tip of the cone.

3.4. Injection

The injection test area is 85·8 mm across stream and 396 mm downstream and has 32 copper-constantan thermocouples fitted into the surface so that the wall temperature can be interpolated for individual traverses. The boundary layer has been under the influence of injection for about 200 mm so that the boundary layer is characteristic of equilibrium conditions in the constant-pressure flow before the pressure gradients are imposed. The porous test plate is made of porosint Grade A which enables a relatively large pressure difference across the surface to exist for low blowing rates in comparison with the change in wall static pressure along the designed pressure gradients. Therefore the local mass-injection rate varied by only 5 per cent of the mean value along the porous plate under the pressure gradient.

When referring to a particular flow development, the injection rate is then referred to by the variable $m = \rho_w v_w / (\rho_1 U_1)_{\text{ref}}$ which only exhibits this small variation along the pressure gradient. The reference conditions refer to a mean value of $\rho_1 U_1$ upstream of the designed pressure gradient where the flow is nominally at a Mach number of 2·5, whereas $\rho_w v_w$ refer to the local conditions. The significant injection parameter, however, is $F = \rho_w v_w / \rho_1 U_1$ where all the variables are evaluated locally and hence the variation of F along the gradient is dependent upon $\rho_1 U_1$ which varies by as much as 100 per cent along the pressure gradient.

Since a change in static-pressure distribution anywhere over the plate will affect the local injection rate and hence the injection rate all over the plate, it is necessary to consider the static-pressure distribution behind the probe and under the probe-holder extension. Except for a small disturbance caused by the compression shock from the front of the probe and minor ones from edges on the extension, the designed pressure gradients were not affected and the effect on the quoted values of m was negligible.

Spanwise variations of static pressure were shown to be small by Jeromin[31] who traversed 25 mm either side of the centre line of the test section when making sure that negligible three-dimensional effects existed. By comparing the static pressure distributions with and without the probe holder extension in position it would appear that the effect of the designed expansions upon the test section is almost unaffected by the presence of the holder.

For Gradients A and C, there occurs a severe adverse pressure gradient after the induced reflected shock which separates the boundary layer on the test section for the highest blowing rates. The position and nature of this adverse gradient were taken into account when calculating the local mass-injection rates.

The above factors can only influence the injection rate by changing the static-pressure distribution. Since measurements through the boundary layer must be performed using a porous plate without static-pressure holes so as not to disturb the local injection rate, the static-pressure distributions produced were recorded during runs using another plate containing pressure tappings. It is estimated that all the combined effects mentioned above produce only a change of less than ± 1 per cent of the mean injection rate whereas the change due to the designed gradients is of the order of ± 5 per cent. The variations of local mass-injection rate m and the blowing parameter F as a function of streamwise station are shown in Fig. 4.

The temperature of the air supply upon entering the plenum chamber under the porous test plate was just below room temperature and since the test plate normally cools below this temperature during a tunnel run with zero blowing, there will be heat transfer from the injected air to the porous plate and from the porous plate to the free stream. In practice these small-heat transfer rates balance so that the porous plate has a steady wall temperature for positive injection.

The maximum injection rates were fixed by safety limits on the injection equipment. Besides the zero-injection developments, it was possible to obtain:

    (a) two blowing rates for Gradient A, namely $m = 0\cdot001$ and $0\cdot002$,

    (b) three blowing rates for Gradient B, namely $m = 0\cdot001$, $0\cdot002$ and $0\cdot003$, and

    (c) only one blowing rate for Gradient C, that of $m = 0\cdot001$.

3.5. Test Procedure

The first upstream traverse was made 145 mm downstream of the start of injection which was thought sufficient for the boundary-layer profiles to be characteristic of fully developed profiles in zero pressure gradient. This leaves 220 mm of boundary layer development for the measurements, of which the first 50 mm are still in a nominally zero pressure gradient.

The pressure traverses were conducted away from the wall to the free stream and then reversed since the probe was sufficiently flexible to be wound 'into' the wall to record the wall position. This also allowed the temperature of the air in the pitot system to adjust to the running conditions on the outward traverse whilst measurements were taken on the inward traverse. This was possible during the length of running time because of the quick response of the system used. This was not the case for the temperature traverses where there was an obvious time lag if an outward and inward traverse were carried out. The time lag per Kelvin for the metal cone for the range of temperature used was calculated of the order of 4 to 6 seconds. Thus a continuous X–Y plot would be meaningless without taking this lag into account on the scale. It was decided to produce a series of readings at intervals through the boundary layer which were clustered near the wall where the laminar recovery-temperature drop on the cone is largest. By this method it was possible to obtain a traverse as accurate as the error involved in reading the X–Y traces.

Because the temperature probe is much larger than the pressure probe, it is necessary to extrapolate the temperature trace to the local wall temperature.

Boundary-layer traverses were conducted at intervals of $12\cdot7$ mm downstream until the boundary layer was either influenced by the reflection of the compression shock or by the presence of the traverse gear. Such an influence can be detected on the X–Y pressure traces when blow-off or unsteadiness may occur through the boundary layer making it difficult to interpret the trace.

For Gradients A and B the pressure gradient can be regarded as commencing between stations 3 and 4. For Gradient C traverses start an extra station upstream and the pressure gradient starts between stations 4 and 5.

With increasing injection rates causing an increase in the boundary-layer thickness, the influence of the pressure gradients is felt further upstream.

For the case of Gradient B, $m = 0$, traverses were carried out at intervals of 6·35 mm instead of the usual 12·7 mm so that any disturbances would be exposed from the bulk of data measurements. For injection, it was found that with the general increase in boundary-layer growth the effect of these disturbances upon the pressure traces was considerably reduced. For the two highest blowing rates no distortion of the traces could be detected. It is clear, however, that non-linearity in the pressure gradient is magnified by increased injection as can be seen from the Mach number distribution.

3.6. The Reduction of the Experimental Data

The raw data collected from the wind tunnel comprise the X–Y recorder traces through the boundary layer of:

(a) the pitot pressure; behind a normal shock in the case of supersonic flow,

(b) the laminar recovery temperature on a 5 degree cone which is used to determine the local static temperature,

and

(c) the tunnel stagnation pressure, temperature and the wall temperature.

With certain assumptions, the above form a complete set of data with which to determine the velocity and temperature profiles and parameters.

Since the imposed pressure gradients produced neither a measurable transverse-static-pressure gradient nor any shocks in the adverse pressure gradient in the boundary layer itself, the assumption that the flow is isentropic and has constant static pressure through the boundary layer does not appear to be violated when the results are examined. Consequently a data-reduction program similar to that described by Dunbar[3] can be used.

The behaviour of the local air density at any point through the boundary layer was calculated using the perfect-gas-state equation which reduces to $\rho/\rho_1 = T_1/T$. The distribution of viscosity through the boundary layer was determined using Sutherland's formula in the form $\mu = \mu_{273}(T/273)^{\frac{3}{2}}(383\cdot2/T + 110\cdot2)$ where $\mu_{273} = 0\cdot551$ centi poises. A laminar Prandtl number of 0·72 was assumed for the determination of static temperatures from the laminar recovery temperature as measured by the probe.

Probably the largest uncertainty in the evaluation of the collected data is the determination of the free-stream total pressure for the adverse pressure gradient B. The adverse pressure gradient is produced by many weak compression disturbances imposed onto the boundary layer. When a slightly stronger disturbance coincides with the edge of the boundary layer at a traverse station then a distorted pressure trace is recorded on the X–Y recorder. Luckily, this happened at only three or four out of twenty-eight traverse sections in Gradient B, $m = 0$ and such disturbances were less marked with the presence of air injection.

Fig. 5 demonstrates a normal pressure traverse and two types of trace deformed in the outer part of the layer. The dashed line represents the estimated profile used to describe the boundary layer at that station. The estimated profile is that with which the inner part of the layer would appear compatible if the disturbance had not been present. Since the disturbances do not propagate far into the boundary layer perpendicularly to the wall, it was found that only the outer 20 per cent of the boundary layer was affected at the disturbed stations. No effect of disturbances was noticeable at the adjacent downstream station since the boundary layer had already adjusted to the conditions downstream of the disturbance. The change of profile shape from that of constant pressure equilibrium to the developed profile in the pressure gradient was always systematic so that a profile in between stations could be predicted with little error. The estimated profile can be tested by plotting u/U_1 against y/δ and observing that the profile fits the local trend of profile development. Clearly an unsuitable choice for the free-stream total pressure would result in a disturbed value for the free-stream Mach number, M_1, and hence an unsatisfactory value of U_1 with which to scale the local velocity.

Rapid changes in the boundary layer parameters, however, are more commonly caused by a rapid change in the boundary layer thickness, δ itself, rather than a disturbed velocity profile. The effect of having to estimate the free-stream velocity produces smaller changes in boundary-layer parameters than those caused by the disturbances in the boundary-layer thickness. These profiles appear similar when plotted u/U_1 against y/δ and only exhibit disturbed profile shapes when plotted u/U_1 against y. Fortunately such traverse stations exhibiting either of these disturbances were few compared with the number performed for Gradient B.

4. The Skin Friction Coefficient

One of the purposes of investigating the present layers was to determine the validity of various forms of the inner law under these circumstances. For this purpose some degree of knowledge is required of the wall shear stress. An absolutely accurate value of the skin-friction coefficient C_f is often not essential. For uniform flows with small disturbance a mean value obtained from the momentum equation is quite adequate. Unfortunately it was difficult to use this equation over various ranges of the present developments without further knowledge of the expected variation of C_f in pressure gradients of this order of magnitude.

Over a range of boundary layer near the start of the pressure gradients, rapid change in the measured momentum thickness θ were recorded. These usually diminished to leave some range of the pressure-gradient flow with a smooth variation where a momentum balance could be attempted. However, the nature of the continuous change from the upstream constant-pressure flow to such reasonably smooth portions could not be estimated through the disturbed region of rapid change. It was therefore clear that other means of determining C_f was essential in analysing the changeover between the two regions of the flow. Apart from this, extremely large percentage errors are incurred when the momentum integral equation is used for blowing rates when the value of C_f is very small.

For mild pressure gradients, where the magnitude does not vary rapidly, and for low blowing rates, the skin friction appears to be satisfactorily predicted by fitting the velocity profile to some appropriate form of inner law. Direct measurement of C_f in a pressure gradient flow using a floating element balance is difficult since secondary forces on the element must be calculated. Usually the accuracy of these results is worse than using Preston or Stanton tubes, provided that an accurate calibration, which takes into account any normal pressure gradient, is used. Sivasegaram[18] has noted that the floating element cannot be used reliably in pressure gradients with magnitudes similar to those of the present experiments.

4.1. The Measurement of Skin Friction for Zero Injection

The variation of wall shear stress along the test plate for zero injection was found using the razor-blade technique devised by Smith, Gaudet and Winter.[32] This method requires a calibration of the razor blades against skin-friction coefficient. However, in the present investigation a skin-friction balance was not available so that neither a direct measurement of C_f nor a calibration of the razor blades in pressure gradients was possible.

The calibration used by Smith et al. could not be used in the present experiments since the size of the static pressure holes in the test section was only a third of that used by Smith et al. This meant that the geometry of the blades above the static-pressure holes would be different unless both faces of the razor blades were machined to produce much thinner razor blades. This usually caused the razor blades to bow, rendering them useless for the purpose required.

Differences in razor-blade calibrations have been shown by Hopkins and Keener[33] when the position of the blade relative to the wall tapping was varied, and by East[34] when the chamfer height on top of the razor blade and the position of the leading edge were varied. It was therefore decided to place the front of the razor blades over the leading edge of the wall tapping and remove the chamfer from the top surface of the blades so that only 10 per cent remained (see Fig. 6). This would ensure that the boundary layer recovered as quickly as possible so that closer spacing of the blades could be used. To calibrate the razor blades it was decided to use the Spalding–Chi values for constant-pressure flows since several experimental uniform flows of Squire[2] and Jeromin[1] had demonstrated a very close agreement between these values and those obtained from the momentum growth.

The calibration reached by a dimensional argument for such blades is of the form

$$\frac{\tau_w \rho_w h^2}{\mu_w^2} = F\left(\frac{\Delta P \rho_w h^2}{\mu_w^2}\right).$$

That of Smith et al. originally took the form of:

$$\frac{\tau_w \rho_w h^2}{\mu_w^2} = 0 \cdot 207 \left(\frac{\Delta P \rho_w h^2}{\mu_w^2}\right)^{0 \cdot 764}.$$

To check that this form of the calibration did not apply to the present arrangement it was necessary to vary at least two of the variables in the calibration. The simplest manner seemed to be the use of a constant-Mach-number flow at different stagnation pressures. Several razor blades could be mounted along the test plate and

used for the various runs. Since the individual heights of the razor blades should remain constant and the local wall temperatures remain constant, a calibration of the form

$$\frac{\tau_w \rho_w h^2}{\mu_w^2} = a \left(\frac{\Delta P \rho_w h^2}{\mu_w^2} \right)^b \text{ reduces to } \frac{(\tau_w \rho_w) \text{ ref. 1}}{(\tau_w \rho_w) \text{ ref. 2}} = \left(\frac{(\Delta P \rho_w) \text{ ref. 1}}{(\Delta P \rho_w) \text{ ref. 2}} \right)^b.$$

The different reference conditions apply to any of the different stagnation pressures.

From the experiments of Squire and Jeromin, the values of C_f expected for certain of the tests were known from the momentum growth. These agreed with the values predicted using the Spalding–Chi calibration.[35] Therefore the ratio of $(\tau_w \rho_w)$ref. 1/$(\tau_w \rho_w)$ref. 2 was well known; for example for $M = 2 \cdot 5$ at $P_0 = 3 \times 10^5$ N/m^2 and $P_0 = 5 \times 10^5$ N/m^2. The calculated value of b obtained did not agree with the value of $0 \cdot 764$ quoted by Smith *et al.* and was consistently higher than this value for all the razor blades.

The value of b found from the present readings which gave reasonable values of (C_f) ref. 1/(C_f) ref. 2 as predicted by the Spalding–Chi calibration was $b = 0 \cdot 794$. This was representative of all the razor blades, for the three Mach numbers of $1 \cdot 8$, $2 \cdot 5$ and $3 \cdot 6$ for their ranges of stagnation pressure, to within ± 4 per cent of $0 \cdot 794$. If however, only the results where log $(\Delta P \rho_w)$ ref. 1 and log $(\Delta P \rho_w)$ ref. 2 differ by more than 1 per cent are used, the calculated values of b are clustered to within ± 2 per cent of $b = 0 \cdot 794$. If this difference is much smaller than 1 per cent then the solutions for b are not so reliable.

By finding the value of b in this manner there is as yet no reliance upon absolute values of C_f. The ratio of skin-friction coefficients for the relevant values of R_θ is probably better known than their absolute values, for compressible flow. The mean values obtained from the momentum growth agree with the Spalding–Chi values. The values of C_f produced by the method of Winter and Gaudet[36] are generally of the order of 1 or 2 per cent below the values of Spalding and Chi, but produce the same ratio of (C_f) ref. 1/(C_f) ref. 2 for the range used here.

The value of the constant a in the calibration depends upon the absolute value of C_f used and upon the effective height h of the Stanton tube, which depends upon the height of the leading edge from the test plate and to a lesser extent upon the chamfer height on the top surface of the blade. Since the chamfer heights used here are relatively small, the effective heights of the razor blades were taken as the height of the leading edge from the surface of the test plate. The small error involved due to the neglect of the chamfer height is automatically compensated for in the calculated value of a in the calibration. The value of a which gave the best mean fit with the Spalding–Chi values of C_f, for all the razor blades, was $0 \cdot 151$. The scatter about this value was within the experimental error involved in measuring the heights of the razor blades. These were measured using tallysurf traverses to an accuracy of approximately $\pm 1 \cdot 5$ per cent. The shadowgraph and travelling microscope verified the heights with a lower accuracy of ± 4 per cent.

If the heights of the razor blades could be measured more accurately then a better method would have been to calibrate each razor blade individually to account for differences in the individual geometries which must exist. The accuracy of the calibration would then depend mainly upon the error in obtaining the required values of C_f to determine the constant a.

The calibration obtained to represent Mach numbers between $1 \cdot 8$ and $3 \cdot 6$ for stagnation pressures from 2×10^5 N/m^2 to 10^6 N/m^2 for zero pressure gradient is then:

$$\frac{\tau_w \rho_w h^2}{\mu_w^2} = 0 \cdot 151 \left(\frac{\Delta P \rho_w h^2}{\mu_w^2} \right)^{0 \cdot 794}.$$

The three sets of authors previously mentioned who have used razor blades have shown that calibrations of the form log $\tau_w \rho_w h^2 / \mu_w^2$ against log $\Delta P \rho_w h^2 / \mu_w^2$ are in fact non-linear, but over the limited range of $\Delta P \rho_w h^2 / \mu_w^2$ used in the present experiments, the calibration may be taken as linear, well within the bounds of experimental error. Over the same range, the calibration of Hopkins and Keener[33] can be approximated by a linear calibration with $b = 0 \cdot 833$ as opposed to that of $b = 0 \cdot 764$ by Smith *et al.* The value of $0 \cdot 794$ for b in the present experiments is therefore reasonable since the geometry of the razor blade relative to the wall tapping also lies between that of the above two sets of authors.

In the present experiments it was found that the static pressure in the boundary layer had readjusted to the undisturbed value within 25 mm downstream of a razor blade. The razor blades for the calibration at different Mach numbers and stagnation pressures were positioned at approximately 50 mm intervals along the plate. The series was then repeated with the razor blades shifted by 25 mm. In each case the first run was repeated at the end of the series to check whether a razor blade had shifted. The tallysurf traverse was also repeated.

Although the razor blade technique of determining wall shear stress has already been used in pressure gradients, the effect of pressure gradient upon the calibration cannot be evaluated at present because of a lack

of reliable skin friction data in pressure gradients. Consequently the calibration as found above, was used to determine the skin friction distribution of Gradients B and C. The readings were taken in two stages so that the shear stress could be evaluated at intervals of 25 mm along the test section.

If the calibration holds for pressure gradients, this would then produce skin friction measurements in the pressure gradients as accurate as those predicted by the Spalding–Chi calibration for zero pressure gradient.

4.2. An Estimation of Skin Friction for Injection

Measurements similar to those upon the solid plate could not be made for the porous plate because of the inevitable disturbance of the local mass-injection rate. Consequently some means of transforming the skin-friction results for zero injection, incorporating the effect of injection, had to be used. Some evidence for such a correlation in zero pressure gradient does exist. For example, it would be possible to estimate the effect of an injection rate at a particular Mach number between 1·8 and 3·6 by interpolating upon the figure of C_f/C_{f0} against $2F/C_{f0}$ in Ref. 37.

Some similar type of interpolation could be used for flows in pressure gradients if C_{f0} were taken to be the measured skin friction in the pressure gradient without injection. This would by no means be rigorous but would serve as an estimate for finding C_f in injected pressure gradients. For example, the assumption that C_f/C_{f0} or $C_{f0} - C_f$ remained the same value as for the equivalent constant pressure flow at that Mach number and Reynolds number, may produce C_f to the required accuracy if the use of theoretical prediction methods cannot be used. Any interpolation or extrapolation method has obvious flaws. For example, if C_f/C_{f0} for the pressure-gradient flow were assumed to remain the same as for the equivalent constant-pressure flow at that Mach number then separation caused by injection in the constant-pressure flow gives $C_f/C_{f0} = 0$. If this value is used for the pressure-gradient flow it prevents a favourable pressure gradient delaying separation. For an adverse pressure gradient, where an equivalent value in constant-pressure flow at C_f/C_{f0} is non-zero, then if C_{f0} tends to zero in the adverse pressure gradient, C_f must also tend to zero for any injection rate, and separation must occur at the same position with and without injection. This is illogical since injection is observed to accelerate the onset of separation. Assuming that C_f/C_{f0} remains constant is therefore inaccurate close to separation. From a comparison of the predicted developments with the estimated values of C_f, in Figs. 8 to 10, using this assumption, it is clear that the estimation holds reasonably well for the two favourable pressure gradients but overestimates the predicted values in the adverse pressure gradient and does not show the separation indicated by the predicted developments. Since C_f/C_{f0} is non-zero for the constant-pressure flow equivalent to a station in Gradient B, and since C_{f0} is non-zero along Gradient B, then the estimation cannot produce a zero value for C_f and the estimation must overestimate C_f for adverse pressure gradients with low skin-friction values. The errors produced by this method of estimating C_f seem to be much larger in adverse pressure gradients than in favourable pressure gradients as conditions move away from separation.

Similar limitations exist if $C_{f0} - C_f$ is assumed to remain constant, for $C_{f0} - C_f$ can be non-zero in the constant-pressure flow whereas both C_{f0} and C_f can be zero in a strong adverse-pressure gradient. This assumption seemed likely to produce much larger errors in the estimation of C_f and was therefore not considered.

The estimates of C_f for the injected flows, assuming that C_f/C_{f0} remains constant, and the measured values for zero injection are shown with other boundary-layer parameters in Table II. A rigorous correlation between skin-friction coefficients in pressure gradient and constant-pressure flows for various injection rates does not seem worthwhile when so little experimental data exists and when satisfactory results can be obtained from theoretical boundary-layer-prediction methods.

5. The Comparison of the Present Results with Two Prediction Methods

This aspect of the work is to be covered in greater detail by Marriott and Thomas but a brief explanation of the theoretical developments which appear in the Figures is necessary.

One theory is that of Verma[5] which was written for compressible flow with injection. Verma solves the enthalpy and momentum equations with the aid of an eddy-viscosity model and the hypothesis used was basically the same as that of Cebeci and Smith.[22] Differences between the two methods exist in the manner of solving the finite difference equations.

The other theory is the author's extension of the Bradshaw–Ferriss method for compressible flow with zero heat transfer to include injection. The program was modified in a similar manner to that suggested by Ferriss and Bradshaw[38] for incompressible flow with injection. Before this modification was made it was necessary to change the length scale, L_{max}, from $0·096\delta_{995}$ as used by Bradshaw to $0·075\delta_{995}$, and also to increase the value of the mixing length constant k to 0·418 from 0·4. As the program originally stood, it predicted the

12

developments of displacement and momentum thickness and skin friction satisfactorily. However it could not produce the non-dimensional equilibrium velocity profiles for constant-pressure flows measured in the Cambridge University Engineering Department wind tunnels and those of the present experiments for zero injection. For similar Mach numbers and Reynolds numbers these profiles are almost identical to those of Coles;[39] Rubesin, Maydew and Varga;[40] Peake, Brakmann and Romeskie;[41] Michel;[42] Sivasegaram[43] and Baker.[29] However, the profiles of Winter and Gaudet[36] at much higher Reynolds numbers and those of Adcock, Peterson and McRee[44] at much higher Mach numbers are predicted better by a value of $0.096\delta_{995}$ for $L_{\max}$. Another way in which the difference in profile shapes between the data of Winter and Gaudet and those mentioned is shown in the relation between the incompressible and compressible momentum thicknesses as a function of Mach number. Winter and Gaudet propose a relation of the form,

$$\theta_i/\theta = 1 + \alpha M_1^2$$

with $\alpha = 0.056$, whereas the value of α should be increased by the order of 20 per cent for the parameters measured by other authors. A detailed comparison between the present experimental profiles and much of the existing constant pressure and pressure-gradient flows with and without injection is given by Thomas.[8]

With a value of $0.096\delta_{995}$ for $L_{\max}$ in the Bradshaw–Ferriss method the predicted velocities were too high in the inner region and slightly too low in the outer region of the boundary layer, thus compensating for the displacement thickness. With a value of $0.075\delta_{995}$ for $L_{\max}$ the profiles were very similar to those measured at Mach numbers and Reynolds numbers in the same range as the present experiments without a noticeable change in displacement and momentum thicknesses. With a value of 0.4 for k the skin friction development was now underestimated and the value of 0.418, which is characteristic of the boundary layers in the Cambrdige University Engineering Department supersonic wind tunnel, returned the development in close agreement with the Spalding–Chi development which in turn agreed with the skin friction values obtained from the experimental momentum growth.

To incorporate injection, the form of the inner law proposed by Bradshaw and Ferriss

$$\frac{2}{V_w}[(uV_w + U_\tau^2)^{\frac{1}{2}} - U_\tau] = \frac{1}{k}\log\frac{U_\tau y}{\nu w} + A$$

where A is now a function of Mach number and V_w/U_τ was finally chosen as giving best agreement with experiment with minimum computing time.

These are then the two methods used to produce the theoretical developments which appear in the Figures.

6. Discussion of the Boundary Layer Profiles

The basic experimental results are tabulated in Tables 1 and 2. The smoothed Mach-number distributions used for the theoretical predictions are shown in Fig. 7. Similar presentations of each gradient follow for C_f, δ^* and θ in Figs. 8 to 12. Typical temperature profiles in the zero pressure gradient region, at $X = 0$ mm, and downstream, at $X = 127$ mm, where the profiles are typical of the pressure gradient are shown in Figs. 26 to 28. The full boundary-layer developments for the flows are shown in the form of velocity profiles at intervals of 25.4 mm in Figs. 13 to 21.

The inner law is considered in the form

$$G(u) = \int_0^u \frac{(\rho)^{\frac{1}{2}}du'}{(\tau_w + \rho_w v_w u')^{\frac{1}{2}}}$$

versus $\log y^+$ for some of the developments in Figs. 30 to 35. The outer law is also considered in the form $(U_\tau - u)/U^*$ versus y/δ for typical profiles in Figs. 39 and 40.

6.1. The Velocity Profiles

When the velocity profiles are plotted in non-dimensional form all three pressure gradients demonstrate the increase in fullness associated with the presence of injection and it is clear that the adverse pressure gradient deforms the profile in the same manner as injection. The shape of the profiles for the two highest blowing rates in Gradient B is similar to those of Jeromin[1] and Marriott[4] for high blowing rates at a Mach number of 3.6 towards the last test stations of the developments. In these cases there was an upstream history of an adverse pressure gradient. For all these flows the skin-friction is very low so that the logarithmic region may be so small as to be immeasurable and the profiles are dominated by the wake component. This behaviour is very similar to that of the profiles measured by Stratford[13] with a nominally zero skin-friction coefficient. Neither of the

13

prediction methods show this kind of behaviour when approaching separation although both methods predict a gradual fall in skin friction until separation is predicted.

The change in the profile shape close to the wall, between that in a constant-pressure flow and that in a favourable pressure gradient, indicates an increase in wall shear stress with the presence of a favourable pressure gradient. In pressure Gradient C there is a trace of an inflection in the profiles close to the wall, as in the profiles of Michel et al.[17] This is not shown by either of the two prediction methods.

With the addition of injection the profiles become fuller and the wall shear stress reduces with an increase in injection rate. The injection profiles for favourable pressure gradients resemble those for lower injection rates in constant-pressure flows or still lower injection rates in adverse-pressure gradients. For example, for $m = 0.001$ the velocity profiles in Gradient A resemble zero-pressure-gradient profiles for zero injection.

6.2. A Comparison of Velocity profiles in Pressure Gradients with Injection

When a comparison of velocity profiles is made it is essential to know the immediate history of the boundary layer upstream. Although local conditions of two profiles may be similar their immediate upstream histories may differ greatly so that the profile shapes also differ noticeably. The profile shapes with which the present profiles are compared are taken after as long a development as was measured in the particular pressure gradient. In some cases the local conditions vary continually along the flow and the state of the flow is mentioned when considering the profile shape.

The adverse-pressure-gradient profiles are shown in Figs. 22 and 23. The profile shape, onto which the present measurements along each flow collapse, represents a pressure-gradient parameter β of between 0.5 and 0.6. The injection rate is considered in the form V_w/U_1 so that both compressible and incompressible data can be considered. The profiles are plotted versus y/θ_i for the same reason.

In Fig. 22 the profiles of Ludwieg and Tillman[45] and Sivasegaram[18] for $\beta \simeq 0.5$ are very similar to those of the present experiments. The profile for $\beta = 0.235$ of Sivasegaram is still influenced by the upstream favourable pressure gradient and resembles a zero-pressure-gradient profile. All the other profiles are at nominally higher values of β. The profiles of Schubauer and Klebanoff[46] represent profiles at lower values of β than shown since the pressure gradient starts only 50 mm upstream of that for $\beta = 1.74$ and follows a favourable pressure gradient. The later profile represents a lower value of β than $\beta = 12$ since the flow causes a rapid increase in β and does not adjust to local conditions. The profile for Baker[29] for $\beta = 1.18$ is similarly affected but that for $\beta = 0.98$ is characteristic of local conditions. The flow of Stratford[13] has a rapid β variation and only close to the wall does the profile show the fullness associated with a very low skin friction. All the profiles of Peake, Brakmann and Romeskie[4] appear under-developed which is associated with the under-developed flow in the constant-pressure region upstream of this pressure gradient. The profiles of Voisinet et al.[19] also represent lower values of β than calculated since the flow follows a strong favourable pressure gradient and β increases rapidly.

For injection in Fig. 23 the profiles of McQuaid[26] are characteristic of local conditions and the profiles for $V_w/U_1 = 0.002$ are almost identical with the present experiments. The developed profiles of Baker for $\beta = 0.98$ agree with the present profiles, except close to the wall, where the present profiles demonstrate higher velocities, associated with the onset of separation. Baker's profiles for $\beta = 1.18$ again seem representative of lower values of β.

Figs. 24 and 25 show the profiles for favourable pressure gradients. For zero injection the profile of Herring and Norbury[12] is very similar to those of Gradient A and only varies slightly close to the wall. The profiles of Sivasegaram are representative of a value of $-\beta$ less than 0.6 as indicated and the profile for $-\beta = +0.16$ probably corresponds to a value higher than this, since full development in the constant-pressure flow does not occur until after this station. The profile of Baker for $-\beta + 0.47$ is similar to that for Gradient A except near the wall. The profile for $-\beta = +0.78$ again corresponds to a higher value of $-\beta$ due to the stronger pressure gradient upstream. The profiles of Michel et al.[17] are taken from the downstream stations of the developments D1, D2 and D3 but all the profiles demonstrate the influence of the stronger pressure gradients upstream, which are respectively $-\beta = 1.4$, $+1.6$ and $+1.8$. The profile shapes of both Loyd[28] and Julien[27] seem characteristic of stronger pressure gradients, but unlike the flows of Michel et al. there is no stronger pressure gradient upstream. Instead, the boundary layer in the constant-pressure region upstream of the test pressure gradients is not in equilibrium and is considerably under-developed and resembles that in a mild favourable pressure gradient.

A comparison between profiles for injection into favourable pressure gradients is not as simple as that for adverse pressure gradients since the effects of injection and a favourable pressure gradient on the profile shape are in opposite senses. Injection tends to make the profile fuller with lower velocities for a given value of y/θ_i

14

whereas the favourable pressure gradient has the opposite effect. This holds through the inner half of the boundary layer, but as can be seen in the figures the profile shapes cross and the reverse is true in the outer region of the layer. Nevertheless, the profiles of Loyd and Julien are under-developed for the local values of β. The profiles of Baker and McQuaid, for similar values of β and V_w/U_1 resemble the present profiles.

The profiles of Baker for freon injection show that close to the wall the profiles are similar to those of air injection into boundary layers with very low skin-friction coefficients, since the profiles approach the u/U_1 axis steeply close to the wall. In general the profiles show higher velocities for a given value of y/θ_i than for air injection, since the free-stream value of y/θ_i is less than that for the equivalent flow with air injection.

It is concluded that the present experimental flows are substantially developed under the influence of the pressure gradients. Similarly the flows of McQuaid and Baker for either favourable or adverse pressure gradients are also developed but the favourable–adverse pressure gradient of Baker and the flows of Loyd and Julien do not attain a developed state under local conditions.

For developed flows theoretical methods can predict profile shapes quite adequately but when the flow is under-developed and influenced by upstream conditions which are different from the local conditions, differences between theory and measurement will exist unless the upstream history is also considered in the theory.

6.3. The Temperature Profiles

For compressible flow with zero heat transfer one would expect that the flux of total energy would remain constant through the boundary layer. Since the wall temperature under these conditions would be below the stagnation temperature, T_0, this implies that T_0 is not constant through the boundary layer and that there is an overshoot in T_0 near to the edge of the boundary layer, since $u = 0$ at the wall. In the present experiments, for zero blowing the measured wall temperatures were generally slightly higher than the calculated wall recovery temperature using a recovery factor of $r = 0.89$. The reduction of the wall temperature usually attributed to the effect of injection is not noticed, as can be seen from Table 2, since the heat transfer from the injected air supply to the wall maintains the wall temperature very close to the room temperature. For zero blowing the heat transfer is from the wall to the boundary layer and an observed cooling of the wall is noticed.

The variation of static temperature in the zero pressure gradient and in the pressure gradient for stations $X = 0$ mm and $X = 127$ mm respectively are shown in Figs. 26 to 28. The effect of the pressure gradient upon these is not so marked as upon the velocity profiles but the same tendency to be fuller with blowing and adverse pressure gradients exists. The obvious change upon the profiles is caused by the change in the scaling factor T_1 due to the variation in M_1 along the pressure gradient.

From a theoretical analysis with a range of turbulent Prandtl numbers, Spence[47] found that a good approximation to his results was given by

$$\frac{T}{T_1} = \frac{T_w}{T_1} + \frac{T_r - T}{T_1} \cdot \frac{u}{U_1} - \frac{T_r - T_1}{T_1} \cdot \left(\frac{u}{U}\right)^2$$

where r refers to adiabatic wall recovery conditions. The recovery factor used in this equation for the case of injection profiles was evaluated using the empirical relation

$$\frac{r}{r_0} = \left(1 + 0.83\frac{2F}{C_{fo}}\right)^{-0.04}$$

as used by Dunbar[3] and a value of $r_0 = 0.89$ was used.

Except for the case of the two blowing rates of $m = 0.002, 0.003$ for Gradient B, the agreement of Spence's equation with measured temperature profiles is remarkably good in all three pressure gradients. It is in general slightly better than the temperature distribution produced by solving the energy equation from the theory of Verma. The measured temperature profile is very similar to the velocity profile for the two cases exempted above. The particular shape is also produced by Spence's equation. The same feature of rapid change between wall conditions and the first experimental values is evident, since the velocity and temperature are inter-related.

The assumption of constant T_0 through the boundary layer is clearly not true when the measured distribution is calculated. Typical distributions for the three gradients are shown plotted in Fig. 29 since interest has been shown lately in these, concerning the existence of the temperature overshoot in the outer part of the boundary layer. This is not noticed in these experiments to a significant extent although very small overshoots are indicated. However, the rapid changes close to the wall are very interesting.

6.4. Boundary Layer Relations in the Inner and Outer Layers

It is generally held that the boundary layer can be sub-divided into three distinct regions: (1) the region nearest the wall being the viscous sublayer, (2) the region known as the inner region which is influenced largely by the imposed boundary conditions of the wall, and (3) the outer region where the effect of the wall is small and the flow bears the characteristics of a 'wake' region.

Although pitot pressure probes with an outside diameter of less than 0·1 mm were made, it was found impossible to obtain sufficient satisfactory data in the sublayer region of the present boundary layers to be able to consider comparisons between theory and experiment in this region. Consequently, such comparisons will be concerned only with the inner and outer regions.

(a) The inner region

For compressible flow with combined pressure gradient and injection, the boundary-layer equations can be integrated with the usual assumptions to produce an inner law of the form:

$$G(u) = \int_0^u \frac{\rho^{\frac{1}{2}} \, du'}{(\rho_w v_w u' + \tau_w + (dp/dx)y)^{\frac{1}{2}}} = \frac{1}{k} \log \frac{U_\tau y}{\nu_w} + B.$$

For large pressure gradients, the dominant term in the expression $\rho_w v_w u' + \tau_w + dp/dx \cdot y$ is the last component. For severe adverse pressure gradients a plot of $G(u)$ versus $\log y^+$ produces little region where the slope is as large as $1/k$ and removes any sign of a wake region where one might expect a very large wake component. For severe favourable gradients there will occur a value of y through the boundary layer where $\tau_w + \rho_w v_w u + (dp/dx)y$ is zero so that any linearity of the plot existing initially is quickly destroyed. Fig. 36 shows typical plots of this form of $G(u)$ versus $\log y^+$ for the present experiments when $G(u)$ is calculated using linear interpolation with small step changes in u'.

At present there appears little to be gained from such plots and one could argue that where the linearity and slope differ from $1/k$, then the equation $\tau = \tau_w + \rho_w v_w u + (dp/dx)y$ no longer holds and that second order terms cannot be neglected in the boundary-layer equations. If, however, the term $(dp/dx)y$ is neglected, the resulting plots of $G(u)$ versus $\log y^+$ bear similar characteristics to the usual inner law especially for favourable pressure gradients where one might expect the inner law to hold further through the boundary layer due to the much smaller wake components associated with favourable pressure gradients. Since the more logical equation to produce an inner law should include the pressure gradient term it is difficult to justify the removal of this term to produce plots which do exhibit a linear region.

For adverse pressure gradients the inner law holds only very close to the wall and it is here that experimental scatter can occur in the velocity profiles so that the law does not produce a significant linear region at all.

The amount of scatter in the $G(u)$ plots as shown in the initial pressure gradient region in Figs. 30 and 34 is observed by most experimenters (e.g. Michel et al.[17] and Sivasegaram[18]) but towards the end of the pressure gradients A and C, some of the profiles bear remarkably linear characteristics although the slopes may vary considerably. For Gradient C, it can be seen that the inner region describes nearly all the boundary layer and this effect is more pronounced for the blown profiles which is contrary to some characteristics of blown profiles which bear similarities to adverse-pressure-gradient profiles.

In the figures of the $G(u)$ profiles (Figs. 30 to 35), Coles'[16] wake function is shown to describe the wake exceptionally well. In Figs. 37 and 38 the variations of π and the law of the wall constant B are shown along the flows for the different injection parameters. The possible error in B due to the uncertainty in C_f is shown on Fig. 38 by the side of each flow. With the onset of separation at the highest injection rates in Gradient B the constant B falls rapidly along the flows and becomes negative. In the favourable pressure gradients the value of B increased slightly over the initial pressure-gradient region and settled to a constant value along the flows.

The value of π increased more rapidly along the adverse pressure gradient for increasing injection. For the favourable pressure gradients the value dropped and remained virtually unchanged for increasing injection up to the maximum used in these experiments. The value of π did not reach zero and increased in the last one or two stations when the magnitudes of the pressure gradients were reduced.

(b) The outer region

It has been shown by McQuaid[48] and Squire[2] that the law in the form $(U_1 - u)/U_\tau = g(y/\delta)$ can be transformed to account for the compressible flow with injection and pressure gradient by using it in the form:

$$\frac{U_1 - u}{U^*} = g(y/\delta) \quad \text{where} \quad U^* = U_1 \left(\frac{T_w}{T_1} \frac{d\theta}{dx} \right)^{\frac{1}{2}}$$

The present experiments are compared with the transformed velocity defect law in Figs. 39 and 40. For zero and adverse pressure-gradient profiles, the collapse is excellent for all blowing rates while the velocity defects for the favourable gradients show vast differences. This is to be expected since it has already been shown that these profiles are satisfied by the inner law almost to the edge of the boundary layer.

It is noticeable that the velocity defects of the theories in Fig. 41 are very similar to the experimental defects. This is significant for the case of Gradient B, $m = 0\cdot002$ and $0\cdot003$ where the overall developments are poorly predicted.

In Fig. 42 the range of velocity defects of the present flows in Gradient B is compared against other data. Apart from the defect profiles of Voisinet et al.[19] the rest of the data shown agrees with the range found in Gradient B. The defects of Voisinet et al. show the influence of the strong favourable pressure gradient upstream.

6.5. General Comments

The experiments of many authors have shown that the collapse of non-dimensional velocity profiles for all blowing rates in zero pressure gradient is good, as would be expected for equilibrium profiles. Small deviations from such profiles occur when small pressure gradients are present. To the same degree of accuracy, the initial profiles of the present experiments collapse onto similar shaped profiles. The profiles then undergo a transition from this equilibrium profile shape when the boundary layer experiences the initial pressure gradient and rapidly tend towards a new shape characteristic of the particular gradient even though it is impossible for it to have reattained equilibrium conditions in a constant pressure gradient since the blowing rate varies from station to station along the gradient.

The initial profiles of Gradient C show signs of the presence of a mild favourable gradient upstream of the first station which would account for the increase in Mach number from the start of Gradient A. This increase was caused by attempts to smooth the Araldite-Dural join on the rear of the liner when forming Gradient B. This produced a small expansion which could not easily be removed later, and the effect upon Gradient C is to change the initial Mach number from $2\cdot55$ to $2\cdot58$.

Similarly this join produced a slight compression in Gradient B which reduced the upstream Mach number $2\cdot51$, but since it would appear that the effect upon the profiles of an adverse gradient, of similar magnitude, is less, there appears no change in the upstream profile from that of the equilibrium shape.

The favourable gradients were free from further disturbance until reaching separation at the downstream stations. One or two weak disturbances were evident in Gradient B and these did affect some of the boundary-layer parameters. In general, disturbances tended initially to increase the skin-friction coefficient, boundary-layer thickness and consequently δ^*, θ and R_θ without changing the shape of the velocity profiles plotted in non-dimensional terms. The increase in skin friction and Reynolds number were invariably accompanied by a drop in Mach number. It was difficult to conclude anything concisely due to the experimental error involved in measuring C_f, but it would suffice to add that different razor blades at stations 10, 13 and 15 in Gradient B indicated a higher level of skin friction than predicted by the two theories considered.

For disturbed profiles in Gradient B, which were relatively few, the error involved in measuring δ^* and θ for the worst possible configuration could be as much as ± 10 per cent, whereas for any undisturbed profiles the respective estimates would be ± 1 per cent for δ^* and ± 5 per cent for θ.

A comparison of the two predicted developments in Fig. 11 with Gradient B, $m = 0$ shows that at $X = 30$ mm the start of the adverse pressure gradient has compressed the boundary layer which develops, with a minor disturbance at $X = 7\cdot5$ mm, until a stronger disturbance increases the boundary-layer thickness from $X = 125$ mm onwards. After this change in boundary-layer thickness the non-dimensional profile shape remains unchanged.

Where differences occur in the initial values of δ^* for the two theoretical predictions in Fig. 11 the method of Verma[5] was started with a slightly different value, by choice, so that the mean θ development in the adverse pressure gradient was in reasonable agreement with experiment. This was to ensure that the value of R_θ was not too far in error below experimental values so that the predicted C_f developments would be under similar conditions as the experimental values. The error in the estimated values of C_f for injection is then due to the estimation used rather than differences in conditions.

In the flows where δ^* coincides at the initial station for the two methods, their developments are almost identical and when the initial values are different, interchanging the starting values produces similar developments. Thus in the velocity profile development in Fig. 16, the apparent lack of agreement between the prediction of Bradshaw and Ferriss and the measured profiles is due to the initial value of δ^* used, whereas the

17

initial value of δ^* and boundary-layer thickness was scaled down for the method of Verma. When the boundary layer was compressed after 25 mm by the disturbance at the start of the pressure gradient, the development predicted by Verma, starting with an initial low value of δ^*, coincides with the experimental development, whereas that of Bradshaw and Ferriss continues at the higher level. If this method were started at the same low value it produces similar agreement as the method of Verma. Direct comparisons between the two methods must be taken from developments starting from identical values of δ^*. Small differences in θ occur at the initial station due to the difference in the temperature distributions through the boundary layer for the two methods.

7. Concluding Remarks

In many of the experimental data on two-dimensional pressure-gradient flows it is difficult to analyse qualitatively the effect of the pressure gradient itself upon the boundary layer. This is basically because the fully developed profile for those particular conditions in zero pressure gradient is unknown. Most experimental work studies the transition from a constant-pressure flow to one in the pressure gradient, but often an insufficient length of boundary layer in the upstream constant pressure flow exists to allow the flow to become fully developed before the start of the designed pressure gradient. Consequently the initial profiles in the pressure gradient often exhibit characteristics associated with the strong upstream favourable pressure gradient which commences at the throat of the wind tunnel. Alternatively, the study of the boundary layer under the imposed pressure gradient does not progress sufficiently far downstream for the boundary layer to adjust to the local pressure-gradient conditions. In a pressure gradient where the magnitude varies rapidly along the entire flow, the boundary layer will never be representative of local conditions.

Although it is probably unrealistic to expect the boundary layer to obtain fully developed equilibrium conditions because of minor fluctuations in the imposed pressure gradient, these conditions can be approached to an extent where the velocity profiles collapse onto a profile characteristic of the pressure-gradient parameter describing the local flow, provided the parameter varies slowly along this flow. It is also reasonable to expect that the profiles in adverse pressure gradients should resemble some form of velocity-defect profile in the outer part of the boundary layer, provided the magnitude of the pressure gradient and injection rate can be successfully represented in such a velocity-defect law. Similarly, one would expect the deviation from some form of inner law to be a systematic and continuous function in the range of favourable pressure gradients through to adverse pressure gradients.

From a comparison of these various forms of velocity profiles it is concluded that most of the other data considered have signs of incomplete development or only one or two profiles which resemble full development. It would seem that very few of the profiles of Julien or Loyd were near to full development, whereas most of the profiles of McQuad and Baker, apart from his favourable-adverse pressure gradient, appeared well developed for the velocity profiles, velocity defect and inner law profiles.

For zero injection, the velocity profiles of Peake *et al.* do not resemble developed profiles in adverse pressure gradients. Those of Voisinet *et al.* were clearly not in local equilibrium but provide well behaved inner law and wake component profiles. The profiles of Sivasegaram seem quite reasonable whenever the flow develops for sufficient length with slowly varying β. The developments of Michel *et al.* do not readjust to the local value of β after the initial larger pressure gradients. Although the inner law profiles of the strongest pressure gradient bear no linear region and are marked throughout by experimental fluctuation, it is not thought that relaminarisation has commenced in the down-stream stations since the value of β reduces very quickly to similar values in other flows.

It is not known how much emphasis can be placed on the ability of developed velocity profiles to reflect the magnitude of the individual pressure gradient. It would appear, however, that a parameter of a form similar, if not equal, to β can be used to indicate the shape of the velocity profile for zero injection. For injection into pressure gradient flows, β is unsuitable and a more appropriate parameter, for example, would be of the form $v_w/U_1 \cdot 2/C_f + \beta$, where β is the zero injection value and C_f is the value in the injected boundary layer.

The two prediction methods considered, have been shown to produce excellent overall agreement for the flows considered. For pressure-gradient flows with moderate injection rates where the magnitude of the pressure gradient changes relatively slowly, both methods can be considered reliable. For rapidly changing wall or free-stream conditions it is expected that most prediction methods will be inadequate, unless the semi-empirical functions employed, also reflect the rapid changes.

The poor agreement of the prediction methods with experiments for high injection rates in adverse pressure gradients is also expressed by Baker for freon injection, which produces density variations through the boundary layer.

18

The method adopted for measuring the skin-friction coefficient in compressible-flow pressure gradients, using razor blades which are calibrated in constant-pressure flows against the Spalding–Chi values is thought to provide C_f as accurately as any other method at present available. Comparing the results with those predicted by the two calculation methods shows that an estimate of the probable error is ± 5 per cent. This comparison also suggests that an estimate of the skin-friction in favourable pressure gradients with injection is possible. The particular method used does not apply to adverse pressure gradients but a similar method could be adopted for these.

Theoretical methods of obtaining C_f, such as the momentum integral equation or log-law plots are often unsuitable in pressure-gradient flows, especially with the presence of injection, and are liable to produce very large errors due to experimental fluctuations in the boundary-layer parameters and profiles. For flows where the profiles are close to local equilibrium the use of such methods for calculating C_f is probably outdated now that the development of prediction methods has progressed this far.

Considering the velocity profiles, velocity defect and inner-law profiles, it is thought that the overall development of the author's profile in pressure gradients is substantially complete.

It is concluded that the data of McQuaid, Baker and the author, in flows where the pressure gradient varies slowly, are the most reliable velocity profiles which are representative of fully developed profiles for their magnitude of pressure gradient.

The bulk of the data, with pressure gradients where the magnitude changes more rapidly, is probably of greater use to prediction methods for determining the variation of empirical functions with pressure-gradient magnitude when the flow changes so rapidly that it never achieves full development under local conditions.

LIST OF SYMBOLS

a	Constant in razor-blade calibration
b	Constant in razor-blade calibration
B	Inner-law constant
C_f	Local skin-friction coefficient
C_{f0}	Skin-friction coefficient in equivalent zero injection flow
F	Injection parameter $\dfrac{\rho_w v_w}{\rho_1 U_1}$
$G(u)$	$= \displaystyle\int_0^u \dfrac{(\rho)^{\frac{1}{2}}\, du'}{(\tau_w + \rho_w v_w u')^{\frac{1}{2}}}$
h	Height of razor-blade from wall
k	Mixing-length constant
$L_{\max}$	Maximum value of mixing-length function, L, in the Bradshaw–Ferriss method
m	Injection-rate parameter $\dfrac{\rho_w v_w}{(\rho_1 U_1)_{\mathrm{ref}}}$, where ref refers to the upstream constant-pressure value
M	Mach number
p	Pressure, static pressure
P_0	Stagnation pressure
r	Recovery factor
r_0	Recovery factor for zero-injection conditions
R_θ	Reynolds number based on momentum thickness
T	Temperature
u	Streamwise velocity
U_p	$= U_\tau \beta^{\frac{1}{2}}$
U_τ	$= $ shearing velocity, $\left(\dfrac{\tau_w}{\rho_w}\right)^{\frac{1}{2}}$
U^*	$= \left(\dfrac{T_w}{T_1}\dfrac{d\theta}{dx}\right)^{\frac{1}{2}} U_1$
v	velocity component away from the wall
$w(y/\delta_c)$	Wake function in inner law, taken as $1 - \cos(\pi y/\delta_c)$
x	Distance along plate
X	Distance measured from first traverse of Gradients A, B
X'	Distance measured from first traverse of Gradient C
y	Distance from wall
y^+	$= \dfrac{U_\tau y}{\tau_w}$
α	Constant in equation $\theta_i/\theta = 1 + \alpha M_1^2$
β	Pressure-gradient parameter $\dfrac{\delta_i^*}{\tau_w}\dfrac{dp}{dx}$

δ Boundary-layer thickness, taken as value of y when $\dfrac{u}{U_1} = 0.995$ unless otherwise stated

δ_c Value of y where slope of inner-law profile is $1/k$ in outer part of the boundary layer

δ^* Displacement thickness $\displaystyle\int_0^\delta \left(1 - \frac{\rho u}{\rho_1 U_1}\right) dy$

δ_i^* Kinematic displacement thickness $\displaystyle\int_0^\delta \left(1 - \frac{u}{U_1}\right) dy$

ΔP Difference between Stanton-tube pressure and wall static pressure

θ Momentum thickness $\displaystyle\int_0^\delta \frac{\rho u}{\rho_1 U_1}\left(1 - \frac{u}{U_1}\right) dy$

θ_i Kinematic momentum thickness $\displaystyle\int_0^\delta \frac{u}{U_1}\left(1 - \frac{u}{U_1}\right) dy$

μ Viscosity

μ_{273} Reference viscosity at 273 K

ν Kinematic viscosity

π Pressure-gradient constant in wake component of inner law

ρ Density

τ Shear stress

Subscripts

1   Refers to conditions at edge of boundary layer

0   Refers to stagnation conditions

w Refers to wall conditions

REFERENCES

No.	Author(s)	Title, etc.
1	L. O. F. Jeromin	An experimental investigation of the compressible turbulent boundary layer with air injection. A.R.C. R. & M. 3526 (1966).
2	L. C. Squire	Further experimental investigations of compressible turbulent boundary layers with air injection. A.R.C. R. & M. 3627 (1968).
3	D. I. A. Dunbar	Turbulent boundary layers with foreign gas injection. Ph.D. Thesis, Cambridge University (1968).
4	P. G. Marriott	Compressible turbulent boundary layers with discontinuous injection. Ph.D. Thesis, Cambridge University (1973).
5	L. C. Squire and V. K. Verma	The calculation of compressible turbulent boundary layers with fluid injection. A.R.C. 1265 (1973).
6	P. Bradshaw, D. H. Ferriss and N. P. Atwell	Calculation of boundary layer development using the turbulent energy equation. *J. Fluid Mech.* Vol. 28, pt. 3, p. 593 (1967).
7	P. Bradshaw and D. H. Ferriss	Calculation of boundary layer development using the turbulent energy equation: Compressible flow on adiabatic walls. *J. Fluid Mech.* Vol. 46, pt. 1, p. 83 (1971).
8	G. D. Thomas	Compressible turbulent boundary layers with combined air injection and pressure gradient. Ph.D. Thesis, Cambridge University (1973).
9	D. E. Coles and E. A. Hirst	Proceedings of computation of turbulent boundary layers. AFOSR-JFP-Stanford Conference, Vol. 2 (1968).
10	F. H. Clauser	Turbulent boundary layers in adverse pressure gradients. *J. Aero. Sciences* Vol. 21, p. 91 (1954).
11	G. L. Mellor and D. M. Gibson	Equilibrium turbulent boundary layers. *J. Fluid Mech.* Vol. 24, pt. 2, p. 225 (1966).
12	H. J. Herring and J. F. Norbury	Experiments on equilibrium turbulent boundary layers in favourable pressure gradients. *J. Fluid Mech.* Vol. 27, pt. 3, p. 541 (1967).
13	B. S. Stratford	An experimental flow with zero skin friction through its region of pressure rise. *J. Fluid Mech.* Vol. 5, p. 17 (1959).
14	J. E. Lewis, R. L. Gran and T. Kubota	An experiment on the adiabatic compressible turbulent boundary layer in adverse and favourable pressure gradients. *J. Fluid Mech.* Vol. 51, pt. 4, p. 657 (1972).

15 L. Crocco .... Su di un valore massimo del coefficiente di transmissione del calose da una limina piana a un fluido seconente. *Rendiconti R. Accadmia dei Lincei* Vol. 14, p. 490 (1931).

16 D. E. Coles .... The law of the wake in the turbulent boundary layer. *J. Fluid Mech.* Vol. 1, p. 191 (1956).

17 R. Michel, C. Quemard and M. Elena .... Turbulent boundary layer velocity distributions in a uniform or accelerated compressible flow. *La Recherche Aerospatiale* No. 128, p. 33 (January/February 1969).

18 S. Sivasegaram .... An experimental investigation of supersonic boundary layer flows with pressure gradients. A.R.C. C.P. 1190 (1969).

19 R. L. P. Voisinet, R. E. Lee and W. J. Yanta .... An experimental study of the compressible turbulent boundary layer with an adverse pressure gradient. Proc. AGARD Conference, London (September 1971).

20 S. V. Patankar and D. B. Spalding ... *Heat and mass transfer in boundary layers.* Morgan-Grampian Press, London (1967).

21 A. Walz .... Beitraz zur naherungstheorie kompressibler turbulenter grenzschichten. 2 Teil: Berechnung der universellen funktionen und beispiele. D.V.L. Rept. No. 136, 1960. English translation U.S. Library of Congress. A.I.D. Rept. No. T-63-110 (1963).

22 T. Cebeci and A. M. O. Smith ...... A finite difference method for calculating compressible laminar and turbulent boundary layers. *J. Basic Eng.*, p. 523 (September 1970).

23 S. Sivasegaram and J. H. Whitelaw .. The prediction of turbulent supersonic two-dimensional boundary layer flows. *Aero. Quarterly*, Vol. 22, pt. 3, p. 274 (August 1971).

24 T. Cebeci .... Behaviour of turbulent flow near a porous wall with pressure gradient. *AIAA Vol. 8*, No. 12, p. 2152 (December 1970).

25 L. Pasiuk, S. M. Hastings and R. Chatham .... Experimental Reynolds analogy factor for a compressible turbulent boundary layer with a pressure gradient. Naval Ordnance Lab., White Oak, Maryland, Rept. No. NOLTR 64-200 (1964).

26 J. McQuaid .... Experiments on incompressible turbulent boundary layers with distributed injection. A.R.C. R. & M. 3549 (1967).

27 H. L. Julien .... The turbulent boundary layer on a porous plate; experimental study of the effects of a favourable pressure gradient. Ph.D. Thesis, Stanford University (1969).

23

28 R. J. Loyd, R. J. Moffat and M. W. Kays .... The turbulent boundary layer on a porous plate: An experimental study of the fluid dynamics with strong favourable pressure gradients and blowing. Stanford Univ., Rept. No. HMT-13 (May 1970).

29 R. J. Baker .... The turbulent boundary layer with streamwise pressure gradient and foreign gas injection. Ph.D. Thesis, Imperial College, London 1971, also Rep. No. EHT/TN/G/31 (1971).

30 V. C. Patel .... Calibration of the Preston tube and limitations on its use in pressure gradients. *J. Fluid Mech.* Vol. 23, pt. 1, p. 185 (1965).

31 L. O. F. Jeromin .... Compressible turbulent boundary layers with fluid injection. Ph.D. Thesis, Cambridge University (1966).

32 K. G. Smith, L. Gaudet and K. G. Winter .... The use of surface pitot tubes as skin friction meters at supersonic speeds. A.R.C. R. & M. 3351 (1962).

33 E. J. Hopkins and E. R. Keener ..... Study of surface pitots for measuring turbulent skin friction at supersonic Mach numbers: Adiabatic wall. N.A.S.A. TN D-3478 (1966).

34 L. F. East .... Measurement of skin friction at low subsonic speeds by the razor-blade technique. A.R.C. R. & M. 3525 (1966).

35 D. B. Spalding and S. W. Chi .... The drag of a compressible turbulent boundary layer on a smooth flat plate with and without heat transfer. *J. Fluid Mech.*, Vol. 18, pt. 1, p. 117 (1964).

36 K. G. Winter and L. Gaudet .... Turbulent boundary layer studies at high Reynolds numbers, at Mach numbers between 0.2 and 2.8. N.A.S.A. Rept. No. SP-216, 1969; or R.A.E. TN 70251 (1971).

37 L. C. Squire .... A law of the wall for compressible turbulent boundary layers with air injection. *J. Fluid Mech.* Vol. 37, pt. 3, p. 449 (1969).

38 D. H. Ferriss and P. Bradshaw ...... A computer program for the calculation of boundary layer development using the turbulent energy equation. N.P.L. Rept. No. 1269, A.R.C. 30, 231 (1968).

39 D. E. Coles .... Measurements in the turbulent boundary layer on a smooth flat plate in supersonic flow. Jet Propulsion Lab., Pasadena, Repts. 20-69, 20-70, 20-71 (1953).

40 M. W. Rubesin, R. C. Maydew and S. A. Varga .... An analytical and experimental investigation of the skin friction of the turbulent boundary layer on a flat plate at supersonic speeds. N.A.C.A. TN 2305 (1951).

41 D. J. Peake, G. Brakmann and J. M. Romeskie ....   Comparisons between some high Reynolds number turbulent boundary layer experiments at Mach 4, and various recent calculation procedures. Proc. A.G.A.R.D. Conference, London (September 1971).

42 R. Michel ....   Data for the high speed turbulent boundary layer. O.N.E.R.A. publication, 102 (1961).

43 S. Sivasegaram and B. Edwards .....   An experimental investigation of Mach 2.2, turbulent boundary layers in nominally zero pressure gradient Imperial College report BL/TN/3 (1968).

44 J. B. Adcock, J. B. Peterson and I. McRee   Experimental investigation of a turbulent boundary layer at Mach 6, high Reynolds number and zero heat transfer. N.A.S.A. TN D-3882 (1967).

45 H. Ludwieg and W. Tillman ....   Investigation of the wall shearing stress in turbulent boundary layers. N.A.C.A. TM 1285 (May 1950).

46 G. B. Schubauer and P. S. Klebanoff   Investigation of separation of the turbulent boundary layer. N.A.C.A. TN 1030 (1951).

47 D. A. Spence ....   Velocity and enthalpy distributions in the compressible turbulent boundary layer on a flat plate. *J. Fluid Mech.* Vol. 8, pt. 3, p. 368 (1960).

48 J. McQuaid ....   A velocity defect relationship for the outer part of equilibrium and near-equilibrium turbulent boundary layers. A.R.C. C.P. 885 (1965).

The experimental results are presented in the following pages as Tables 1 and 2. The Tables are headed by the particular pressure gradients A, B or C and the respective injection rate, m.

TABLE 1
Velocity and Temperature Profiles

GRADIENT A—0·000

X(mms)	0	12·7	25·4	38·1	50·8	63·5	76·2	88·9	101·6	114·3	127·0	139·7	152·4	165·1	177·8
M_1	2·56	2·56	2·56	2·59	2·63	2·67	2·71	2·75	2·79	2·84	2·88	2·90	2·93	2·96	3·00
θ(mms)	0·424	0·435	0·431	0·479	0·474	0·471	0·463	0·493	0·511	0·519	0·539	0·543	0·558	0·598	0·574
δ (mms)	1·790	1·843	1·899	2·050	2·083	2·115	2·160	2·248	2·377	2·478	2·587	2·695	2·814	2·942	2·937
Y(mms)	U/U_1	U/U_1	U/U_1	U/U_1	U/U_1	U/U_1	U/U_1	U/U_1	U/U_1	U/U_1	U/U_1	U/U_1	U/U_1	U/U_1	U/U_1
0·1	0·511	0·528	0·531	0·520	0·518	0·501	0·533	0·514	0·534	0·515	0·519	0·519	0·511	0·490	0·510
0·2	0·556	0·587	0·588	0·579	0·577	0·566	0·603	0·595	0·622	0·595	0·600	0·600	0·588	0·546	0·601
0·3	0·600	0·623	0·629	0·625	0·635	0·617	0·654	0·661	0·673	0·648	0·656	0·654	0·643	0·610	0·650
0·4	0·636	0·650	0·657	0·660	0·673	0·664	0·693	0·705	0·696	0·683	0·690	0·686	0·683	0·659	0·681
0·5	0·665	0·670	0·681	0·681	0·698	0·693	0·722	0·724	0·712	0·703	0·712	0·708	0·711	0·691	0·701
0·6	0·686	0·686	0·701	0·698	0·714	0·712	0·741	0·739	0·725	0·718	0·728	0·724	0·728	0·712	0·723
0·8	0·711	0·716	0·727	0·723	0·736	0·741	0·761	0·757	0·751	0·738	0·749	0·751	0·753	0·736	0·750
1·0	0·734	0·736	0·747	0·742	0·754	0·756	0·771	0·771	0·766	0·757	0·763	0·766	0·768	0·756	0·761
1·2	0·754	0·757	0·765	0·756	0·769	0·767	0·784	0·782	0·778	0·773	0·776	0·777	0·778	0·769	0·778
1·4	0·772	0·773	0·780	0·771	0·782	0·782	0·796	0·793	0·790	0·790	0·791	0·789	0·789	0·785	0·791
1·6	0·791	0·789	0·794	0·784	0·794	0·793	0·806	0·805	0·815	0·804	0·801	0·800	0·801	0·796	0·802
1·8	0·807	0·804	0·809	0·799	0·808	0·805	0·817	0·826	0·826	0·818	0·813	0·812	0·813	0·804	0·812
2·0	0·824	0·820	0·823	0·811	0·818	0·815	0·828	0·826	0·826	0·827	0·824	0·823	0·823	0·813	0·822
2·2	0·839	0·835	0·837	0·824	0·829	0·828	0·839	0·835	0·837	0·836	0·833	0·831	0·831	0·829	0·832
2·4	0·853	0·850	0·848	0·836	0·840	0·839	0·848	0·844	0·846	0·845	0·843	0·839	0·840	0·832	0·840
2·6	0·869	0·863	0·862	0·850	0·850	0·851	0·857	0·854	0·856	0·853	0·852	0·849	0·850	0·841	0·849
2·8	0·882	0·874	0·875	0·861	0·861	0·863	0·869	0·863	0·863	0·861	0·860	0·858	0·858	0·849	0·856
3·0	0·892	0·886	0·887	0·873	0·871	0·874	0·879	0·871	0·872	0·868	0·868	0·866	0·865	0·856	0·863
3·3	0·910	0·905	0·902	0·889	0·887	0·889	0·890	0·883	0·883	0·879	0·878	0·875	0·873	0·867	0·871
3·6	0·927	0·921	0·919	0·903	0·901	0·903	0·904	0·895	0·894	0·891	0·887	0·885	0·883	0·877	0·881
3·9	0·942	0·938	0·935	0·918	0·917	0·916	0·916	0·908	0·901	0·901	0·896	0·894	0·893	0·887	0·891
4·2	0·956	0·951	0·948	0·932	0·929	0·929	0·927	0·919	0·917	0·911	0·906	0·903	0·903	0·895	0·899
4·5	0·970	0·962	0·962	0·945	0·941	0·941	0·939	0·930	0·923	0·920	0·916	0·912	0·911	0·903	0·908
4·8	0·981	0·975	0·972	0·956	0·953	0·952	0·950	0·940	0·932	0·929	0·924	0·920	0·919	0·911	0·915
5·2	0·990	0·987	0·985	0·971	0·968	0·966	0·961	0·953	0·944	0·941	0·935	0·932	0·928	0·920	0·924
5·6	0·996	0·995	0·993	0·981	0·980	0·978	0·973	0·963	0·954	0·951	0·945	0·941	0·937	0·931	0·933
6·0	0·999	0·999	0·999	0·989	0·988	0·988	0·981	0·973	0·965	0·961	0·954	0·951	0·946	0·940	0·942
6·4	1·000	1·000	1·000	0·994	0·994	0·994	0·989	0·981	0·973	0·971	0·963	0·960	0·955	0·948	0·950
6·8				0·996	0·996	0·998	0·994	0·989	0·981	0·979	0·972	0·968	0·963	0·956	0·956
7·2				0·998	0·998	0·999	0·998	0·995	0·987	0·985	0·980	0·976	0·971	0·963	0·965
7·6				0·999	0·999	1·000	1·000	0·997	0·992	0·990	0·986	0·983	0·978	0·971	0·972
8·0				1·000	1·000			0·998	0·996	0·994	0·989	0·987	0·983	0·978	0·977
8·5								0·999	0·998	0·997	0·993	0·994	0·988	0·985	0·985
9·0								1·000	0·999	1·000	0·996	0·997	0·992	0·989	0·991
9·5									1·000		0·999	0·999	0·996	0·993	0·995
10·0											1·000	1·000	0·998	0·995	0·997
10·5													0·999	0·997	0·998
11·0													1·000	0·999	0·999
11·5														1·000	1·000

27

TABLE 1 (Cont.)

							GRADIENT A—0·000								
X (mms)	0	12·7	25·4	38·1	50·8	63·5	76·2	88·9	101·6	114·3	127·0	139·7	152·4	165·1	177·8
M_1	2·56	2·56	2·56	2·59	2·63	2·67	2·71	2·75	2·79	2·84	2·88	2·90	2·93	2·96	3·00
R_θ	16500	17100	17200	18200	17700	17300	16800	17100	17500	17400	17700	17900	18400	18700	17700
T_w/T_1	2·258	2·260	2·295	2·271	2·315	2·363	2·429	2·422	2·473	2·534	2·581	2·626	2·681	2·653	2·722
Y (mms)	T/T_1	T/T_1	T/T_1	T/T_1	T/T_1	T/T_1	T/T_1	T/T_1	T/T_1	T/T_1	T/T_1	T/T_1	T/T_1	T/T_1	T/T_1
0·1	1·962	1·946	1·979	1·956	2·000	2·050	2·080	2·086	2·105	2·167	2·197	2·230	2·305	2·298	2·331
0·2	1·885	1·852	1·885	1·861	1·903	1·940	1·965	1·955	1·951	2·029	2·049	2·085	2·167	2·196	2·158
0·3	1·808	1·786	1·809	1·781	1·806	1·845	1·869	1·835	1·848	1·924	1·940	1·977	2·053	2·072	2·050
0·4	1·742	1·731	1·749	1·717	1·734	1·761	1·789	1·747	1·793	1·846	1·863	1·904	1·960	1·966	1·970
0·5	1·688	1·687	1·697	1·674	1·680	1·700	1·723	1·697	1·750	1·795	1·807	1·849	1·887	1·886	1·912
0·6	1·645	1·649	1·655	1·639	1·643	1·654	1·676	1·658	1·713	1·756	1·762	1·803	1·833	1·830	1·851
0·8	1·592	1·587	1·597	1·589	1·592	1·592	1·612	1·606	1·639	1·693	1·688	1·719	1·742	1·753	1·764
1·0	1·555	1·549	1·555	1·552	1·549	1·556	1·571	1·566	1·599	1·639	1·639	1·654	1·667	1·685	1·711
1·2	1·522	1·519	1·520	1·525	1·520	1·535	1·539	1·536	1·569	1·597	1·602	1·618	1·633	1·649	1·658
1·4	1·491	1·484	1·492	1·499	1·493	1·507	1·509	1·509	1·536	1·555	1·567	1·585	1·606	1·605	1·619
1·6	1·457	1·456	1·466	1·476	1·470	1·482	1·486	1·486	1·506	1·518	1·540	1·560	1·572	1·577	1·589
1·8	1·429	1·429	1·440	1·448	1·445	1·459	1·463	1·456	1·478	1·489	1·513	1·530	1·540	1·553	1·559
2·0	1·397	1·402	1·415	1·421	1·425	1·438	1·440	1·436	1·454	1·463	1·483	1·503	1·517	1·529	1·533
2·2	1·370	1·377	1·389	1·400	1·405	1·413	1·413	1·416	1·430	1·443	1·461	1·478	1·494	1·506	1·507
2·4	1·343	1·348	1·367	1·379	1·382	1·391	1·393	1·396	1·408	1·420	1·437	1·457	1·470	1·483	1·481
2·6	1·313	1·323	1·340	1·353	1·361	1·365	1·373	1·376	1·388	1·403	1·415	1·435	1·446	1·459	1·460
2·8	1·287	1·301	1·315	1·330	1·341	1·344	1·349	1·356	1·366	1·384	1·392	1·413	1·423	1·435	1·440
3·0	1·260	1·277	1·292	1·309	1·320	1·323	1·326	1·338	1·346	1·367	1·373	1·392	1·404	1·416	1·421
3·3	1·221	1·241	1·260	1·279	1·291	1·290	1·301	1·309	1·321	1·340	1·348	1·366	1·382	1·390	1·394
3·6	1·178	1·202	1·226	1·248	1·261	1·264	1·271	1·281	1·299	1·311	1·325	1·339	1·356	1·364	1·368
3·9	1·139	1·165	1·188	1·219	1·227	1·234	1·243	1·256	1·281	1·287	1·301	1·316	1·331	1·338	1·342
4·2	1·100	1·128	1·156	1·186	1·199	1·205	1·217	1·232	1·243	1·261	1·278	1·297	1·305	1·315	1·318
4·5	1·069	1·097	1·117	1·156	1·173	1·176	1·190	1·204	1·228	1·238	1·252	1·276	1·282	1·295	1·294
4·8	1·040	1·064	1·086	1·126	1·143	1·148	1·165	1·181	1·206	1·217	1·230	1·253	1·262	1·273	1·273
5·2	1·019	1·029	1·051	1·089	1·105	1·115	1·134	1·151	1·176	1·187	1·205	1·223	1·238	1·248	1·248
5·6	1·007	1·008	1·023	1·054	1·072	1·081	1·103	1·122	1·146	1·158	1·180	1·198	1·212	1·221	1·223
6·0	1·001	1·001	1·007	1·029	1·044	1·050	1·076	1·094	1·119	1·132	1·152	1·170	1·187	1·199	1·199
6·4	1·000	1·000	1·002	1·013	1·020	1·027	1·049	1·066	1·090	1·106	1·125	1·145	1·164	1·175	1·176
6·8			1·000	1·006	1·009	1·013	1·026	1·043	1·067	1·082	1·102	1·119	1·138	1·154	1·156
7·2				1·000	1·002	1·003	1·014	1·024	1·045	1·061	1·077	1·097	1·112	1·129	1·130
7·6					1·001	1·002	1·006	1·012	1·024	1·041	1·055	1·071	1·094	1·105	1·110
8·0					1·000	1·000	1·003	1·006	1·012	1·021	1·039	1·051	1·071	1·085	1·094
8·5							1·000	1·002	1·004	1·010	1·021	1·030	1·048	1·059	1·066
9·0								1·000	1·001	1·004	1·012	1·014	1·028	1·041	1·047
9·5									1·000	1·002	1·004	1·009	1·015	1·024	1·030
10·0										1·001	1·001	1·003	1·008	1·013	1·017
10·5										1·000	1·000	1·000	1·002	1·005	1·010
11·0													1·000	1·001	1·005
11.5														1·000	1·000

TABLE 1 (Cont.)

GRADIENT A—0·001

X(mms)	0	12·7	25·4	38·1	50·8	63·5	76·2	88·9	101·6	114·3	127·0	139·7	152·4	165·1
M_1	2·54	2·53	2·56	2·59	2·61	2·67	2·71	2·75	2·76	2·81	2·84	2·88	2·82	2·73
θ(mms)	0·572	0·584	0·578	0·592	0·638	0·632	0·659	0·695	0·742	0·747	0·785	0·781	0·878	0·939
δ^x(mms)	2·497	2·509	2·476	2·543	2·777	2·910	3·037	3·269	3·437	3·532	3·759	3·948	4·102	4·175
Y(mms)	U/U_1	U/U_1	U/U_1	U/U_1	U/U_1	U/U_1	U/U_1	U/U_1	U/U_1	U/U_1	U/U_1	U/U_1	U/U_1	U/U_1
0·1	0·410	0·396	0·422	0·468	0·428	0·443	0·444	0·422	0·439	0·448	0·448	0·490	0·501	0·623
0·2	0·451	0·439	0·461	0·512	0·474	0·489	0·497	0·489	0·494	0·492	0·497	0·524	0·530	0·631
0·3	0·478	0·473	0·498	0·542	0·511	0·526	0·529	0·525	0·535	0·536	0·529	0·552	0·551	0·639
0·4	0·498	0·501	0·528	0·567	0·521	0·556	0·558	0·553	0·564	0·562	0·555	0·575	0·568	0·646
0·5	0·515	0·525	0·549	0·590	0·538	0·578	0·582	0·576	0·586	0·582	0·578	0·592	0·583	0·652
0·6	0·534	0·546	0·567	0·608	0·578	0·597	0·603	0·592	0·603	0·603	0·599	0·607	0·597	0·658
0·8	0·570	0·576	0·598	0·634	0·619	0·627	0·631	0·624	0·632	0·634	0·630	0·635	0·622	0·668
1·0	0·601	0·602	0·626	0·655	0·646	0·652	0·657	0·650	0·654	0·660	0·651	0·658	0·643	0·677
1·2	0·630	0·627	0·651	0·674	0·670	0·674	0·675	0·671	0·674	0·682	0·673	0·678	0·662	0·687
1·4	0·651	0·650	0·668	0·692	0·686	0·694	0·694	0·690	0·692	0·697	0·688	0·696	0·679	0·696
1·6	0·675	0·672	0·688	0·707	0·701	0·708	0·710	0·705	0·706	0·713	0·705	0·713	0·693	0·706
1·8	0·697	0·693	0·707	0·721	0·715	0·721	0·723	0·720	0·719	0·727	0·720	0·727	0·709	0·716
2·0	0·717	0·714	0·727	0·737	0·729	0·734	0·737	0·732	0·728	0·739	0·734	0·739	0·718	0·726
2·2	0·738	0·734	0·746	0·754	0·743	0·746	0·747	0·745	0·740	0·750	0·744	0·748	0·729	0·735
2·4	0·756	0·753	0·763	0·768	0·756	0·759	0·760	0·754	0·752	0·760	0·753	0·756	0·739	0·744
2·6	0·774	0·771	0·779	0·782	0·772	0·771	0·772	0·763	0·763	0·771	0·765	0·765	0·749	0·752
2·8	0·792	0·789	0·795	0·795	0·785	0·782	0·783	0·775	0·772	0·779	0·774	0·774	0·758	0·761
3·0	0·806	0·804	0·810	0·810	0·798	0·793	0·795	0·785	0·784	0·787	0·784	0·785	0·767	0·770
3·3	0·832	0·830	0·833	0·830	0·817	0·811	0·812	0·801	0·796	0·803	0·798	0·799	0·783	0·781
3·6	0·858	0·854	0·858	0·850	0·835	0·829	0·826	0·816	0·810	0·818	0·807	0·811	0·794	0·792
3·9	0·880	0·877	0·881	0·870	0·851	0·848	0·839	0·830	0·823	0·828	0·819	0·822	0·805	0·801
4·2	0·901	0·898	0·898	0·888	0·870	0·863	0·855	0·845	0·836	0·841	0·831	0·832	0·816	0·812
4·5	0·922	0·917	0·916	0·905	0·888	0·880	0·874	0·860	0·850	0·852	0·843	0·843	0·828	0·823
4·8	0·939	0·936	0·933	0·921	0·902	0·895	0·888	0·872	0·863	0·863	0·855	0·853	0·839	0·834
5·2	0·961	0·956	0·953	0·944	0·924	0·916	0·906	0·889	0·879	0·878	0·871	0·868	0·851	0·846
5·6	0·978	0·975	0·972	0·962	0·943	0·934	0·924	0·907	0·895	0·892	0·884	0·881	0·867	0·859
6·0	0·990	0·984	0·986	0·977	0·959	0·953	0·939	0·924	0·910	0·908	0·896	0·894	0·877	0·870
6·4	0·995	0·994	0·995	0·989	0·974	0·967	0·954	0·940	0·925	0·920	0·910	0·906	0·889	0·881
6·8	0·997	0·997	0·998	0·996	0·984	0·980	0·968	0·954	0·938	0·934	0·921	0·919	0·900	0·891
7·2	0·999	0·999	1·000	0·999	0·992	0·991	0·980	0·967	0·951	0·945	0·932	0·930	0·910	0·901
7·6	1·000	1·000		1·000	0·996	0·996	0·990	0·977	0·964	0·957	0·944	0·941	0·920	0·911
8·0					0·999	0·999	0·996	0·987	0·975	0·968	0·956	0·951	0·931	0·921
8·5					1·000	1·000	0·999	0·995	0·985	0·979	0·969	0·962	0·943	0·933
9·0							1·000	0·999	0·992	0·987	0·979	0·973	0·956	0·942
9·5								1·000	0·996	0·992	0·987	0·981	0·967	0·964
10·0									0·998	0·996	0·992	0·989	0·977	0·972
10·5									0·999	0·998	0·995	0·993	0·986	0·977
11·0									1·000	0·999	0·997	0·996	0·993	0·982
11·5										1·000	0·999	0·999	0·996	0·987
12·0											1·000	1·000	0·999	0·991
12·5													1·000	0·995
13·0														0·997
13·5														0·999
14·0														1·000

TABLE 1 (Cont.)

30

							GRADIENT A—0·001							
X(mms)	0	12·7	25·4	38·1	50·8	63·5	76·2	88·9	101·6	114·3	127·0	139·7	152·4	165·1
M_1	2·54	2·53	2·56	2·59	2·61	2·67	2·71	2·75	2·76	2·81	2·84	2·88	2·82	2·73
R_θ	27500	28000	27200	27300	29500	28900	29100	29900	31700	31300	32100	32100	36300	41000
T_w/T_1	2·198	2·176	2·204	2·243	2·264	2·345	2·376	2·417	2·418	2·479	2·503	2·578	2·479	2·379
Y(mms)	T/T_1	T/T_1	T/T_1	T/T_1	T/T_1	T/T_1	T/T_1	T/T_1	T/T_1	T/T_1	T/T_1	T/T_1	T/T_1	T/T_1
0·1	2·028	2·020	2·024	2·011	2·076	2·134	2·155	2·211	2·199	2·245	2·247	2·268	2·158	1·906
0·2	1·970	1·968	1·970	1·947	2·010	2·066	2·079	2·121	2·113	2·170	2·166	2·202	2·108	1·884
0·3	1·927	1·920	1·915	1·895	1·953	2·004	2·023	2·056	2·041	2·094	2·106	2·144	2·066	1·862
0·4	1·890	1·875	1·867	1·848	1·925	1·949	1·971	2·001	1·985	2·040	2·053	2·094	2·028	1·842
0·5	1·858	1·836	1·828	1·801	1·889	1·904	1·922	1·954	1·937	1·992	2·006	2·049	1·993	1·824
0·6	1·824	1·802	1·792	1·762	1·823	1·863	1·877	1·915	1·898	1·942	1·959	2·009	1·958	1·805
0·8	1·763	1·746	1·731	1·703	1·744	1·790	1·808	1·839	1·826	1·865	1·882	1·937	1·901	1·768
1·0	1·716	1·700	1·683	1·662	1·693	1·732	1·749	1·777	1·772	1·803	1·830	1·879	1·849	1·735
1·2	1·675	1·664	1·647	1·628	1·651	1·689	1·707	1·735	1·732	1·752	1·784	1·827	1·808	1·710
1·4	1·645	1·632	1·617	1·598	1·622	1·651	1·672	1·700	1·697	1·719	1·749	1·789	1·771	1·688
1·6	1·611	1·601	1·586	1·574	1·598	1·626	1·644	1·670	1·670	1·681	1·711	1·749	1·740	1·668
1·8	1·577	1·569	1·556	1·551	1·575	1·600	1·616	1·642	1·647	1·654	1·681	1·720	1·707	1·646
2·0	1·546	1·539	1·528	1·524	1·551	1·577	1·591	1·619	1·624	1·630	1·654	1·692	1·689	1·625
2·2	1·516	1·510	1·498	1·498	1·528	1·555	1·570	1·594	1·602	1·605	1·633	1·671	1·664	1·609
2·4	1·487	1·478	1·469	1·474	1·506	1·530	1·547	1·575	1·578	1·584	1·610	1·651	1·643	1·591
2·6	1·458	1·448	1·444	1·450	1·481	1·508	1·523	1·553	1·556	1·560	1·586	1·632	1·624	1·573
2·8	1·429	1·423	1·418	1·429	1·458	1·488	1·503	1·529	1·537	1·544	1·567	1·610	1·603	1·555
3·0	1·404	1·396	1·390	1·403	1·434	1·466	1·478	1·511	1·515	1·526	1·545	1·583	1·581	1·538
3·3	1·363	1·352	1·353	1·366	1·382	1·432	1·444	1·477	1·488	1·492	1·515	1·551	1·548	1·515
3·6	1·314	1·310	1·309	1·330	1·441	1·397	1·416	1·445	1·459	1·460	1·493	1·521	1·520	1·494
3·9	1·271	1·270	1·266	1·295	1·335	1·361	1·387	1·419	1·433	1·437	1·468	1·494	1·496	1·476
4·2	1·230	1·229	1·232	1·261	1·302	1·329	1·353	1·388	1·403	1·408	1·440	1·469	1·471	1·454
4·5	1·189	1·193	1·199	1·228	1·266	1·299	1·318	1·355	1·377	1·382	1·412	1·444	1·441	1·430
4·8	1·149	1·153	1·165	1·195	1·236	1·264	1·285	1·330	1·350	1·358	1·384	1·418	1·414	1·407
5·2	1·096	1·106	1·116	1·145	1·188	1·224	1·248	1·291	1·312	1·327	1·350	1·384	1·386	1·382
5·6	1·056	1·061	1·071	1·106	1·146	1·186	1·209	1·255	1·281	1·297	1·319	1·351	1·351	1·353
6·0	1·025	1·035	1·037	1·067	1·108	1·147	1·173	1·217	1·245	1·260	1·291	1·318	1·322	1·325
6·4	1·012	1·016	1·011	1·038	1·069	1·112	1·143	1·182	1·213	1·229	1·260	1·288	1·293	1·301
6·8	1·008	1·003	1·002	1·019	1·039	1·078	1·108	1·146	1·181	1·199	1·232	1·256	1·266	1·278
7·2	1·002	1·001	1·000	1·010	1·019	1·050	1·078	1·115	1·150	1·171	1·203	1·229	1·242	1·256
7·6	1·001	1·000		1·003	1·007	1·031	1·048	1·089	1·119	1·140	1·177	1·202	1·213	1·232
8·0	1·000			1·002	1·002	1·017	1·028	1·061	1·087	1·112	1·146	1·175	1·189	1·210
8·5				1·000	1·000	1·008	1·012	1·032	1·057	1·079	1·112	1·143	1·157	1·182
9·0						1·004	1·005	1·016	1·038	1·054	1·080	1·114	1·124	1·160
9·5						1·003	1·002	1·006	1·019	1·034	1·055	1·086	1·099	1·136
10·0						1·002	1·000	1·002	1·008	1·020	1·037	1·062	1·074	1·112
10·5						1·001		1·000	1·003	1·010	1·023	1·042	1·051	1·087
11·0						1·000			1·001	1·003	1·012	1·027	1·033	1·062
11·5									1·000	1·001	1·009	1·017	1·018	1·050
12·0										1·000	1·002	1·009	1·011	1·034
12·5											1·001	1·005	1·006	1·025
13·0											1·000	1·003	1·003	1·018
13·5												1·002	1·002	1·012
14·0												1·000	1·000	1·008
15·0														1·002
16·0														

TABLE 1 (Cont.)

31

X(mms)	0	12·7	25·4	38·1	50·8	63·5	76·2	88·9	101·6	114·3	127·0	139·7
						GRADIENT A—0·002						
M_1	2·53	2·54	2·55	2·58	2·61	2·67	2·70	2·72	2·77	2·81	2·83	2·87
θ(mms)	0·655	0·689	0·738	0·779	0·808	0·812	0·870	0·934	0·939	0·967	0·976	1·071
δ (mms)	3·050	3·194	3·407	3·523	3·720	3·853	4·041	4·402	4·535	4·704	4·910	5·387
Y(mms)	U/U_1	U/U_1	U/U_1	U/U_1	U/U_1	U/U_1	U/U_1	U/U_1	U/U_1	U/U_1	U/U_1	U/U_1
0·1	0·304	0·320	0·314	0·346	0·330	0·350	0·353	0·316	0·344	0·336	0·346	0·315
0·2	0·332	0·358	0·366	0·396	0·378	0·403	0·402	0·362	0·394	0·384	0·392	0·360
0·3	0·367	0·390	0·405	0·430	0·417	0·444	0·445	0·417	0·428	0·453	0·428	0·404
0·4	0·399	0·417	0·442	0·458	0·442	0·474	0·473	0·456	0·461	0·480	0·459	0·437
0·5	0·427	0·443	0·473	0·478	0·472	0·503	0·497	0·484	0·491	0·504	0·485	0·456
0·6	0·451	0·466	0·485	0·496	0·497	0·526	0·516	0·506	0·506	0·525	0·504	0·474
0·8	0·490	0·498	0·516	0·527	0·529	0·561	0·554	0·536	0·545	0·558	0·539	0·507
1·0	0·522	0·527	0·541	0·549	0·558	0·581	0·580	0·562	0·576	0·584	0·569	0·538
1·2	0·546	0·549	0·561	0·570	0·582	0·600	0·600	0·587	0·598	0·604	0·592	0·564
1·4	0·569	0·570	0·581	0·593	0·602	0·617	0·619	0·605	0·616	0·618	0·611	0·585
1·6	0·590	0·592	0·596	0·610	0·617	0·631	0·634	0·620	0·632	0·637	0·627	0·606
1·8	0·617	0·612	0·614	0·625	0·633	0·647	0·650	0·636	0·646	0·646	0·643	0·624
2·0	0·638	0·630	0·633	0·643	0·647	0·660	0·662	0·650	0·661	0·658	0·655	0·637
2·2	0·659	0·650	0·653	0·658	0·659	0·674	0·674	0·662	0·675	0·671	0·668	0·652
2·4	0·679	0·671	0·670	0·670	0·672	0·688	0·686	0·673	0·688	0·684	0·681	0·665
2·6	0·698	0·689	0·688	0·682	0·686	0·700	0·699	0·686	0·700	0·697	0·694	0·677
2·8	0·717	0·707	0·705	0·695	0·700	0·712	0·709	0·696	0·710	0·707	0·706	0·688
3·0	0·738	0·726	0·720	0·709	0·716	0·725	0·720	0·707	0·718	0·717	0·714	0·698
3·3	0·766	0·753	0·744	0·735	0·734	0·743	0·738	0·722	0·734	0·733	0·728	0·712
3·6	0·794	0·777	0·763	0·756	0·754	0·761	0·747	0·738	0·748	0·746	0·742	0·727
3·9	0·819	0·804	0·786	0·777	0·771	0·776	0·761	0·754	0·761	0·759	0·756	0·737
4·2	0·846	0·829	0·809	0·796	0·788	0·792	0·782	0·768	0·788	0·771	0·771	0·750
4·5	0·871	0·852	0·831	0·819	0·806	0·809	0·797	0·781	0·788	0·784	0·782	0·761
4·8	0·892	0·873	0·854	0·839	0·827	0·826	0·812	0·796	0·800	0·797	0·794	0·770
5·2	0·922	0·904	0·881	0·863	0·849	0·848	0·834	0·816	0·816	0·814	0·809	0·783
5·6	0·947	0·929	0·904	0·888	0·874	0·868	0·851	0·835	0·831	0·829	0·823	0·797
6·0	0·968	0·952	0·928	0·914	0·893	0·887	0·871	0·851	0·849	0·845	0·837	0·813
6·4	0·985	0·972	0·950	0·935	0·914	0·906	0·890	0·867	0·865	0·861	0·850	0·827
6·8	0·994	0·988	0·968	0·952	0·934	0·925	0·906	0·883	0·881	0·874	0·864	0·841
7·2	0·999	0·997	0·981	0·969	0·953	0·942	0·922	0·899	0·894	0·887	0·879	0·855
7·6	1·000	0·999	0·990	0·982	0·969	0·957	0·938	0·915	0·909	0·901	0·891	0·869
8·0		1·000	0·995	0·991	0·982	0·970	0·952	0·931	0·923	0·914	0·904	0·882
8·5			0·999	0·996	0·992	0·983	0·968	0·948	0·938	0·931	0·920	0·897
9·0			1·000	0·998	0·996	0·991	0·982	0·964	0·954	0·945	0·935	0·912
9·5				1·000	0·999	0·997	0·990	0·977	0·968	0·959	0·949	0·927
10·0					1·000	0·999	0·996	0·985	0·979	0·970	0·961	0·940
10·5						1·000	0·998	0·991	0·988	0·979	0·974	0·954
11·0							0·999	0·996	0·993	0·987	0·984	0·966
11·5							1·000	0·998	0·997	0·992	0·992	0·977
12·0								1·000	0·999	0·995	0·998	0·986
12·5									1·000	0·999	1·000	0·992
13·0										1·000		0·995
13·5												0·998
14·0												0·999
15·0												1·000

TABLE 1 (Cont.)

32

X(mms)	0	12·7	25·4	38·1	50·8	63·5	76·2	88·9	101·6	114·3	127·0	139·7
						GRADIENT A—0·002						
M_1	2·53	2·54	2·55	2·58	2·61	2·67	2·70	2·72	2·77	2·81	2·83	2·87
R_6	32500	34200	36800	37900	38800	38400	39100	41800	41300	41400	41200	44400
T_w/T_1	2·229	2·246	2·284	2·287	2·328	2·411	2·394	2·422	2·486	2·520	2·543	2·575
Y(mms)	T/T_1	T/T_1	T/T_1	T/T_1	T/T_1	T/T_1	T/T_1	T/T_1	T/T_1	T/T_1	T/T_1	T/T_1
0·1	2·107	2·108	2·140	2·132	2·178	2·248	2·224	2·283	2·319	2·357	2·376	2·429
0·2	2·059	2·056	2·076	2·073	2·115	2·178	2·156	2·224	2·253	2·293	2·315	2·374
0·3	2·015	2·013	2·019	2·024	2·054	2·113	2·098	2·155	2·201	2·200	2·259	2·313
0·4	1·976	1·976	1·972	1·977	2·013	2·066	2·053	2·101	2·152	2·152	2·208	2·259
0·5	1·940	1·939	1·932	1·940	1·967	2·014	2·013	2·056	2·103	2·108	2·161	2·222
0·6	1·910	1·908	1·913	1·909	1·931	1·974	1·974	2·016	2·066	2·066	2·124	2·187
0·8	1·864	1·862	1·866	1·862	1·880	1·905	1·905	1·950	1·991	1·993	2·049	2·115
1·0	1·823	1·823	1·827	1·826	1·832	1·863	1·857	1·899	1·927	1·934	1·983	2·041
1·2	1·794	1·791	1·802	1·791	1·796	1·826	1·822	1·854	1·883	1·892	1·932	1·987
1·4	1·762	1·766	1·772	1·754	1·763	1·796	1·788	1·821	1·849	1·864	1·894	1·947
1·6	1·735	1·738	1·751	1·729	1·742	1·772	1·759	1·795	1·822	1·838	1·863	1·911
1·8	1·699	1·710	1·723	1·704	1·717	1·745	1·731	1·769	1·795	1·809	1·832	1·878
2·0	1·667	1·683	1·696	1·677	1·693	1·722	1·712	1·744	1·766	1·788	1·810	1·851
2·2	1·637	1·654	1·668	1·655	1·675	1·696	1·692	1·723	1·737	1·763	1·784	1·823
2·4	1·608	1·623	1·643	1·637	1·655	1·672	1·668	1·700	1·713	1·734	1·757	1·796
2·6	1·579	1·597	1·614	1·614	1·633	1·650	1·646	1·676	1·690	1·711	1·733	1·772
2·8	1·549	1·569	1·589	1·593	1·610	1·630	1·627	1·659	1·668	1·693	1·711	1·751
3·0	1·520	1·540	1·565	1·571	1·580	1·608	1·608	1·639	1·652	1·672	1·692	1·731
3·3	1·473	1·500	1·526	1·532	1·549	1·570	1·575	1·610	1·622	1·637	1·662	1·703
3·6	1·432	1·459	1·493	1·497	1·514	1·538	1·559	1·579	1·595	1·610	1·633	1·675
3·9	1·386	1·415	1·454	1·461	1·488	1·510	1·533	1·549	1·569	1·583	1·605	1·648
4·2	1·341	1·372	1·417	1·427	1·457	1·480	1·492	1·526	1·543	1·559	1·574	1·621
4·5	1·296	1·333	1·377	1·389	1·425	1·447	1·463	1·501	1·514	1·532	1·550	1·597
4·8	1·255	1·294	1·333	1·356	1·388	1·416	1·432	1·471	1·489	1·504	1·518	1·578
5·2	1·194	1·233	1·286	1·309	1·345	1·372	1·391	1·433	1·455	1·467	1·490	1·550
5·6	1·137	1·183	1·239	1·261	1·301	1·331	1·356	1·394	1·422	1·435	1·460	1·518
6·0	1·088	1·128	1·188	1·212	1·261	1·290	1·318	1·365	1·387	1·400	1·427	1·483
6·4	1·047	1·081	1·138	1·168	1·221	1·253	1·280	1·331	1·352	1·366	1·400	1·451
6·8	1·019	1·039	1·094	1·129	1·179	1·212	1·245	1·296	1·316	1·336	1·369	1·418
7·2	1·008	1·020	1·056	1·087	1·135	1·173	1·211	1·265	1·285	1·306	1·335	1·388
7·6	1·001	1·006	1·032	1·054	1·098	1·136	1·177	1·229	1·256	1·275	1·304	1·357
8·0	1·000	1·002	1·014	1·032	1·066	1·103	1·141	1·194	1·223	1·245	1·275	1·326
8·5		1·000	1·006	1·015	1·036	1·069	1·100	1·154	1·184	1·207	1·238	1·288
9·0			1·001	1·005	1·019	1·039	1·066	1·117	1·146	1·172	1·200	1·253
9·5			1·000	1·002	1·008	1·022	1·038	1·078	1·110	1·138	1·165	1·216
10·0				1·000	1·001	1·010	1·018	1·054	1·078	1·106	1·133	1·181
10·5					1·000	1·004	1·008	1·033	1·055	1·077	1·103	1·144
11·0						1·001	1·002	1·018	1·032	1·052	1·077	1·116
11·5						1·000	1·000	1·010	1·018	1·035	1·049	1·086
12·0								1·005	1·008	1·021	1·033	1·057
12·5								1·000	1·004	1·012	1·023	1·039
13·0									1·001	1·007	1·013	1·027
13·5									1·000	1·004	1·008	1·018
14·0										1·002	1·006	1·014
15·0										1·000	1·002	1·008
16·0											1·001	1·004
17·0											1·000	1·002
18·0												1·001
19·0												

TABLE 1 (Cont.)

							GRADIENT B—0·000								
X(mms)	0	12·7	25·4	38·1	50·8	63·5	76·2	88·9	101·6	114·3	127·0	139·7	152·4	165·1	177·8
M_1	2·52	2·52	2·53	2·52	2·48	2·45	2·44	2·41	2·39	2·34	2·33	2·30	2·28	2·27	2·21
θ(mms)	0·496	0·474	0·450	0·456	0·455	0·469	0·496	0·513	0·517	0·566	0·538	0·593	0·604	0·615	0·680
δ^x(mms)	2·018	2·027	1·913	1·933	1·920	2·004	2·033	2·059	2·059	2·216	2·185	2·218	2·228	2·258	2·500
Y(mms)	U/U_1	U/U_1	U/U_1	U/U_1	U/U_1	U/U_1	U/U_1	U/U_1	U/U_1	U/U_1	U/U_1	U/U_1	U/U_1	U/U_1	U/U_1
0·1	0·498	0·532	0·531	0·539	0·528	0·527	0·513	0·518	0·558	0·501	0·533	0·506	0·518	0·545	0·479
0·2	0·558	0·578	0·589	0·606	0·578	0·582	0·572	0·577	0·599	0·568	0·583	0·563	0·572	0·583	0·537
0·3	0·605	0·622	0·626	0·640	0·610	0·613	0·607	0·603	0·625	0·607	0·614	0·601	0·606	0·614	0·578
0·4	0·636	0·648	0·657	0·663	0·635	0·638	0·629	0·625	0·645	0·627	0·634	0·620	0·624	0·632	0·603
0·5	0·660	0·668	0·678	0·681	0·654	0·660	0·647	0·644	0·660	0·645	0·651	0·636	0·643	0·647	0·621
0·6	0·674	0·684	0·693	0·698	0·672	0·675	0·664	0·655	0·676	0·658	0·668	0·650	0·656	0·660	0·635
0·8	0·702	0·711	0·720	0·720	0·698	0·700	0·689	0·684	0·698	0·680	0·690	0·673	0·677	0·680	0·657
1·0	0·722	0·731	0·738	0·738	0·719	0·721	0·711	0·706	0·712	0·698	0·707	0·691	0·693	0·696	0·679
1·2	0·741	0·749	0·757	0·756	0·737	0·738	0·730	0·724	0·727	0·712	0·722	0·707	0·709	0·712	0·692
1·4	0·758	0·763	0·774	0·771	0·754	0·755	0·749	0·744	0·743	0·725	0·738	0·723	0·724	0·726	0·704
1·6	0·775	0·777	0·787	0·786	0·771	0·773	0·763	0·758	0·757	0·741	0·752	0·738	0·739	0·739	0·718
1·8	0·789	0·791	0·803	0·801	0·786	0·785	0·779	0·774	0·772	0·755	0·766	0·752	0·753	0·752	0·729
2·0	0·802	0·805	0·817	0·814	0·803	0·801	0·793	0·788	0·787	0·768	0·780	0·765	0·766	0·764	0·742
2·2	0·816	0·819	0·830	0·827	0·819	0·815	0·805	0·804	0·801	0·780	0·793	0·778	0·779	0·777	0·753
2·4	0·829	0·831	0·844	0·840	0·833	·0·828	0·820	0·817	0·814	0·794	0·805	0·791	0·791	0·788	0·765
2·6	0·843	0·846	0·856	0·855	0·848	0·845	0·833	0·832	0·828	0·808	0·817	0·803	0·802	0·801	0·778
2·8	0·856	0·858	0·868	0·868	0·862	0·856	0·846	0·844	0·842	0·820	0·831	0·814	0·814	0·812	0·791
3·0	0·867	0·870	0·882	0·879	0·875	0·870	0·860	0·858	0·864	0·833	0·844	0·829	0·825	0·824	0·802
3·3	0·883	0·888	0·899	0·896	0·888	0·881	0·881	0·878	0·873	0·852	0·862	0·848	0·844	0·843	0·818
3·6	0·901	0·906	0·915	0·913	0·914	0·905	0·899	0·895	0·892	0·871	0·881	0·865	0·863	0·861	0·837
3·9	0·917	0·922	0·930	0·930	0·931	0·924	0·917	0·912	0·909	0·888	0·898	0·885	0·881	0·877	0·854
4·2	0·931	0·936	0·945	0·944	0·949	0·940	0·932	0·929	0·925	0·907	0·915	0·901	0·899	0·893	0·872
4·5	0·942	0·951	0·957	0·956	0·964	0·955	0·948	0·943	0·941	0·924	0·928	0·917	0·915	0·910	0·889
4·8	0·955	0·961	0·969	0·967	0·979	0·968	0·961	0·955	0·955	0·940	0·946	0·933	0·930	0·924	0·904
5·2	0·968	0·975	0·981	0·980	0·991	0·982	0·976	0·970	0·971	0·956	0·964	0·952	0·947	0·942	0·924
5·6	0·982	0·986	0·991	0·990	0·994	0·991	0·988	0·984	0·983	0·974	0·981	0·967	0·964	0·960	0·943
6·0	0·991	0·992	0·997	0·995	0·997	0·998	0·995	0·994	0·992	0·986	0·992	0·982	0·976	0·975	0·958
6·4	0·997	0·998	1·000	0·998	0·998	1·000	0·999	0·997	0·998	0·995	0·997	0·992	0·987	0·987	0·971
6·8	1·000	1·000		1·000	1·000		1·000	0·999	0·998	0·999	0·999	0·997	0·995	0·995	0·984
7·2								1·000	0·999	1·000	1·000	1·000	0·999	0·998	0·992
7·6									1·000				1·000	0·999	0·995
8·0														1·000	0·997
8·5															0·999
9·0															1·000
9·5															

TABLE 1 (Cont.)

	GRADIENT B—0·000														
X(mms)	0	12·7	25·4	38·1	50·8	63·5	76·2	88·9	101·6	114·3	127·0	139·7	152·4	165·1	177·8
M_1	2·52	2·52	2·53	2·52	2·48	2·45	2·44	2·41	2·39	2·34	2·33	2·30	2·28	2·27	2·21
R_θ	14200	14200	13100	13300	13600	14400	15100	16000	16500	18400	17900	19500	20000	20700	24000
T_w/T_1	2·168	2·231	2·214	2·203	2·166	2·163	2·129	2·112	2·100	2·058	2·081	2·005	1·991	1·992	1·957
Y(mms)	T/T_1	T/T_1	T/T_1	T/T_1	T/T_1	T/T_1	T/T_1	T/T_1	T/T_1	T/T_1	T/T_1	T/T_1	T/T_1	T/T_1	T/T_1
0·1	1·915	1·939	1·916	1·902	1·887	1·888	1·868	1·847	1·799	1·826	1·813	1·767	1·747	1·722	1·760
0·2	1·835	1·868	1·829	1·798	1·813	1·815	1·785	1·769	1·739	1·744	1·747	1·699	1·684	1·675	1·702
0·3	1·760	1·795	1·766	1·738	1·763	1·763	1·727	1·726	1·696	1·691	1·700	1·651	1·639	1·632	1·655
0·4	1·710	1·746	1·716	1·695	1·716	1·688	1·695	1·688	1·660	1·657	1·669	1·621	1·612	1·606	1·622
0·5	1·670	1·705	1·675	1·659	1·679	1·681	1·667	1·654	1·632	1·627	1·637	1·597	1·582	1·582	1·597
0·6	1·641	1·671	1·643	1·626	1·646	1·652	1·638	1·633	1·603	1·604	1·608	1·574	1·561	1·560	1·575
0·8	1·589	1·611	1·588	1·581	1·599	1·604	1·590	1·583	1·562	1·563	1·571	1·535	1·524	1·523	1·543
1·0	1·547	1·567	1·545	1·543	1·557	1·563	1·551	1·543	1·533	1·532	1·541	1·507	1·498	1·496	1·511
1·2	1·517	1·533	1·513	1·513	1·524	1·532	1·519	1·515	1·504	1·509	1·513	1·482	1·473	1·472	1·492
1·4	1·488	1·506	1·483	1·485	1·495	1·503	1·485	1·484	1·497	1·487	1·488	1·461	1·453	1·449	1·473
1·6	1·460	1·480	1·457	1·459	1·469	1·475	1·464	1·460	1·454	1·464	1·464	1·441	1·433	1·433	1·452
1·8	1·437	1·454	1·430	1·433	1·441	1·451	1·437	1·437	1·432	1·441	1·443	1·419	1·412	1·412	1·438
2·0	1·410	1·430	1·405	1·411	1·412	1·426	1·412	1·414	1·409	1·423	1·423	1·400	1·394	1·396	1·422
2·2	1·386	1·404	1·380	1·387	1·384	1·401	1·393	1·390	1·387	1·402	1·403	1·382	1·376	1·379	1·404
2·4	1·363	1·383	1·357	1·364	1·361	1·375	1·367	1·369	1·367	1·380	1·382	1·364	1·359	1·360	1·389
2·6	1·340	1·356	1·333	1·337	1·335	1·347	1·346	1·340	1·344	1·359	1·364	1·347	1·340	1·341	1·373
2·8	1·317	1·334	1·310	1·313	1·310	1·327	1·324	1·330	1·321	1·341	1·342	1·330	1·322	1·325	1·353
3·0	1·297	1·311	1·284	1·290	1·286	1·303	1·300	1·297	1·286	1·320	1·322	1·308	1·306	1·307	1·338
3·3	1·266	1·274	1·250	1·260	1·246	1·269	1·267	1·261	1·270	1·291	1·293	1·280	1·278	1·279	1·315
3·6	1·232	1·240	1·219	1·224	1·212	1·238	1·233	1·233	1·238	1·264	1·258	1·253	1·251	1·253	1·2$8
3·9	1·197	1·208	1·188	1·188	1·179	1·202	1·201	1·202	1·208	1·236	1·231	1·224	1·225	1·228	1·261
4·2	1·166	1·174	1·154	1·160	1·144	1·168	1·169	1·171	1·178	1·206	1·201	1·199	1·197	1·204	1·236
4·5	1·140	1·141	1·126	1·129	1·110	1·136	1·139	1·141	1·147	1·180	1·177	1·173	1·173	1·177	1·212
4·8	1·110	1·111	1·091	1·098	1·076	1·107	1·110	1·116	1·120	1·149	1·144	1·146	1·149	1·154	1·187
5·2	1·072	1·073	1·057	1·061	1·045	1·071	1·075	1·076	1·085	1·113	1·113	1·111	1·117	1·125	1·155
5·6	1·042	1·044	1·026	1·033	1·024	1·041	1·043	1·052	1·053	1·077	1·075	1·082	1·084	1·095	1·125
6·0	1·016	1·024	1·011	1·014	1·013	1·020	1·022	1·027	1·032	1·048	1·049	1·051	1·058	1·065	1·098
6·4	1·004	1·007	1·003	1·006	1·004	1·008	1·008	1·012	1·014	1·025	1·032	1·028	1·038	1·041	1·071
6·8	1·000	1·001	1·000	1·003	1·001	1·001	1·004	1·005	1·006	1·010	1·018	1·017	1·015	1·023	1·043
7·2		1·000		1·000	1·000	1·000	1·003	1·001	1·001	1·003	1·010	1·007	1·007	1·014	1·025
7·6							1·000	1·000	1·000	1·002	1·006	1·002	1·003	1·007	1·016
8·0										1·000	1·002	1·000	1·002	1·003	1·008
8·5											1·000		1·000	1·000	1·003
9·0															1·001
9·5															1·000

TABLE 1 (Cont.)

GRADIENT B—0.001

X(mms)	0	12·7	25·4	38·1	50·8	63·5	76·2	88·9	101·6	114·3	127·0	139·7	152·4	165·1	177·8
M_1	2·51	2·50	2·55	2·48	2·46	2·44	2·41	2·39	2·38	2·35	2·32	2·27	2·28	2·27	2·19
θ(mms)	0·674	0·665	0·614	0·671	0·671	0·724	0·752	0·773	0·815	0·822	0·842	0·913	0·904	0·926	0·991
δ^x (mms)	2·877	2·905	2·689	2·941	2·975	2·997	3·152	3·164	3·310	3·321	3·397	3·523	3·502	3·596	3·767
Y(mms)	U/U_1	U/U_1	U/U_1	U/U_1	U/U_1	U/U_1	U/U_1	U/U_1	U/U_1	U/U_1	U/U_1	U/U_1	U/U_1	U/U_1	U/U_1
0·1	0·411	0·374	0·464	0·408	0·411	0·416	0·403	0·406	0·397	0·405	0·413	0·385	0·394	0·403	0·357
0·2	0·444	0·403	0·485	0·434	0·445	0·448	0·433	0·435	0·437	0·442	0·444	0·419	0·438	0·450	0·390
0·3	0·477	0·443	0·509	0·462	0·470	0·479	0·464	0·466	0·469	0·476	0·472	0·445	0·468	0·478	0·419
0·4	0·502	0·473	0·530	0·492	0·494	0·501	0·487	0·484	0·485	0·495	0·494	0·466	0·490	0·507	0·443
0·5	0·523	0·500	0·549	0·516	0·516	0·519	0·504	0·501	0·504	0·514	0·510	0·482	0·506	0·525	0·462
0·6	0·540	0·519	0·566	0·534	0·532	0·534	0·517	0·516	0·517	0·533	0·521	0·495	0·518	0·536	0·478
0·8	0·562	0·556	0·593	0·561	0·557	0·557	0·542	0·540	0·541	0·560	0·543	0·514	0·542	0·556	0·505
1·0	0·594	0·584	0·617	0·585	0·578	0·578	0·561	0·560	0·562	0·573	0·562	0·531	0·556	0·573	0·527
1·2	0·616	0·607	0·640	0·605	0·598	0·535	0·581	0·578	0·578	0·590	0·577	0·550	0·571	0·587	0·544
1·4	0·635	0·628	0·660	0·624	0·613	0·613	0·599	0·594	0·593	0·602	0·592	0·563	0·587	0·598	0·559
1·6	0·655	0·645	0·676	0·645	0·632	0·629	0·613	0·612	0·611	0·616	0·609	0·579	0·600	0·612	0·571
1·8	0·673	0·661	0·694	0·662	0·651	0·647	0·630	0·625	0·624	0·631	0·625	0·593	0·612	0·627	0·584
2·0	0·691	0·682	0·712	0·677	0·670	0·665	0·645	0·641	0·636	0·644	0·639	0·610	0·625	0·640	0·601
2·2	0·708	0·698	0·729	0·697	0·686	0·680	0·660	0·658	0·653	0·654	0·654	0·624	0·641	0·652	0·612
2·4	0·724	0·718	0·744	0·714	0·705	0·696	0·678	0·674	0·669	0·670	0·668	0·638	0·653	0·664	0·624
2·6	0·742	0·735	0·762	0·732	0·721	0·715	0·697	0·691	0·685	0·686	0·680	0·652	0·667	0·676	0·639
2·8	0·759	0·751	0·778	0·748	0·740	0·731	0·713	0·705	0·700	0·700	0·693	0·663	0·680	0·688	0·651
3·0	0·775	0·769	0·793	0·766	0·758	0·748	0·727	0·723	0·717	0·712	0·706	0·678	0·694	0·701	0·664
3·3	0·795	0·795	0·814	0·787	0·778	0·771	0·750	0·745	0·736	0·733	0·726	0·698	0·716	0·720	0·685
3·6	0·818	0·817	0·837	0·809	0·804	0·794	0·773	0·766	0·761	0·754	0·751	0·719	0·733	0·741	0·701
3·9	0·837	0·839	0·857	0·831	0·826	0·814	0·797	0·789	0·783	0·777	0·770	0·744	0·758	0·757	0·719
4·2	0·858	0·858	0·877	0·854	0·848	0·833	0·817	0·812	0·804	0·796	0·791	0·764	0·778	0·777	0·742
4·5	0·876	0·878	0·897	0·874	0·870	0·855	0·838	0·833	0·823	0·816	0·811	0·785	0·798	0·794	0·760
4·8	0·897	0·898	0·917	0·894	0·889	0·867	0·859	0·856	0·845	0·835	0·830	0·805	0·817	0·813	0·780
5·2	0·918	0·920	0·940	0·919	0·914	0·904	0·887	0·884	0·871	0·863	0·857	0·832	0·844	0·837	0·804
5·6	0·940	0·941	0·958	0·941	0·939	0·927	0·913	0·912	0·896	0·890	0·883	0·860	0·863	0·860	0·832
6·0	0·958	0·961	0·974	0·961	0·960	0·949	0·938	0·934	0·918	0·914	0·908	0·886	0·890	0·881	0·857
6·4	0·970	0·977	0·987	0·978	0·977	0·967	0·959	0·955	0·939	0·936	0·929	0·910	0·912	0·902	0·880
6·8	0·983	0·988	0·995	0·988	0·992	0·981	0·976	0·972	0·957	0·954	0·947	0·934	0·934	0·921	0·900
7·2	0·992	0·994	0·998	0·993	0·998	0·991	0·990	0·985	0·973	0·971	0·964	0·954	0·951	0·939	0·926
7·6	0·997	0·997	1·000	0·995	1·000	0·996	0·996	0·994	0·982	0·982	0·978	0·971	0·967	0·956	0·949
8·0	0·999	0·999		0·997		0·999	0·998	0·997	0·989	0·992	0·988	0·985	0·979	0·971	0·967
8·5	1·000	1·000		0·999		1·000	0·999	0·998	0·994	0·998	0·995	0·994	0·990	0·984	0·983
9·0				1·000			1·000	0·999	0·998	1·000	0·999	0·998	0·995	0·991	0·995
9·5								1·000	1·000		1·000	1·000	0·997	0·996	0·998
10·0													0·998	0·998	1·000
10·5													1·000	1·000	
11·0															

35

TABLE 1 (Cont.)

							GRADIENT B—0·001								
X(mms)	0	12·7	25·4	38·1	50·8	63·5	76·2	88·9	101·6	114·3	127·0	139·7	152·4	165·1	177·8
M_1	2·51	2·50	2·55	2·48	2·46	2·44	2·41	2·39	2·38	2·35	2·32	2·27	2·28	2·27	2·19
R_θ	19900	20000	18200	20800	21200	22300	23900	24600	26200	27100	28400	30900	30700	31800	35500
T_w/T_1	2·153	2·164	2·216	2·165	2·165	2·099	2·079	2·051	2·046	2·037	2·020	1·941	1·974	1·974	1·910
Y(mms)	T/T_1	T/T_1	T/T_1	T/T_1	T/T_1	T/T_1	T/T_1	T/T_1	T/T_1	T/T_1	T/T_1	T/T_1	T/T_1	T/T_1	T/T_1
0·1	1·970	2·008	1·968	1·983	1·977	1·914	1·910	1·878	1·883	1·869	1·852	1·800	1·820	1·814	1·789
0·2	1·930	1·974	1·937	1·954	1·940	1·878	1·875	1·848	1·846	1·834	1·820	1·767	1·783	1·772	1·763
0·3	1·890	1·925	1·899	1·919	1·907	1·838	1·842	1·811	1·810	1·798	1·790	1·742	1·752	1·742	1·737
0·4	1·859	1·893	1·866	1·879	1·876	1·813	1·812	1·789	1·789	1·771	1·765	1·720	1·729	1·708	1·713
0·5	1·830	1·858	1·836	1·847	1·848	1·790	1·791	1·768	1·766	1·748	1·744	1·702	1·712	1·684	1·695
0·6	1·807	1·829	1·808	1·820	1·826	1·770	1·772	1·748	1·749	1·726	1·726	1·688	1·697	1·667	1·678
0·8	1·768	1·779	1·762	1·778	1·783	1·737	1·735	1·714	1·710	1·688	1·698	1·664	1·667	1·641	1·646
1·0	1·721	1·735	1·722	1·740	1·751	1·703	1·708	1·688	1·682	1·664	1·672	1·642	1·647	1·619	1·625
1·2	1·691	1·703	1·684	1·709	1·718	1·676	1·681	1·663	1·660	1·640	1·649	1·622	1·625	1·605	1·603
1·4	1·663	1·672	1·653	1·683	1·696	1·653	1·658	1·643	1·640	1·625	1·628	1·609	1·604	1·591	1·585
1·6	1·633	1·649	1·630	1·651	1·668	1·629	1·638	1·621	1·617	1·606	1·608	1·590	1·588	1·574	1·572
1·8	1·603	1·624	1·598	1·627	1·642	1·605	1·615	1·605	1·600	1·588	1·590	1·572	1·574	1·557	1·558
2·0	1·576	1·592	1·571	1·606	1·615	1·580	1·594	1·581	1·585	1·574	1·573	1·553	1·557	1·543	1·542
2·2	1·550	1·569	1·544	1·577	1·594	1·561	1·574	1·561	1·563	1·556	1·552	1·538	1·539	1·528	1·531
2·4	1·525	1·539	1·519	1·551	1·565	1·537	1·551	1·539	1·544	1·536	1·534	1·521	1·525	1·515	1·519
2·6	1·499	1·511	1·489	1·525	1·538	1·511	1·525	1·517	1·522	1·516	1·519	1·503	1·508	1·501	1·504
2·8	1·473	1·486	1·461	1·499	1·509	1·488	1·505	1·498	1·480	1·498	1·503	1·490	1·490	1·486	1·489
3·0	1·447	1·457	1·436	1·471	1·480	1·462	1·486	1·473	1·479	1·483	1·487	1·472	1·472	1·471	1·473
3·3	1·412	1·418	1·400	1·436	1·448	1·425	1·452	1·441	1·453	1·454	1·460	1·448	1·445	1·446	1·450
3·6	1·378	1·379	1·360	1·399	1·411	1·394	1·418	1·414	1·417	1·425	1·427	1·424	1·422	1·420	1·431
3·9	1·344	1·345	1·322	1·366	1·374	1·359	1·384	1·379	1·387	1·396	1·400	1·395	1·389	1·398	1·410
4·2	1·309	1·310	1·283	1·325	1·335	1·326	1·352	1·346	1·359	1·367	1·370	1·368	1·365	1·371	1·383
4·5	1·275	1·273	1·247	1·289	1·297	1·288	1·321	1·312	1·329	1·336	1·340	1·342	1·335	1·348	1·361
4·8	1·235	1·234	1·209	1·252	1·261	1·254	1·286	1·278	1·297	1·310	1·315	1·317	1·300	1·324	1·336
5·2	1·197	1·192	1·163	1·201	1·215	1·214	1·241	1·234	1·255	1·267	1·273	1·281	1·274	1·293	1·307
5·6	1·149	1·150	1·119	1·156	1·164	1·170	1·195	1·190	1·217	1·227	1·235	1·243	1·245	1·259	1·272
6·0	1·109	1·106	1·078	1·111	1·118	1·128	1·151	1·151	1·179	1·187	1·196	1·206	1·206	1·230	1·240
6·4	1·077	1·067	1·042	1·072	1·076	1·086	1·111	1·113	1·141	1·150	1·160	1·170	1·171	1·198	1·207
6·8	1·045	1·038	1·021	1·042	1·042	1·058	1·074	1·076	1·106	1·113	1·125	1·133	1·138	1·166	1·176
7·2	1·020	1·024	1·009	1·025	1·019	1·029	1·040	1·047	1·075	1·077	1·095	1·101	1·110	1·137	1·138
7·6	1·006	1·012	1·004	1·012	1·007	1·012	1·018	1·024	1·049	1·052	1·066	1·067	1·083	1·110	1·102
8·0	1·001	1·006	1·000	1·006	1·004	1·003	1·008	1·010	1·032	1·031	1·044	1·043	1·056	1·083	1·074
8·5	1·000	1·002		1·002	1·002	1·000	1·002	1·002	1·018	1·015	1·024	1·018	1·033	1·057	1·045
9·0		1·000		1·000	1·000	1·000	1·000	1·000	1·009	1·006	1·010	1·006	1·018	1·037	1·026
9·5									1·004	1·002	1·003	1·001	1·008	1·024	1·012
10·0									1·001	1·000	1·000	1·000	1·004	1·014	1·005
10·5									1·000				1·002	1·005	1·002
11·0													1·000	1·002	1·000
11·5														1·000	

TABLE 1 (Cont.)

GRADIENT B—0·002

X(mms)	0	12·7	25·4	38·1	50·8	63·5	76·2	88·9	101·6	114·3	127·0	139·7	152·4	165·1	177·8
M_1	2·50	2·51	2·52	2·46	2·43	2·42	2·39	2·38	2·36	2·33	2·29	2·23	2·29	2·25	2·12
θ(mms)	0·816	0·798	0·845	0·868	0·923	0·953	0·982	1·031	1·095	1·113	1·184	1·253	1·207	1·270	1·435
δ (mms)	3·676	3·673	3·864	3·986	4·149	4·261	4·426	4·491	4·643	4·638	4·904	5·047	4·851	5·003	5·768
Y(mms)	U/U_1	U/U_1	U/U_1	U/U_1	U/U_1	U/U_1	U/U_1	U/U_1	U/U_1	U/U_1	U/U_1	U/U_1	U/U_1	U/U_1	U/U_1
0·1	0·344	0·335	0·382	0·350	0·348	0·339	0·320	0·348	0·325	0·356	0·322	0·282	0·381	0·377	0·243
0·2	0·362	0·353	0·394	0·372	0·364	0·360	0·347	0·365	0·359	0·374	0·353	0·315	0·400	0·388	0·269
0·3	0·381	0·371	0·404	0·383	0·380	0·374	0·363	0·386	0·382	0·394	0·371	0·338	0·418	0·403	0·286
0·4	0·401	0·388	0·416	0·404	0·394	0·386	0·378	0·398	0·401	0·407	0·384	0·350	0·434	0·412	0·294
0·5	0·418	0·410	0·428	0·420	0·408	0·399	0·391	0·411	0·414	0·416	0·396	0·361	0·443	0·421	0·303
0·6	0·432	0·425	0·440	0·431	0·420	0·414	0·404	0·422	0·425	0·426	0·406	0·371	0·451	0·432	0·315
0·8	0·459	0·455	0·462	0·449	0·438	0·439	0·425	0·438	0·446	0·446	0·427	0·393	0·469	0·448	0·336
1·0	0·484	0·483	0·482	0·469	0·456	0·460	0·441	0·453	0·462	0·460	0·437	0·410	0·480	0·461	0·351
1·2	0·507	0·506	0·501	0·488	0·473	0·477	0·461	0·464	0·478	0·477	0·454	0·425	0·490	0·475	0·368
1·4	0·527	0·527	0·519	0·506	0·491	0·493	0·474	0·484	0·491	0·494	0·468	0·438	0·501	0·487	0·384
1·6	0·548	0·546	0·539	0·522	0·507	0·508	0·491	0·502	0·503	0·507	0·481	0·454	0·511	0·497	0·398
1·8	0·568	0·563	0·556	0·539	0·526	0·524	0·509	0·514	0·516	0·518	0·495	0·466	0·520	0·507	0·412
2·0	0·587	0·579	0·573	0·555	0·541	0·538	0·524	0·525	0·528	0·531	0·508	0·480	0·531	0·521	0·422
2·2	0·606	0·594	0·588	0·573	0·558	0·554	0·537	0·540	0·542	0·544	0·519	0·492	0·541	0·529	0·434
2·4	0·623	0·612	0·603	0·591	0·573	0·567	0·551	0·556	0·557	0·556	0·531	0·507	0·552	0·538	0·444
2·6	0·642	0·634	0·621	0·608	0·588	0·581	0·569	0·568	0·572	0·568	0·542	0·519	0·560	0·547	0·456
2·8	0·659	0·652	0·638	0·626	0·605	0·598	0·584	0·583	0·584	0·580	0·554	0·529	0·573	0·556	0·470
3·0	0·675	0·671	0·654	0·641	0·621	0·613	0·598	0·596	0·595	0·591	0·565	0·543	0·586	0·569	0·479
3·3	0·699	0·695	0·679	0·664	0·645	0·637	0·618	0·616	0·612	0·609	0·584	0·560	0·600	0·588	0·499
3·6	0·722	0·720	0·703	0·692	0·668	0·656	0·641	0·640	0·633	0·627	0·603	0·582	0·613	0·605	0·519
3·9	0·746	0·747	0·726	0·715	0·693	0·681	0·664	0·662	0·652	0·644	0·621	0·603	0·633	0·621	0·534
4·2	0·771	0·771	0·750	0·741	0·717	0·704	0·687	0·683	0·675	0·663	0·643	0·622	0·651	0·638	0·553
4·5	0·793	0·795	0·775	0·766	0·740	0·729	0·708	0·705	0·696	0·683	0·663	0·642	0·672	0·657	0·571
4·8	0·816	0·818	0·798	0·789	0·763	0·751	0·732	0·727	0·719	0·706	0·684	0·663	0·688	0·676	0·593
5·2	0·848	0·846	0·828	0·819	0·794	0·783	0·764	0·757	0·746	0·728	0·710	0·690	0·715	0·699	0·620
5·6	0·877	0·876	0·856	0·849	0·825	0·814	0·794	0·783	0·773	0·757	0·736	0·715	0·741	0·723	0·647
6·0	0·902	0·909	0·885	0·877	0·855	0·842	0·823	0·812	0·800	0·791	0·764	0·742	0·764	0·748	0·675
6·4	0·926	0·935	0·912	0·904	0·884	0·871	0·849	0·838	0·827	0·819	0·790	0·770	0·788	0·773	0·700
6·8	0·948	0·957	0·936	0·928	0·912	0·895	0·878	0·864	0·852	0·846	0·816	0·795	0·813	0·799	0·726
7·2	0·969	0·974	0·955	0·948	0·934	0·919	0·906	0·893	0·876	0·872	0·842	0·823	0·839	0·824	0·755
7·6	0·984	0·987	0·973	0·967	0·955	0·944	0·930	0·916	0·897	0·897	0·867	0·848	0·863	0·846	0·784
8·0	0·991	0·994	0·986	0·982	0·972	0·965	0·952	0·939	0·920	0·921	0·891	0·872	0·884	0·869	0·812
8·5	0·995	1·000	0·994	0·992	0·987	0·983	0·976	0·964	0·945	0·947	0·920	0·903	0·914	0·898	0·844
9·0	0·999		0·999	0·997	0·994	0·993	0·992	0·981	0·966	0·966	0·946	0·928	0·939	0·925	0·875
9·5	1·000		1·000	0·999	0·997	0·997	0·999	0·993	0·980	0·979	0·967	0·951	0·959	0·948	0·906
10·0				1·000	1·000	0·999	1·000	0·998	0·988	0·989	0·982	0·973	0·978	0·969	0·931
10·5						1·000		0·999	0·992	0·995	0·992	0·989	0·991	0·982	0·951
11·0								1·000	0·996	0·997	0·996	0·997	0·998	0·991	0·969
11·5									0·997	0·998	0·999	1·000	1·000	0·996	0·979
12·0									0·999	0·999	1·000			0·998	0·987
12·5									1·000	1·000				1·000	0·992
13·0															0·996
13·5															0·999
14·0															1·000

TABLE 1 (Cont.)

GRADIENT B—0·002

X (mms)	0	12·7	25·4	38·1	50·8	63·5	76·2	88·9	101·6	114·3	127·0	139·7	152·4	165·1	177·8
M_1	2·50	2·51	2·52	2·46	2·43	2·42	2·39	2·38	2·36	2·33	2·29	2·23	2·29	2·25	2·12
R_6	24300	23800	25200	27300	29200	29800	31500	33400	35300	36200	39900	42600	40200	43100	52100
T_w/T_1	2·170	2·186	2·204	2·174	2·130	2·108	2·095	2·089	2·051	2·022	1·999	1·919	1·984	1·938	1·838
Y (mms)	T/T_1	T/T_1	T/T_1	T/T_1	T/T_1	T/T_1	T/T_1	T/T_1	T/T_1	T/T_1	T/T_1	T/T_1	T/T_1	T/T_1	T/T_1
0·1	2·027	2·049	2·027	2·042	1·993	1·979	1·979	1·953	1·936	1·889	1·887	1·841	1·844	1·804	1·780
0·2	2·003	2·021	2·005	2·023	1·971	1·954	1·952	1·931	1·903	1·869	1·860	1·814	1·821	1·786	1·763
0·3	1·974	1·996	1·983	2·014	1·949	1·934	1·930	1·906	1·878	1·845	1·841	1·792	1·797	1·767	1·747
0·4	1·951	1·971	1·962	1·992	1·930	1·916	1·914	1·886	1·854	1·827	1·823	1·776	1·777	1·752	1·735
0·5	1·927	1·945	1·944	1·984	1·912	1·898	1·896	1·868	1·839	1·813	1·809	1·764	1·766	1·738	1·727
0·6	1·906	1·924	1·923	1·953	1·895	1·878	1·878	1·851	1·824	1·801	1·796	1·752	1·754	1·725	1·717
0·8	1·868	1·882	1·887	1·879	1·868	1·844	1·849	1·823	1·794	1·772	1·771	1·728	1·727	1·703	1·695
1·0	1·837	1·848	1·860	1·849	1·838	1·819	1·826	1·801	1·773	1·750	1·751	1·709	1·711	1·685	1·681
1·2	1·807	1·818	1·835	1·823	1·815	1·799	1·803	1·787	1·753	1·731	1·730	1·695	1·694	1·671	1·668
1·4	1·783	1·792	1·812	1·804	1·793	1·777	1·787	1·767	1·736	1·713	1·718	1·682	1·683	1·662	1·657
1·6	1·755	1·770	1·787	1·782	1·771	1·759	1·769	1·745	1·725	1·699	1·703	1·670	1·672	1·649	1·648
1·8	1·730	1·749	1·764	1·764	1·750	1·743	1·746	1·729	1·713	1·689	1·687	1·658	1·662	1·641	1·637
2·0	1·706	1·725	1·744	1·744	1·731	1·728	1·730	1·717	1·699	1·674	1·673	1·646	1·651	1·625	1·629
2·2	1·682	1·706	1·723	1·721	1·713	1·710	1·711	1·702	1·683	1·660	1·661	1·633	1·638	1·617	1·622
2·4	1·659	1·683	1·700	1·699	1·696	1·692	1·697	1·683	1·663	1·647	1·649	1·619	1·627	1·607	1·613
2·6	1·634	1·654	1·677	1·678	1·674	1·676	1·677	1·668	1·646	1·632	1·638	1·609	1·619	1·596	1·603
2·8	1·611	1·628	1·654	1·656	1·653	1·655	1·660	1·652	1·633	1·618	1·624	1·599	1·603	1·588	1·593
3·0	1·588	1·602	1·632	1·636	1·633	1·638	1·644	1·637	1·619	1·605	1·611	1·583	1·589	1·575	1·583
3·3	1·553	1·566	1·595	1·605	1·603	1·604	1·620	1·610	1·596	1·583	1·589	1·467	1·574	1·557	1·568
3·6	1·517	1·528	1·560	1·565	1·572	1·578	1·592	1·580	1·572	1·561	1·569	1·546	1·559	1·536	1·553
3·9	1·482	1·486	1·528	1·531	1·538	1·549	1·563	1·552	1·548	1·540	1·549	1·525	1·533	1·518	1·537
4·2	1·446	1·451	1·490	1·493	1·504	1·518	1·533	1·524	1·518	1·517	1·524	1·503	1·512	1·500	1·520
4·5	1·411	1·410	1·452	1·454	1·469	1·481	1·503	1·496	1·491	1·492	1·501	1·479	1·488	1·478	1·505
4·8	1·373	1·373	1·413	1·421	1·439	1·450	1·469	1·468	1·464	1·466	1·476	1·457	1·468	1·456	1·485
5·2	1·319	1·326	1·365	1·372	1·391	1·402	1·423	1·427	1·427	1·438	1·443	1·425	1·434	1·432	1·460
5·6	1·269	1·270	1·313	1·325	1·345	1·357	1·383	1·389	1·391	1·399	1·409	1·399	1·400	1·403	1·434
6·0	1·222	1·213	1·262	1·275	1·298	1·311	1·338	1·348	1·354	1·355	1·374	1·366	1·371	1·371	1·406
6·4	1·175	1·160	1·212	1·225	1·251	1·266	1·299	1·307	1·315	1·314	1·339	1·333	1·339	1·340	1·379
6·8	1·130	1·115	1·160	1·180	1·202	1·229	1·256	1·268	1·280	1·276	1·302	1·303	1·305	1·308	1·351
7·2	1·083	1·076	1·116	1·136	1·157	1·187	1·208	1·223	1·241	1·239	1·268	1·269	1·270	1·277	1·321
7·6	1·042	1·040	1·068	1·096	1·116	1·141	1·166	1·182	1·209	1·199	1·232	1·236	1·237	1·248	1·290
8·0	1·021	1·020	1·033	1·061	1·080	1·101	1·126	1·142	1·169	1·163	1·197	1·203	1·206	1·218	1·259
8·5	1·005	1·008	1·012	1·030	1·042	1·057	1·077	1·092	1·125	1·119	1·155	1·164	1·163	1·177	1·222
9·0	1·002	1·004	1·001	1·009	1·022	1·029	1·037	1·052	1·086	1·082	1·112	1·128	1·124	1·142	1·185
9·5	1·000	1·000	1·000	1·001	1·009	1·013	1·017	1·024	1·053	1·051	1·076	1·091	1·090	1·108	1·147
10·0				1·000	1·001	1·006	1·010	1·009	1·031	1·031	1·048	1·056	1·056	1·073	1·112
10·5					1·000	1·002	1·002	1·004	1·018	1·015	1·025	1·026	1·032	1·047	1·083
11·0						1·000	1·001	1·000	1·011	1·007	1·011	1·009	1·016	1·029	1·057
11·5							1·000		1·005	1·004	1·005	1·003	1·006	1·015	1·037
12·0									1·003	1·001	1·001	1·000	1·003	1·008	1·023
12·5									1·000	1·000	1·000		1·001	1·004	1·013
13·0													1·000	1·002	1·005
13·5														1·000	1·002
14·0															1·000

GRADIENT B—0·003

X(mms)	0	12·7	25·4	38·1	50·8	63·5	76·2	88·9	101·6	114·3	127·0	139·7	152·4	165·1	177·8
M_1	2·51	2·50	2·50	2·45	2·44	2·40	2·37	2·36	2·34	2·29	2·27	2·21	2·24	2·11	2·07
θ (mms)	0·957	0·992	1·026	1·084	1·162	1·184	1·250	1·306	1·378	1·478	1·536	1·604	1·680	1·756	1·877
δ (mms)	4·574	4·854	4·937	5·331	5·689	5·925	6·040	6·120	6·423	6·727	7·065	7·397	7·292	8·303	8·546
Y(mms)	U/U_1	U/U_1	U/U_1	U/U_1	U/U_1	U/U_1	U/U_1	U/U_1	U/U_1	U/U_1	U/U_1	U/U_1	U/U_1	U/U_1	U/U_1
0·1	0·332	0·330	0·345	0·308	0·296	0·258	0·251	0·284	0·286	0·257	0·261	0·217	0·309	0·133	0·112
0·2	0·340	0·334	0·352	0·315	0·304	0·267	0·262	0·294	0·296	0·264	0·269	0·227	0·314	0·143	0·127
0·3	0·350	0·341	0·358	0·322	0·311	0·275	0·273	0·305	0·303	0·267	0·276	0·236	0·320	0·154	0·134
0·4	0·359	0·347	0·364	0·329	0·319	0·284	0·283	0·313	0·310	0·274	0·284	0·242	0·328	0·163	0·146
0·5	0·368	0·353	0·369	0·335	0·330	0·292	0·292	0·319	0·316	0·281	0·290	0·247	0·333	0·172	0·161
0·6	0·376	0·359	0·379	0·342	0·335	0·300	0·301	0·326	0·325	0·289	0·296	0·253	0·338	0·180	0·173
0·8	0·392	0·376	0·389	0·353	0·347	0·314	0·320	0·344	0·341	0·308	0·309	0·266	0·344	0·194	0·183
1·0	0·411	0·395	0·401	0·365	0·360	0·327	0·337	0·358	0·352	0·320	0·318	0·279	0·349	0·208	0·192
1·2	0·429	0·409	0·417	0·374	0·367	0·343	0·345	0·366	0·362	0·332	0·325	0·294	0·358	0·219	0·201
1·4	0·446	0·422	0·430	0·387	0·379	0·360	0·356	0·376	0·372	0·343	0·335	0·303	0·366	0·231	0·210
1·6	0·462	0·438	0·442	0·403	0·395	0·377	0·366	0·384	0·381	0·352	0·346	0·309	0·370	0·243	0·217
1·8	0·480	0·454	0·457	0·418	0·409	0·391	0·382	0·399	0·391	0·363	0·355	0·316	0·376	0·253	0·227
2·0	0·497	0·471	0·471	0·430	0·422	0·405	0·398	0·413	0·405	0·375	0·366	0·324	0·383	0·263	0·242
2·2	0·512	0·488	0·486	0·444	0·435	0·419	0·413	0·423	0·417	0·386	0·375	0·333	0·390	0·273	0·253
2·4	0·528	0·503	0·503	0·459	0·447	0·431	0·426	0·432	0·428	0·395	0·384	0·344	0·398	0·282	0·263
2·6	0·544	0·522	0·520	0·473	0·457	0·445	0·437	0·444	0·440	0·403	0·389	0·358	0·405	0·291	0·273
2·8	0·560	0·536	0·534	0·488	0·471	0·460	0·448	0·453	0·451	0·414	0·398	0·372	0·414	0·298	0·286
3·0	0·576	0·551	0·550	0·505	0·488	0·474	0·462	0·467	0·460	0·427	0·409	0·381	0·425	0·308	0·298
3·3	0·605	0·571	0·574	0·531	0·509	0·494	0·480	0·486	0·476	0·445	0·425	0·397	0·438	0·321	0·316
3·6	0·631	0·593	0·597	0·552	0·530	0·516	0·499	0·502	0·494	0·461	0·441	0·413	0·449	0·337	0·333
3·9	0·658	0·620	0·619	0·576	0·553	0·534	0·520	0·525	0·513	0·476	0·459	0·425	0·462	0·355	0·349
4·2	0·681	0·646	0·643	0·602	0·574	0·555	0·541	0·545	0·531	0·495	0·477	0·443	0·476	0·373	0·369
4·5	0·709	0·669	0·663	0·622	0·598	0·577	0·567	0·564	0·550	0·515	0·495	0·464	0·495	0·391	0·387
4·8	0·732	0·693	0·687	0·642	0·619	0·602	0·581	0·585	0·568	0·533	0·513	0·484	0·511	0·408	0·402
5·2	0·762	0·727	0·722	0·676	0·650	0·632	0·609	0·611	0·592	0·555	0·536	0·510	0·531	0·431	0·432
5·6	0·794	0·757	0·752	0·712	0·681	0·663	0·642	0·638	0·619	0·585	0·560	0·534	0·552	0·456	0·460
6·0	0·823	0·790	0·784	0·744	0·713	0·700	0·672	0·668	0·644	0·612	0·588	0·558	0·578	0·482	0·486
6·4	0·850	0·821	0·813	0·775	0·743	0·732	0·700	0·694	0·672	0·634	0·611	0·582	0·602	0·507	0·512
6·8	0·879	0·852	0·843	0·804	0·772	0·754	0·728	0·725	0·699	0·662	0·636	0·607	0·624	0·537	0·536
7·2	0·906	0·883	0·872	0·836	0·802	0·783	0·759	0·752	0·727	0·695	0·664	0·630	0·648	0·561	0·562
7·6	0·932	0·909	0·900	0·867	0·831	0·812	0·788	0·779	0·755	0·719	0·691	0·656	0·674	0·587	0·587
8·0	0·948	0·935	0·925	0·894	0·859	0·842	0·815	0·804	0·781	0·745	0·717	0·685	0·699	0·613	0·613
8·5	0·969	0·963	0·951	0·927	0·893	0·876	0·852	0·849	0·810	0·784	0·751	0·722	0·729	0·647	0·645
9·0	0·987	0·987	0·974	0·955	0·923	0·907	0·889	0·874	0·844	0·815	0·784	0·757	0·763	0·682	0·677
9·5	0·995	0·996	0·989	0·976	0·951	0·938	0·921	0·903	0·875	0·848	0·818	0·791	0·794	0·715	0·709
10·0	0·998	0·999	0·996	0·993	0·972	0·963	0·951	0·929	0·904	0·879	0·849	0·824	0·825	0·747	0·736
10·5	1·000	1·000	0·998	0·998	0·985	0·980	0·972	0·954	0·934	0·907	0·878	0·856	0·853	0·778	0·764
11·0			0·999	1·000	0·992	0·990	0·998	0·974	0·957	0·933	0·907	0·886	0·881	0·809	0·792
11·5			1·000		0·996	0·995	0·995	0·987	0·973	0·958	0·935	0·914	0·907	0·841	0·820
12·0					0·998	0·998	0·999	0·995	0·987	0·976	0·956	0·939	0·927	0·869	0·849
12·5					0·999	0·999	1·000	0·999	0·995	0·988	0·973	0·959	0·945	0·896	0·876
13·0					1·000	1·000		1·000	0·999	0·994	0·986	0·974	0·961	0·923	0·902
13·5									1·000	0·998	0·994	0·986	0·974	0·951	0·924
14·0										0·999	0·997	0·991	0·982	0·973	0·939
15·0										1·000	1·000	0·999	0·993	0·993	0·965
16·0												1·000	0·997	1·000	0·981
17·0													1·000		0·992
18·0															0·997
19·0															0·999
20·0															1·000

TABLE 1 (Cont.)

GRADIENT B—0.003

X(mms)	0	12.7	25.4	38.1	50.8	63.5	76.2	88.9	101.6	114.3	127.0	139.7	152.4	165.1	177.8
M_1	2.51	2.50	2.50	2.45	2.44	2.40	2.37	2.36	2.34	2.29	2.27	2.21	2.24	2.11	2.07
R_t	28100	29500	30700	33600	36300	38200	40000	41800	44800	48500	51900	55400	56800	63100	69000
T_w/T_1	2.186	2.192	2.192	2.152	2.147	2.133	2.065	2.063	2.048	1.994	1.978	1.921	1.934	1.830	1.796
Y(mms)	T/T_1	T/T_1	T/T_1	T/T_1	T/T_1	T/T_1	T/T_1	T/T_1	T/T_1	T/T_1	T/T_1	T/T_1	T/T_1	T/T_1	T/T_1
0.1	2.057	2.062	2.054	2.043	2.047	2.058	1.996	1.973	1.962	1.928	1.911	1.871	1.844	1.754	1.781
0.2	2.039	2.050	2.038	2.029	2.032	2.047	1.982	1.959	1.948	1.919	1.897	1.861	1.831	1.750	1.772
0.3	2.019	2.038	2.025	2.014	2.019	2.034	1.969	1.945	1.937	1.907	1.886	1.848	1.819	1.748	1.762
0.4	2.000	2.026	2.010	2.002	2.007	2.023	1.958	1.934	1.926	1.897	1.875	1.838	1.808	1.746	1.754
0.5	1.989	2.010	1.999	1.991	1.993	2.011	1.945	1.925	1.916	1.887	1.867	1.830	1.802	1.740	1.744
0.6	1.976	2.001	1.986	1.982	1.982	2.003	1.931	1.917	1.905	1.877	1.860	1.822	1.793	1.738	1.737
0.8	1.952	1.976	1.966	1.961	1.962	1.984	1.910	1.891	1.884	1.857	1.844	1.810	1.783	1.733	1.724
1.0	1.927	1.950	1.945	1.943	1.946	1.965	1.891	1.879	1.870	1.840	1.828	1.797	1.773	1.726	1.712
1.2	1.906	1.930	1.928	1.929	1.933	1.947	1.880	1.866	1.857	1.829	1.820	1.784	1.763	1.722	1.705
1.4	1.888	1.914	1.912	1.915	1.919	1.927	1.868	1.852	1.845	1.817	1.811	1.776	1.755	1.715	1.699
1.6	1.871	1.895	1.898	1.898	1.903	1.910	1.858	1.843	1.836	1.806	1.801	1.773	1.749	1.710	1.694
1.8	1.849	1.879	1.880	1.883	1.888	1.895	1.846	1.828	1.826	1.797	1.793	1.767	1.745	1.706	1.690
2.0	1.828	1.861	1.862	1.870	1.874	1.881	1.832	1.816	1.815	1.789	1.786	1.762	1.738	1.703	1.685
2.2	1.811	1.840	1.843	1.857	1.862	1.869	1.818	1.806	1.803	1.781	1.777	1.756	1.732	1.698	1.680
2.4	1.790	1.820	1.822	1.840	1.849	1.857	1.807	1.797	1.790	1.722	1.770	1.747	1.727	1.691	1.675
2.6	1.770	1.800	1.804	1.822	1.836	1.841	1.794	1.786	1.780	1.765	1.765	1.738	1.720	1.687	1.669
2.8	1.752	1.784	1.784	1.807	1.821	1.825	1.785	1.775	1.768	1.758	1.757	1.727	1.712	1.684	1.663
3.0	1.732	1.763	1.766	1.787	1.804	1.812	1.770	1.763	1.759	1.745	1.748	1.721	1.704	1.677	1.656
3.3	1.695	1.737	1.732	1.755	1.779	1.789	1.752	1.745	1.743	1.730	1.732	1.707	1.691	1.699	1.646
3.6	1.661	1.709	1.702	1.731	1.753	1.764	1.733	1.726	1.725	1.713	1.718	1.695	1.682	1.661	1.637
3.9	1.618	1.671	1.670	1.702	1.727	1.744	1.711	1.701	1.702	1.699	1.701	1.685	1.671	1.650	1.629
4.2	1.584	1.635	1.638	1.672	1.703	1.717	1.686	1.680	1.685	1.680	1.685	1.671	1.657	1.638	1.616
4.5	1.547	1.604	1.610	1.642	1.672	1.694	1.657	1.655	1.663	1.659	1.669	1.655	1.639	1.628	1.604
4.8	1.512	1.567	1.574	1.616	1.643	1.661	1.641	1.631	1.643	1.640	1.651	1.636	1.625	1.618	1.593
5.2	1.465	1.515	1.523	1.571	1.604	1.624	1.610	1.602	1.616	1.619	1.627	1.612	1.606	1.601	1.574
5.6	1.418	1.471	1.475	1.520	1.562	1.579	1.565	1.570	1.585	1.587	1.601	1.589	1.583	1.583	1.556
6.0	1.371	1.421	1.426	1.476	1.517	1.529	1.531	1.532	1.556	1.556	1.573	1.566	1.555	1.564	1.536
6.4	1.327	1.371	1.377	1.428	1.473	1.486	1.496	1.498	1.516	1.530	1.550	1.541	1.530	1.545	1.515
6.8	1.273	1.316	1.328	1.384	1.428	1.453	1.456	1.456	1.483	1.499	1.519	1.515	1.507	1.521	1.497
7.2	1.220	1.262	1.277	1.335	1.384	1.409	1.414	1.419	1.449	1.459	1.486	1.491	1.481	1.501	1.476
7.6	1.171	1.213	1.230	1.281	1.336	1.366	1.374	1.382	1.410	1.428	1.453	1.463	1.451	1.477	1.455
8.0	1.131	1.162	1.182	1.234	1.291	1.322	1.336	1.344	1.373	1.393	1.422	1.431	1.422	1.455	1.430
8.5	1.079	1.100	1.128	1.176	1.234	1.265	1.281	1.279	1.332	1.344	1.382	1.389	1.389	1.428	1.401
9.0	1.036	1.047	1.077	1.119	1.178	1.214	1.224	1.241	1.284	1.299	1.338	1.348	1.348	1.397	1.371
9.5	1.011	1.019	1.041	1.075	1.125	1.159	1.174	1.196	1.237	1.255	1.293	1.306	1.308	1.367	1.339
10.0	1.002	1.008	1.017	1.034	1.076	1.108	1.122	1.154	1.193	1.210	1.248	1.264	1.272	1.335	1.312
10.5	1.001	1.002	1.005	1.017	1.046	1.067	1.077	1.109	1.143	1.169	1.205	1.227	1.236	1.303	1.286
11.0	1.000	1.000	1.002	1.007	1.022	1.037	1.044	1.071	1.105	1.129	1.164	1.189	1.200	1.269	1.256
11.5			1.000	1.002	1.009	1.023	1.024	1.041	1.072	1.087	1.124	1.150	1.164	1.232	1.227
12.0				1.000	1.003	1.012	1.013	1.023	1.047	1.057	1.090	1.112	1.134	1.199	1.196
12.5					1.001	1.006	1.006	1.013	1.029	1.036	1.062	1.084	1.104	1.164	1.165
13.0					1.000	1.003	1.003	1.004	1.014	1.020	1.039	1.060	1.078	1.127	1.139
13.5						1.000	1.000	1.002	1.010	1.009	1.022	1.038	1.059	1.082	1.110
14.0								1.000	1.005	1.003	1.013	1.033	1.040	1.050	1.090
15.0									1.000	1.000	1.004	1.009	1.019	1.018	1.056
16.0											1.002	1.002	1.005	1.003	1.031
17.0											1.000	1.000	1.000	1.000	1.014
18.0															1.002
19.0															1.002
20.0															1.000

TABLE 1 (Cont.)

GRADIENT C—0·000

X(mms)	0	12·7	25·4	38·1	50·8	63·5	76·2	88·9	101·6	114·3	127·0	139·7	152·4	165·1	177·8	190·5	203·2	215·9
M_1	2·57	2·61	2·58	2·61	2·61	2·67	2·72	2·77	2·84	2·90	2·96	3·01	3·05	3·10	3·13	3·17	3·22	3·24
θ (mms)	0·404	0·398	0·439	0·414	0·484	0·442	0·446	0·486	0·487	0·504	0·519	0·532	0·538	0·571	0·571	0·612	0·615	0·733
δ (mms)	1·727	1·710	1·869	1·812	2·046	1·985	2·062	2·214	2·298	2·418	2·530	2·640	2·779	2·963	3·174	3·114	3·200	3·432
Y(mms)	U/U_1	U/U_1	U/U_1	U/U_1	U/U_1	U/U_1	U/U_1	U/U_1	U/U_1	U/U_1	U/U_1	U/U_1	U/U_1	U/U_1	U/U_1	U/U_1	U/U_1	U/U_1
0·1	0·539	0·576	0·543	0·548	0·549	0·568	0·590	0·579	0·598	0·571	0·587	0·584	0·592	0·579	0·568	0·581	0·573	0·586
0·2	0·600	0·625	0·610	0·615	0·610	0·643	0·659	0·644	0·649	0·624	0·648	0·644	0·648	0·630	0·627	0·634	0·618	0·613
0·3	0·643	0·658	0·650	0·660	0·649	0·670	0·691	0·681	0·690	0·694	0·693	0·689	0·691	0·676	0·669	0·669	0·657	0·642
0·4	0·672	0·683	0·677	0·687	0·680	0·698	0·727	0·714	0·721	0·721	0·729	0·720	0·719	0·707	0·698	0·698	0·690	0·670
0·5	0·693	0·705	0·702	0·708	0·700	0·720	0·744	0·734	0·744	0·743	0·747	0·741	0·742	0·729	0·722	0·720	0·714	0·697
0·6	0·709	0·723	0·717	0·725	0·716	0·736	0·755	0·748	0·759	0·763	0·762	0·757	0·757	0·748	0·739	0·739	0·731	0·717
0·8	0·734	0·750	0·741	0·748	0·735	0·757	0·774	0·765	0·777	0·779	0·782	0·778	0·779	0·770	0·765	0·761	0·755	0·742
1·0	0·755	0·765	0·755	0·763	0·750	0·775	0·784	0·778	0·788	0·788	0·792	0·791	0·793	0·784	0·782	0·778	0·773	0·759
1·2	0·770	0·780	0·770	0·778	0·762	0·788	0·796	0·789	0·797	0·798	0·803	0·803	0·807	0·795	0·794	0·792	0·789	0·773
1·4	0·788	0·797	0·782	0·791	0·776	0·801	0·806	0·801	0·808	0·808	0·812	0·814	0·818	0·808	0·806	0·804	0·803	0·786
1·6	0·803	0·812	0·796	0·805	0·787	0·813	0·816	0·812	0·819	0·818	0·822	0·824	0·826	0·818	0·818	0·814	0·814	0·798
1·8	0·817	0·826	0·811	0·819	0·800	0·824	0·828	0·821	0·827	0·827	0·830	0·832	0·835	0·828	0·829	0·825	0·823	0·807
2·0	0·831	0·840	0·822	0·833	0·813	0·835	0·837	0·830	0·836	0·835	0·838	0·839	0·843	0·839	0·837	0·833	0·834	0·816
2·2	0·844	0·852	0·836	0·845	0·824	0·846	0·847	0·839	0·844	0·843	0·847	0·848	0·850	0·846	0·844	0·841	0·843	0·824
2·4	0·859	0·863	0·847	0·857	0·834	0·857	0·856	0·848	0·852	0·852	0·855	0·855	0·858	0·853	0·851	0·849	0·851	0·831
2·6	0·873	0·877	0·859	0·870	0·845	0·865	0·864	0·858	0·859	0·860	0·861	0·862	0·864	0·861	0·858	0·857	0·858	0·838
2·8	0·886	0·888	0·873	0·883	0·855	0·876	0·875	0·866	0·867	0·867	0·867	0·869	0·870	0·867	0·865	0·864	0·864	0·846
3·0	0·898	0·901	0·884	0·894	0·867	0·885	0·884	0·875	0·875	0·873	0·876	0·876	0·877	0·873	0·872	0·870	0·869	0·853
3·3	0·916	0·917	0·900	0·910	0·884	0·900	0·896	0·887	0·887	0·885	0·885	0·884	0·884	0·881	0·881	0·878	0·877	0·861
3·6	0·935	0·934	0·917	0·926	0·899	0·913	0·909	0·898	0·897	0·895	0·894	0·893	0·892	0·889	0·889	0·885	0·885	0·867
3·9	0·951	0·948	0·934	0·940	0·915	0·926	0·921	0·910	0·907	0·904	0·902	0·900	0·900	0·896	0·895	0·893	0·892	0·874
4·2	0·964	0·961	0·948	0·953	0·929	0·937	0·933	0·920	0·917	0·913	0·911	0·910	0·908	0·902	0·903	0·899	0·899	0·882
4·5	0·977	0·974	0·960	0·964	0·943	0·948	0·943	0·930	0·926	0·922	0·919	0·917	0·915	0·909	0·909	0·905	0·907	0·888
4·8	0·986	0·985	0·972	0·977	0·955	0·960	0·953	0·940	0·936	0·930	0·926	0·924	0·921	0·916	0·915	0·912	0·913	0·895
5·2	0·994	0·996	0·983	0·990	0·968	0·971	0·965	0·953	0·948	0·941	0·938	0·933	0·931	0·924	0·924	0·915	0·919	0·902
5·6	0·999	0·998	0·992	0·996	0·980	0·982	0·976	0·964	0·959	0·952	0·947	0·942	0·940	0·932	0·932	0·923	0·927	0·909
6·0	1·000	1·000	0·996	0·999	0·989	0·991	0·985	0·974	0·969	0·961	0·956	0·950	0·948	0·940	0·939	0·934	0·933	0·916
6·4			0·999	1·000	0·995	0·995	0·992	0·982	0·978	0·971	0·964	0·959	0·956	0·947	0·945	0·940	0·940	0·922
6·8			1·000		0·998	0·997	0·996	0·989	0·986	0·979	0·971	0·966	0·962	0·955	0·951	0·947	0·946	0·928
7·2					1·000	0·999	0·998	0·993	0·991	0·986	0·978	0·972	0·969	0·961	0·958	0·953	0·952	0·933
7·6						1·000	0·999	0·997	0·994	0·990	0·985	0·979	0·975	0·968	0·965	0·959	0·957	0·940
8·0							1·000	0·999	0·997	0·995	0·989	0·984	0·980	0·972	0·970	0·966	0·963	0·946
8·5								1·000	1·000	0·997	0·992	0·989	0·984	0·979	0·977	0·972	0·970	0·952
9·0										1·000	0·995	0·994	0·991	0·985	0·982	0·979	0·975	0·959
9·5											0·998	0·997	0·995	0·991	0·988	0·984	0·981	0·965
10·0											0·999	0·998	0·997	0·994	0·992	0·989	0·986	0·970
10·5											1·000	0·999	0·998	0·996	0·995	0·993	0·990	0·976
11·0												1·000	0·999	0·998	0·997	0·996	0·993	0·982
11·5													1·000	0·999	0·998	0·997	0·995	0·987
12·0														1·000	0·999	0·998	0·997	0·993
12·5															1·000	0·999	0·998	0·997
13·0																1·000	0·999	0·999
13·5																	1·000	1·000

41

TABLE 1 (Cont.)

GRADIENT C—0·000

X (mms)	0	12·7	25·4	38·1	50·8	63·5	76·2	88·9	101·6	114·3	127·0	139·7	152·4	165·1	177·8	190·5	203·2	215·9
M_1	2·57	2·61	2·58	2·61	2·61	2·67	2·72	2·77	2·84	2·90	2·96	3·01	3·05	3·10	3·13	3·17	3·22	3·24
R_θ	15600	15000	17100	16100	18400	16500	16400	17100	16700	16300	16400	16300	16300	16800	16000	16100	15900	18500
T_w/T_1	2·242	2·272	2·278	2·313	2·291	2·374	2·452	2·478	2·551	2·586	2·670	2·730	2·789	2·832	2·806	2·792	2·847	2·859
Y (mms)	T/T_1	T/T_1	T/T_1	T/T_1	T/T_1	T/T_1	T/T_1	T/T_1	T/T_1	T/T_1	T/T_1	T/T_1	T/T_1	T/T_1	T/T_1	T/T_1	T/T_1	T/T_1
0·1	1·903	1·872	1·916	1·939	1·918	1·963	1·980	2·015	2·039	2·101	2·131	2·181	2·201	2·262	2·259	2·200	2·253	2·221
0·2	1·818	1·793	1·820	1·839	1·827	1·842	1·857	1·894	1·939	1·998	1·999	2·048	2·072	2·141	2·132	2·083	2·152	2·155
0·3	1·747	1·736	1·753	1·763	1·759	1·783	1·784	1·817	1·849	1·854	1·892	1·941	1·969	2·028	2·035	2·000	2·059	2·081
0·4	1·698	1·690	1·701	1·709	1·702	1·724	1·707	1·745	1·773	1·792	1·803	1·860	1·893	1·943	1·962	1·926	1·973	2·004
0·5	1·657	1·647	1·653	1·667	1·661	1·676	1·666	1·658	1·720	1·736	1·751	1·801	1·827	1·881	1·904	1·868	1·910	1·930
0·6	1·624	1·612	1·621	1·629	1·628	1·638	1·636	1·658	1·679	1·685	1·705	1·754	1·779	1·818	1·855	1·821	1·863	1·871
0·8	1·569	1·551	1·569	1·573	1·581	1·585	1·583	1·608	1·620	1·632	1·639	1·687	1·703	1·740	1·781	1·750	1·793	1·795
1·0	1·525	1·518	1·533	1·533	1·544	1·541	1·548	1·568	1·579	1·593	1·604	1·636	1·654	1·686	1·732	1·698	1·736	1·735
1·2	1·494	1·485	1·502	1·501	1·514	1·510	1·518	1·536	1·552	1·561	1·569	1·591	1·609	1·648	1·694	1·654	1·688	1·688
1·4	1·462	1·453	1·476	1·472	1·489	1·479	1·494	1·505	1·518	1·532	1·539	1·557	1·573	1·607	1·658	1·622	1·647	1·647
1·6	1·433	1·426	1·451	1·448	1·463	1·453	1·470	1·480	1·491	1·503	1·512	1·528	1·550	1·578	1·623	1·593	1·613	1·611
1·8	1·404	1·399	1·424	1·417	1·439	1·430	1·445	1·461	1·471	1·482	1·488	1·507	1·521	1·552	1·590	1·563	1·584	1·580
2·0	1·379	1·372	1·403	1·389	1·416	1·408	1·423	1·440	1·445	1·464	1·469	1·487	1·502	1·523	1·565	1·536	1·553	1·550
2·2	1·354	1·348	1·378	1·366	1·395	1·384	1·399	1·416	1·427	1·441	1·448	1·461	1·480	1·500	1·542	1·511	1·524	1·523
2·4	1·325	1·325	1·356	1·341	1·375	1·359	1·380	1·395	1·410	1·417	1·427	1·441	1·457	1·478	1·518	1·489	1·497	1·500
2·6	1·297	1·298	1·333	1·315	1·354	1·341	1·362	1·373	1·390	1·397	1·412	1·423	1·439	1·452	1·497	1·466	1·475	1·477
2·8	1·274	1·274	1·306	1·289	1·334	1·318	1·339	1·355	1·369	1·379	1·395	1·404	1·420	1·432	1·476	1·443	1·455	1·453
3·0	1·252	1·248	1·282	1·268	1·314	1·300	1·318	1·335	1·351	1·364	1·375	1·387	1·399	1·417	1·455	1·427	1·440	1·432
3·3	1·215	1·214	1·250	1·233	1·280	1·267	1·289	1·307	1·322	1·335	1·349	1·362	1·378	1·389	1·424	1·400	1·416	1·408
3·6	1·179	1·181	1·216	1·203	1·249	1·242	1·261	1·280	1·296	1·309	1·325	1·334	1·355	1·365	1·402	1·375	1·387	1·387
3·9	1·144	1·148	1·180	1·172	1·214	1·214	1·234	1·258	1·272	1·287	1·302	1·313	1·332	1·345	1·383	1·352	1·364	1·366
4·2	1·109	1·118	1·147	1·141	1·184	1·188	1·201	1·231	1·246	1·262	1·279	1·287	1·310	1·325	1·361	1·332	1·342	1·341
4·5	1·076	1·085	1·118	1·111	1·156	1·158	1·177	1·205	1·223	1·238	1·258	1·266	1·290	1·304	1·340	1·313	1·318	1·322
4·8	1·049	1·054	1·084	1·083	1·129	1·132	1·152	1·180	1·199	1·217	1·236	1·247	1·272	1·283	1·317	1·292	1·297	1·301
5·2	1·022	1·022	1·053	1·041	1·094	1·099	1·124	1·149	1·168	1·187	1·205	1·219	1·243	1·260	1·292	1·282	1·278	1·276
5·6	1·007	1·010	1·026	1·022	1·061	1·069	1·090	1·118	1·138	1·160	1·178	1·195	1·215	1·237	1·266	1·260	1·252	1·254
6·0	1·001	1·004	1·011	1·010	1·035	1·043	1·063	1·090	1·110	1·135	1·154	1·170	1·193	1·211	1·241	1·225	1·233	1·231
6·4	1·000	1·000	1·002	1·004	1·019	1·024	1·041	1·064	1·084	1·106	1·131	1·145	1·166	1·189	1·216	1·202	1·211	1·212
6·8			1·000	1·002	1·009	1·014	1·022	1·040	1·064	1·081	1·104	1·124	1·144	1·165	1·194	1·181	1·188	1·194
7·2				1·000	1·004	1·007	1·013	1·023	1·039	1·059	1·080	1·100	1·122	1·145	1·173	1·162	1·168	1·174
7·6					1·000	1·002	1·006	1·011	1·021	1·041	1·061	1·077	1·104	1·123	1·153	1·142	1·153	1·155
8·0						1·000	1·002	1·005	1·010	1·026	1·042	1·058	1·082	1·105	1·130	1·119	1·133	1·140
8·5							1·000	1·001	1·004	1·014	1·026	1·037	1·052	1·083	1·107	1·097	1·109	1·121
9·0								1·000	1·000	1·007	1·015	1·021	1·037	1·062	1·087	1·077	1·088	1·100
9·5										1·001	1·005	1·013	1·026	1·040	1·064	1·058	1·070	1·084
10·0										1·000	1·002	1·004	1·015	1·024	1·046	1·042	1·052	1·066
10·5											1·001	1·002	1·010	1·015	1·031	1·026	1·037	1·049
11·0											1·000	1·001	1·002	1·009	1·021	1·018	1·026	1·038
11·5												1·000	1·001	1·004	1·014	1·010	1·015	1·031
12·0													1·000	1·002	1·004	1·006	1·005	1·024
12·5														1·000	1·000	1·003	1·004	1·018
13·0																1·001	1·000	1·014
13·5																1·000		1·010
14·0																		1·006
15·0																		1·003
16·0																		1·001
17·0																		

GRADIENT C—0·001

X (mms)	0	12·7	25·4	38·1	50·8	63·5	76·2	88·9	101·6	114·3	127·0	139·7	152·4	165·1	177·8	190·5	203·2
M_1	2·55	2·55	2·59	2·59	2·61	2·67	2·74	2·80	2·85	2·89	2·93	2·97	3·02	3·05	3·08	3·15	3·18
θ (mms)	0·529	0·551	0·560	0·600	0·648	0·644	0·653	0·663	0·658	0·719	0·716	0·755	0·787	0·832	0·874	0·885	0·885
δ^x (mms)	2·268	2·325	2·426	2·532	2·809	2·818	2·892	3·024	3·070	3·418	3·500	3·692	3·927	4·198	4·632	4·714	4·774
Y (mms)	U/U_1	U/U_1	U/U_1	U/U_1	U/U_1	U/U_1	U/U_1	U/U_1	U/U_1	U/U_1	U/U_1	U/U_1	U/U_1	U/U_1	U/U_1	U/U_1	U/U_1
0·1	0·442	0·435	0·446	0·475	0·433	0·449	0·478	0·481	0·470	0·443	0·473	0·465	0·481	0·476	0·450	0·461	0·499
0·2	0·492	0·489	0·492	0·506	0·467	0·500	0·532	0·533	0·520	0·491	0·511	0·496	0·509	0·498	0·470	0·484	0·505
0·3	0·524	0·529	0·534	0·542	0·499	0·545	0·572	0·576	0·554	0·534	0·546	0·539	0·532	0·524	0·507	0·508	0·514
0·4	0·552	0·559	0·561	0·569	0·532	0·572	0·596	0·603	0·585	0·570	0·581	0·566	0·560	0·551	0·532	0·532	0·524
0·5	0·574	0·583	0·584	0·592	0·568	0·596	0·618	0·626	0·609	0·596	0·604	0·592	0·582	0·575	0·552	0·553	0·534
0·6	0·593	0·601	0·602	0·610	0·588	0·620	0·638	0·645	0·631	0·619	0·625	0·616	0·602	0·594	0·573	0·575	0·545
0·8	0·625	0·640	0·634	0·638	0·623	0·645	0·670	0·674	0·668	0·656	0·658	0·651	0·637	0·630	0·617	0·615	0·566
1·0	0·653	0·658	0·658	0·662	0·647	0·664	0·689	0·694	0·693	0·681	0·688	0·679	0·666	0·659	0·647	0·644	0·593
1·2	0·677	0·679	0·678	0·681	0·665	0·683	0·706	0·711	0·711	0·702	0·708	0·703	0·687	0·680	0·670	0·666	0·620
1·4	0·698	0·698	0·695	0·697	0·683	0·699	0·720	0·725	0·728	0·717	0·723	0·716	0·704	0·698	0·685	0·682	0·643
1·6	0·717	0·716	0·711	0·712	0·700	0·709	0·732	0·737	0·741	0·732	0·736	0·729	0·717	0·715	0·699	0·697	0·665
1·8	0·734	0·733	0·727	0·727	0·715	0·724	0·742	0·751	0·753	0·745	0·748	0·743	0·741	0·727	0·715	0·713	0·686
2·0	0·750	0·749	0·742	0·742	0·729	0·738	0·753	0·763	0·764	0·754	0·758	0·754	0·754	0·740	0·727	0·727	0·707
2·2	0·768	0·764	0·758	0·756	0·741	0·755	0·765	0·772	0·774	0·764	0·768	0·767	0·759	0·753	0·739	0·739	0·726
2·4	0·784	0·779	0·772	0·769	0·755	0·767	0·777	0·783	0·785	0·774	0·779	0·778	0·767	0·765	0·750	0·750	0·741
2·6	0·800	0·796	0·787	0·783	0·769	0·779	0·787	0·790	0·796	0·783	0·789	0·786	0·778	0·774	0·761	0·760	0·756
2·8	0·816	0·812	0·801	0·797	0·780	0·790	0·796	0·793	0·806	0·793	0·799	0·794	0·787	0·783	0·771	0·771	0·772
3·0	0·832	0·829	0·814	0·811	0·790	0·800	0·805	0·810	0·815	0·803	0·807	0·802	0·797	0·790	0·781	0·780	0·785
3·3	0·858	0·850	0·837	0·831	0·807	0·818	0·819	0·824	0·829	0·816	0·819	0·815	0·809	0·802	0·792	0·793	0·798
3·6	0·880	0·871	0·857	0·849	0·827	0·835	0·834	0·832	0·841	0·827	0·830	0·827	0·819	0·814	0·803	0·802	0·810
3·9	0·903	0·892	0·878	0·870	0·845	0·853	0·849	0·843	0·854	0·837	0·841	0·837	0·831	0·825	0·815	0·813	0·822
4·2	0·922	0·912	0·901	0·887	0·862	0·868	0·864	0·861	0·866	0·848	0·852	0·848	0·842	0·835	0·825	0·826	0·832
4·5	0·939	0·928	0·921	0·903	0·880	0·883	0·878	0·876	0·876	0·860	0·863	0·859	0·853	0·845	0·835	0·836	0·842
4·8	0·955	0·944	0·938	0·920	0·895	0·898	0·891	0·888	0·887	0·869	0·873	0·867	0·861	0·853	0·843	0·844	0·851
5·2	0·974	0·964	0·960	0·941	0·918	0·916	0·908	0·902	0·901	0·885	0·886	0·879	0·874	0·865	0·855	0·856	0·863
5·6	0·986	0·979	0·976	0·961	0·936	0·933	0·926	0·918	0·917	0·899	0·900	0·891	0·886	0·877	0·866	0·866	0·873
6·0	0·994	0·992	0·989	0·975	0·955	0·950	0·940	0·933	0·930	0·912	0·912	0·901	0·897	0·887	0·877	0·878	0·884
6·4	0·998	0·996	0·994	0·987	0·971	0·966	0·955	0·948	0·944	0·924	0·925	0·912	0·908	0·897	0·888	0·886	0·893
6·8	1·000	1·000	0·998	0·991	0·985	0·979	0·970	0·961	0·957	0·936	0·936	0·925	0·919	0·907	0·907	0·896	0·902
7·2			1·000	0·999	0·994	0·987	0·981	0·980	0·979	0·960	0·956	0·946	0·935	0·929	0·917	0·906	0·911
7·6				1·000	0·997	0·994	0·992	0·988	0·987	0·970	0·966	0·956	0·944	0·937	0·925	0·915	0·919
8·0					0·999	0·998	0·994	0·988	0·987	0·970	0·966	0·955	0·946	0·935	0·924	0·921	0·927
8·5					1·000	1·000	0·997	0·994	0·993	0·980	0·978	0·966	0·958	0·946	0·933	0·932	0·935
9·0							0·999	0·997	0·997	0·988	0·985	0·976	0·967	0·955	0·945	0·941	0·943
9·5							1·000	1·000	0·999	0·993	0·991	0·983	0·975	0·964	0·954	0·950	0·951
10·0									1·000	0·997	0·996	0·989	0·983	0·972	0·962	0·958	0·958
10·5										1·000	0·998	0·994	0·989	0·980	0·970	0·966	0·964
11·0											1·000	0·997	0·992	0·986	0·977	0·972	0·970
11·5												0·999	0·997	0·994	0·990	0·984	0·980
12·0												1·000	0·998	0·996	0·993	0·989	0·985
12·5													0·999	0·998	0·996	0·993	0·988
13·0													1·000	0·999	0·997	0·995	0·991
13·5														1·000	0·998	0·997	0·994
14·0															0·999	1·000	0·997
15·0															1·000		0·999
16·0																	1·000
17·0																	

TABLE 1 (Concluded)

GRADIENT C—0.001

X (mms)	0	12.7	25.4	38.1	50.8	63.5	76.2	88.9	101.6	114.3	127.0	139.7	152.4	165.1	177.8	190.5	203.2
M_1	2·55	2·55	2·59	2·59	2·61	2·67	2·74	2·80	2·85	2·89	2·93	2·97	3·02	3·05	3·08	3·15	3·18
R_θ	29000	30000	30200	32100	35100	33200	32300	32000	30800	32700	32300	33000	33600	34700	36900	35400	34200
T_w/T_1	2·195	2·175	2·237	2·225	2·279	2·324	2·386	2·453	2·500	2·540	2·607	2·642	2·690	2·725	2·810	2·846	2·856
Y (mms)	T/T_1	T/T_1	T/T_1	T/T_1	T/T_1	T/T_1	T/T_1	T/T_1	T/T_1	T/T_1	T/T_1	T/T_1	T/T_1	T/T_1	T/T_1	T/T_1	T/T_1
0·1	1·973	1·960	1·996	1·960	2·044	2·070	2·085	2·135	2·189	2·254	2·269	2·309	2·322	2·356	2·473	2·489	2·425
0·2	1·909	1·892	1·935	1·913	1·988	2·002	2·001	2·049	2·099	2·178	2·195	2·241	2·260	2·303	2·421	2·430	2·400
0·3	1·862	1·836	1·881	1·859	1·940	1·931	1·931	1·971	2·034	2·104	2·123	2·159	2·207	2·248	2·347	2·376	2·372
0·4	1·821	1·794	1·837	1·814	1·897	1·880	1·884	1·914	1·974	2·035	2·056	2·104	2·145	2·189	2·286	2·318	2·340
0·5	1·787	1·758	1·802	1·776	1·843	1·838	1·837	1·864	1·926	1·979	2·005	2·047	2·096	2·138	2·238	2·267	2·311
0·6	1·754	1·728	1·772	1·743	1·807	1·793	1·795	1·824	1·878	1·933	1·955	1·991	2·046	2·092	2·187	2·215	2·282
0·8	1·698	1·663	1·715	1·693	1·746	1·736	1·729	1·758	1·799	1·850	1·873	1·907	1·959	2·003	2·084	2·114	2·226
1·0	1·649	1·635	1·674	1·648	1·700	1·696	1·684	1·712	1·740	1·790	1·805	1·837	1·889	1·928	2·005	2·038	2·157
1·2	1·613	1·600	1·637	1·618	1·665	1·658	1·647	1·672	1·695	1·741	1·754	1·778	1·836	1·874	1·944	1·980	2·094
1·4	1·581	1·571	1·604	1·587	1·633	1·628	1·618	1·642	1·656	1·704	1·715	1·745	1·793	1·829	1·902	1·933	2·038
1·6	1·552	1·543	1·578	1·563	1·604	1·628	1·595	1·619	1·628	1·669	1·686	1·716	1·765	1·786	1·865	1·893	1·985
1·8	1·524	1·516	1·552	1·539	1·580	1·606	1·574	1·590	1·603	1·638	1·659	1·682	1·705	1·754	1·825	1·851	1·930
2·0	1·497	1·490	1·526	1·514	1·555	1·559	1·554	1·568	1·578	1·619	1·632	1·654	1·673	1·723	1·791	1·812	1·877
2·2	1·466	1·464	1·499	1·489	1·534	1·528	1·531	1·544	1·553	1·597	1·606	1·625	1·658	1·692	1·759	1·780	1·831
2·4	1·439	1·442	1·473	1·467	1·511	1·503	1·507	1·520	1·506	1·552	1·557	1·576	1·613	1·636	1·699	1·722	1·754
2·6	1·413	1·413	1·448	1·445	1·486	1·479	1·487	1·506	1·484	1·527	1·535	1·555	1·589	1·614	1·672	1·695	1·709
2·8	1·386	1·384	1·421	1·421	1·467	1·459	1·469	1·498	1·464	1·504	1·515	1·537	1·566	1·595	1·648	1·669	1·671
3·0	1·358	1·358	1·399	1·394	1·448	1·442	1·449	1·464	1·432	1·476	1·487	1·506	1·536	1·565	1·619	1·631	1·633
3·3	1·318	1·318	1·357	1·357	1·416	1·407	1·426	1·434	1·405	1·450	1·460	1·476	1·509	1·535	1·591	1·606	1·597
3·6	1·276	1·283	1·319	1·327	1·379	1·372	1·394	1·418	1·377	1·425	1·432	1·450	1·478	1·507	1·561	1·576	1·563
3·9	1·234	1·244	1·278	1·290	1·344	1·340	1·365	1·396	1·350	1·400	1·405	1·423	1·451	1·478	1·531	1·540	1·530
4·2	1·195	1·210	1·235	1·258	1·312	1·309	1·333	1·355	1·325	1·375	1·382	1·397	1·427	1·451	1·503	1·515	1·501
4·5	1·158	1·177	1·197	1·227	1·278	1·280	1·301	1·319	1·302	1·352	1·358	1·376	1·401	1·430	1·480	1·490	1·474
4·8	1·122	1·144	1·162	1·192	1·247	1·249	1·274	1·294	1·268	1·312	1·325	1·346	1·365	1·399	1·444	1·455	1·438
5·2	1·076	1·100	1·115	1·150	1·204	1·213	1·238	1·262	1·230	1·281	1·293	1·316	1·334	1·366	1·415	1·425	1·408
5·6	1·042	1·064	1·073	1·107	1·159	1·174	1·200	1·223	1·198	1·250	1·261	1·287	1·308	1·340	1·384	1·391	1·374
6·0	1·016	1·031	1·035	1·071	1·118	1·135	1·166	1·187	1·168	1·220	1·230	1·258	1·281	1·315	1·354	1·366	1·346
6·4	1·001	1·011	1·011	1·039	1·079	1·097	1·130	1·153	1·134	1·188	1·202	1·228	1·250	1·285	1·330	1·338	1·322
6·8	1·000	1·004	1·005	1·024	1·044	1·063	1·093	1·120	1·104	1·160	1·174	1·198	1·222	1·257	1·306	1·310	1·298
7·2		1·000	1·000	1·006	1·022	1·039	1·060	1·092	1·075	1·130	1·145	1·172	1·197	1·233	1·278	1·283	1·273
7·6				1·000	1·008	1·022	1·032	1·065	1·050	1·100	1·120	1·147	1·174	1·207	1·253	1·259	1·247
8·0					1·002	1·009	1·024	1·044	1·034	1·068	1·090	1·116	1·143	1·178	1·224	1·228	1·219
8·5					1·000	1·004	1·010	1·023	1·017	1·044	1·064	1·087	1·114	1·149	1·194	1·201	1·194
9·0						1·002	1·002	1·010	1·005	1·025	1·042	1·058	1·090	1·121	1·165	1·175	1·168
9·5						1·000	1·001	1·004	1·003	1·012	1·025	1·037	1·068	1·097	1·139	1·148	1·148
10·0							1·000	1·001	1·002	1·004	1·015	1·022	1·049	1·073	1·114	1·127	1·130
10·5								1·000	1·000	1·000	1·011	1·013	1·033	1·052	1·093	1·107	1·112
11·0											1·003	1·007	1·021	1·038	1·073	1·084	1·093
11·5											1·001	1·005	1·012	1·019	1·055	1·063	1·078
12·0											1·000	1·003	1·007	1·012	1·038	1·045	1·061
12·5												1·000	1·003	1·004	1·028	1·030	1·045
13·0													1·000	1·001	1·020	1·018	1·033
13·5														1·000	1·014	1·010	1·023
14·0																	
15·0															1·005	1·001	1·008
16·0															1·001	1·000	1·002

44

TABLE 2
Boundary Layer Parameters

Gradient A , m = 0 .
P_o = 4.12 x 10^5 Nm^{-2} , T_o= 291.9°K

X(mm)	δ_i^x(mm)	θ_i(mm)	ε_i(mm)	ε(mm)	T°K	Cfx10^6	mx10	Fx10	-β
0	0.849	0.614	1.087	0.759	289.6	1530	0	0	0
12.7	0.859	0.628	1.117	0.781	289.7	1520	0	0	0
25.4	0.849	0.627	1.118	0.776	289.8	1510	0	0	0
38.1	0.926	0.687	1.227	0.863	289.9	1535	0	0	0.52
50.8	0.910	0.682	1.223	0.858	290.0	1565	0	0	0.52
63.5	0.916	0.683	1.223	0.852	290.1	1565	0	0	0.54
76.2	0.879	0.672	1.215	0.846	290.2	1555	0	0	0.54
88.9	0.923	0.707	1.280	0.901	290.2	1550	0	0	0.58
101.6	0.954	0.737	1.338	0.937	290.2	1550	0	0	0.62
114.3	0.987	0.757	1.372	0.950	290.1	1550	0	0	0.67
127.0	1.012	0.785	1.426	0.989	290.0	1545	0	0	0.71
139.7	1.031	0.800	1.454	0.997	289.9	1535	0	0	0.65
152.4	1.058	0.823	1.499	1.026	289.8	1525	0	0	0.60
165.1	1.140	0.880	1.597	1.097	289.7	1515	0	0	0.53
177.8	1.088	0.849	1.547	1.057	289.6	1505	0	0	0.46

Gradient A , m = 0.001 .
P_o = 5.15 x 10^5 Nm^{-2}, T_o= 294.1°K

X(mm)	δ_i^x(mm)	θ_i(mm)	ε_i(mm)	ε(mm)	T°K	Cfx10^5	mx10^6	Fx10^6
0	1.340	0.872	1.483	0.987	289.8	83	1020	1020
12.7	1.356	0.883	1.503	1.008	289.8	82	1020	1020
25.4	1.303	0.870	1.492	1.004	289.7	81	1020	1020
38.1	1.271	0.884	1.535	1.039	289.7	81	1020	1076
50.8	1.403	0.963	1.666	1.118	289.6	83	1025	1091
63.5	1.388	0.968	1.684	1.112	289.6	80	1031	1154
76.2	1.428	1.008	1.760	1.165	289.5	78	1036	1213
88.9	1.518	1.071	1.872	1.230	289.5	75	1042	1276
101.6	1.581	1.133	1.988	1.319	289.4	75	1047	1290
114.3	1.579	1.142	2.014	1.333	289.4	73	1053	1358
127.0	1.666	1.207	2.127	1.402	289.3	71	1058	1409
139.7	1.661	1.221	2.162	1.400	289.3	68	1064	1461
152.4	1.829	1.341	2.368	1.568	289.2	70	1056	1393
165.1	1.811	1.382	2.470	1.693	289.2	72	1041	1272

Gradient A , m = 0.002
P_o = 5.15 x 10^5 Nm^{-2}, T_o= 291.9°K

X(mm)	δ_i^x(mm)	θ_i(mm)	ε_i(mm)	ε(mm)	T°K	Cfx10^5	mx10^6	Fx10^6
0	1.744	1.037	1.717	1.102	290.7	47	1990	1990
12.7	1.801	1.092	1.814	1.163	290.6	47	1990	1990
25.4	1.871	1.164	1.950	1.254	290.4	46	1990	1990
38.1	1.915	1.218	2.052	1.331	290.3	46	1990	2080
50.8	1.974	1.268	2.146	1.387	290.2	47	1995	2151
63.5	1.942	1.286	2.196	1.406	290.1	44	2001	2271
76.2	2.043	1.364	2.336	1.510	290.0	42	2006	2371
88.9	2.222	1.472	2.518	1.621	289.8	41	2012	2417
101.6	2.205	1.489	2.563	1.639	289.7	39	2017	2534
114.3	2.249	1.535	2.650	1.694	289.6	38	2023	2642
127.0	2.318	1.572	2.708	1.706	289.5	36	2028	2715
139.7	2.593	1.734	2.977	1.867	289.4	35	2034	2809

TABLE 2 (Cont.)

Gradient B , m = 0 .
P_o = 3.08 x 10^5 Nm^{-2}, T_o = 294.1°K

X(mm)	δ_i^x(mm)	Θ_i(mm)	ε_i(mm)	ε(mm)	T°K	Cfx10^6	mx10	Fx10	β
0	0.965	0.707	1.253	0.888	291.6	1885	0	0	0
12.7	0.930	0.686	1.220	0.850	291.6	1590	0	0	0
25.4	0.875	0.647	1.153	0.809	291.7	1605	0	0	0
38.1	0.879	0.654	1.167	0.821	291.7	1620	0	0	0.49
50.8	0.908	0.658	1.162	0.810	291.8	1585	0	0	0.50
63.5	0.932	0.680	1.204	0.837	291.8	1550	0	0	0.52
76.2	0.978	0.710	1.253	0.883	291.9	1515	0	0	0.55
88.9	1.003	0.729	1.287	0.913	292.0	1490	0	0	0.56
101.6	0.992	0.730	1.293	0.923	291.9	1465	0	0	0.55
114.3	1.102	0.799	1.406	1.004	291.8	1445	0	0	0.60
127.0	1.046	0.765	1.352	0.959	291.8	1430	0	0	0.58
139.7	1.135	0.822	1.446	1.051	291.7	1420	0	0	0.61
152.4	1.142	0.832	1.467	1.073	291.7	1410	0	0	0.615
165.1	1.150	0.844	1.491	1.094	291.6	1400	0	0	0.62
177.8	1.307	0.940	1.648	1.203	291.6	1395	0	0	2.84

Gradient B , m = 0.001 .
P_o = 3.08 x 10^5 Nm^{-2}, T_o = 289.1°K

X(mm)	δ_i^x(mm)	Θ_i(mm)	ε_i(mm)	ε(mm)	T°K	Cfx10^5	mx10^6	Fx10^6
0	1.535	1.016	1.733	1.165	285.0	91	1030	1030
12.7	1.567	1.013	1.717	1.143	284.9	91	1030	1030
25.4	1.383	0.935	1.605	1.066	284.9	92	1030	1030
38.1	1.569	1.026	1.743	1.155	284.8	94	1030	996
50.8	1.594	1.035	1.751	1.149	284.7	92	1022	975
63.5	1.656	1.083	1.835	1.241	284.7	90	1014	944
76.2	1.760	1.133	1.909	1.282	284.6	89	1005	907
88.9	1.789	1.152	1.940	1.317	284.5	88	997	883
101.6	1.858	1.205	2.036	1.393	284.4	86	989	866
114.3	1.858	1.215	2.056	1.406	284.4	86	980	838
127.0	1.907	1.243	2.100	1.439	284.3	86	972	811
139.7	2.100	1.326	2.216	1.544	284.3	87	964	762
152.4	2.016	1.309	2.211	1.543	284.2	85	956	770
165.1	2.012	1.334	2.267	1.589	284.2	85	948	759
177.8	2.273	1.426	2.380	1.672	284.1	87	940	702

Gradient B , m = 0.002 .
P_o = 3.08 x 10^5 Nm^{-2}, T_o = 290.2°K

X(mm)	δ_i^x(mm)	Θ_i(mm)	ε_i(mm)	ε(mm)	T°K	Cfx10^5	mx10^6	Fx10^6
0	2.144	1.281	2.112	1.336	288.6	53	2030	2030
12.7	2.147	1.267	2.081	1.331	288.4	53	2030	2030
25.4	2.241	1.346	2.216	1.412	288.3	56	2030	2030
38.1	2.334	1.379	2.262	1.446	288.2	57	2030	1950
50.8	2.485	1.451	2.370	1.531	288.1	56	2024	1885
63.5	2.559	1.493	2.436	1.578	288.0	54	2017	1866
76.2	2.692	1.543	2.504	1.617	287.9	53	2011	1815
88.9	2.730	1.598	2.606	1.705	287.8	51	2005	1793
101.6	2.818	1.668	2.734	1.820	287.7	51	1998	1751
114.3	2.848	1.686	2.757	1.844	287.6	51	1992	1697
127.0	3.089	1.784	2.898	1.949	287.5	52	1985	1630
139.7	3.313	1.850	2.982	2.047	287.4	53	1979	1532
152.4	2.985	1.802	2.958	2.006	287.2	51	1973	1620
165.1	3.141	1.869	3.058	2.103	287.1	54	1966	1548
177.8	3.988	2.086	3.308	2.310	287.0	57	1960	1380

TABLE 2 (Concluded)

Gradient B , $m = 0.003$.
$P_o = 3.08 \times 10^5 Nm^{-2}$, $T_o = 290.2°K$

X(mm)	δ_i^x(mm)	Θ_i(mm)	ε_i(mm)	ε(mm)	T°K	Cfx10^5	mx10^6	Fx10^6
0	2.786	1.552	2.503	1.568	289.8	32	3030	3030
12.7	3.012	1.634	2.608	1.610	289.7	32	3030	3030
25.4	3.027	1.680	2.695	1.673	289.6	33	3030	3030
38.1	3.401	1.778	2.811	1.744	289.5	35	3030	2879
50.8	3.649	1.900	3.002	1.869	289.4	34	3022	2846
63.5	3.842	1.940	3.050	1.897	289.3	33	3014	2762
76.2	4.008	2.007	3.143	1.991	289.2	32	3005	2652
88.9	4.008	2.078	3.278	2.095	289.1	31	2997	2638
101.6	4.217	2.185	3.445	2.209	289.0	31	2989	2583
114.3	4.595	2.277	3.554	2.315	288.9	32	2981	2453
127.0	4.858	2.392	3.723	2.432	288.8	32	2973	2393
139.7	5.247	2.455	3.788	2.519	288.7	33	2965	2264
152.4	4.961	2.555	4.015	2.684	288.6	33	2956	2312
165.1	6.235	2.616	3.973	2.712	288.5	34	2948	2066
177.8	6.455	2.717	4.167	2.936	288.4	36	2940	1988

Gradient C , $m = 0$.
$P_o = 4.12 \times 10^5 Nm^{-2}$, $T_o = 290.2°K$

X'(mm)	δ_i^x(mm)	Θ_i(mm)	ε_i(mm)	ε(mm)	T°K	Cfx10^6	mx10	Fx10	$-\beta$
0	0.784	0.581	1.037	0.727	287.6	1540	0	0	0
12.7	0.755	0.568	1.020	0.720	287.7	1540	0	0	0
25.4	0.835	0.628	1.125	0.793	287.8	1560	0	0	0
38.1	0.790	0.595	1.068	0.749	287.9	1590	0	0	0
50.8	0.912	0.689	1.237	0.875	288.0	1600	0	0	0
63.5	0.819	0.632	1.144	0.808	288.1	1595	0	0	0.57
76.2	0.815	0.639	1.163	0.819	288.2	1585	0	0	0.59
88.9	0.885	0.695	1.266	0.893	288.3	1580	0	0	0.67
101.6	0.881	0.699	1.278	0.897	288.4	1580	0	0	0.70
114.3	0.914	0.725	1.326	0.929	288.5	1580	0	0	0.77
127.0	0.930	0.745	1.369	0.961	288.6	1580	0	0	0.82
139.7	0.955	0.768	1.413	0.986	288.7	1575	0	0	0.88
152.4	0.967	0.782	1.441	0.999	288.8	1565	0	0	0.75
165.1	1.036	0.835	1.536	1.061	288.9	1550	0	0	0.64
177.8	1.058	0.852	1.567	1.061	289.0	1535	0	0	0.53
190.5	1.101	0.889	1.637	1.138	289.1	1520	0	0	0.44
203.2	1.117	0.901	1.657	1.144	289.2	1510	0	0	0.36
215.9	1.301	1.048	1.924	1.359	289.3	1500	0	0	0.30

Gradient C , $m = 0.001$.
$P_o = 5.84 \times 10^5 Nm^{-2}$, $T_o = 289.1°K$

X'(mm)	δ_i^x(mm)	Θ_i(mm)	ε_i(mm)	ε(mm)	T°K	Cfx10^5	mx10^6	Fx10^6
0	1.162	0.792	1.365	0.923	285.1	83	970	970
12.7	1.188	0.816	1.412	0.964	285.2	82	970	970
25.4	1.225	0.844	1.460	0.980	285.4	83	970	1007
38.1	1.266	0.888	1.546	1.055	285.5	86	970	1005
50.8	1.411	0.975	1.690	1.136	285.7	83	970	1085
63.5	1.360	0.965	1.687	1.138	285.9	83	977	1101
76.2	1.335	0.974	1.719	1.164	286.1	79	985	1180
88.9	1.351	0.995	1.764	1.187	286.2	76	992	1255
101.6	1.353	0.994	1.762	1.180	286.4	74	999	1324
114.3	1.498	1.097	1.942	1.289	286.5	72	1006	1386
127.0	1.481	1.097	1.949	1.287	286.7	70	1014	1467
139.7	1.563	1.158	2.059	1.359	286.9	68	1021	1493
152.4	1.642	1.217	2.164	1.417	287.1	65	1028	1600
165.1	1.746	1.295	2.301	1.499	287.2	62	1035	1664
177.8	1.888	1.389	2.463	1.573	287.3	59	1043	1738
190.5	1.910	1.411	2.505	1.595	287.4	56	1050	1844
203.2	1.948	1.420	2.510	1.593	287.5	54	1057	1909
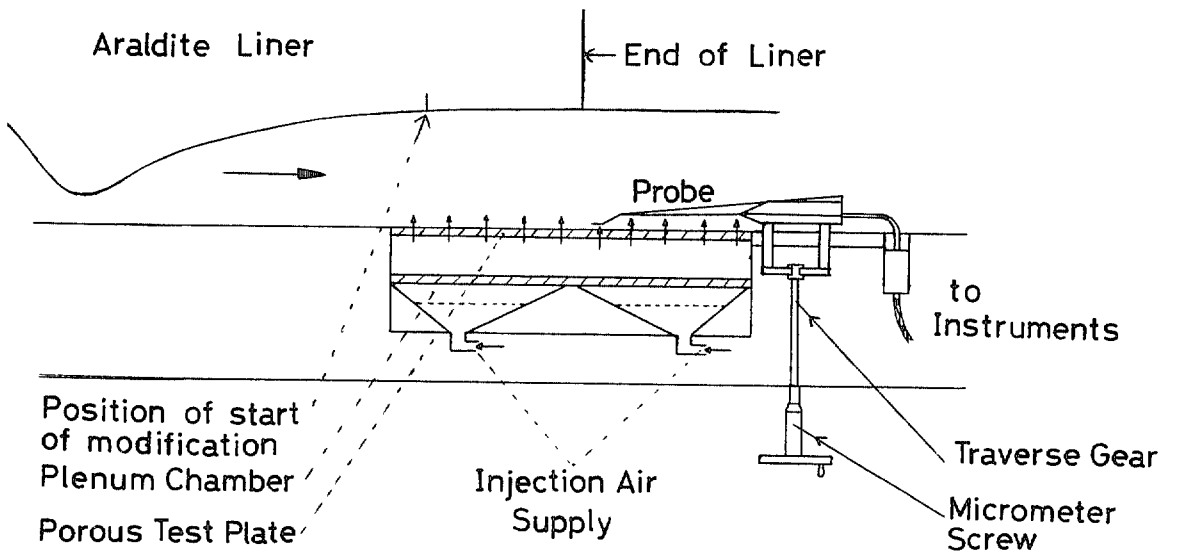
FIG. 1. X-Section of Tunnel.
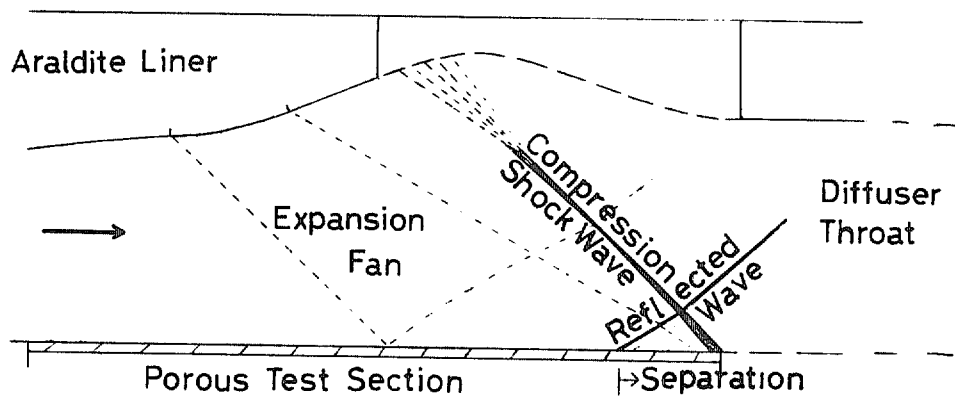
FIG. 2. Design of Pressure Gradients A and C.

PROBE HOLDER

PITOT PROBE MOUTHS

0.06 mm
.032 mm
.032 mm

← 1.05mm →

0.051mm
0.044mm
0.036mm

← 1.55mm →

.0815 mm
0.031 mm
.0405 mm

0.9mm

0.0545mm
0.025mm
0.0535mm

← 1.4mm →

TEMPERATURE PROBE

Hypodermic tube

Ceramic

1.65mm

10°

Thermocouple

← 2.5mm →

STATIC PRESSURE PROBE

1mm

5°

0.4mm

← 20mm →
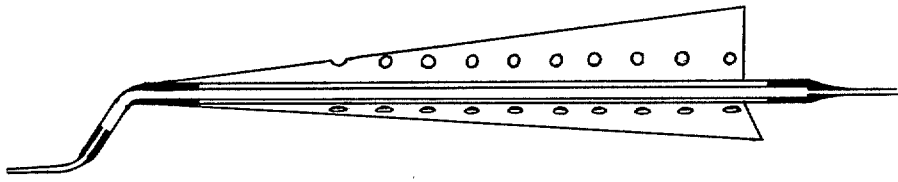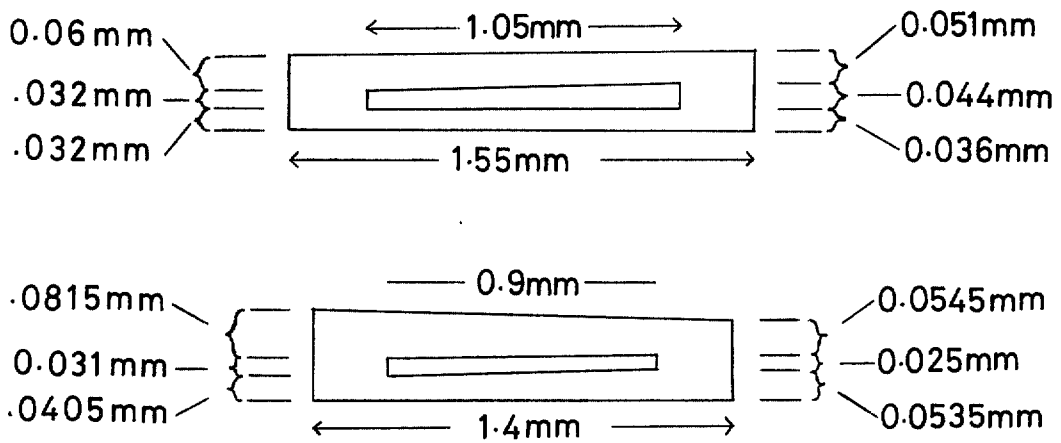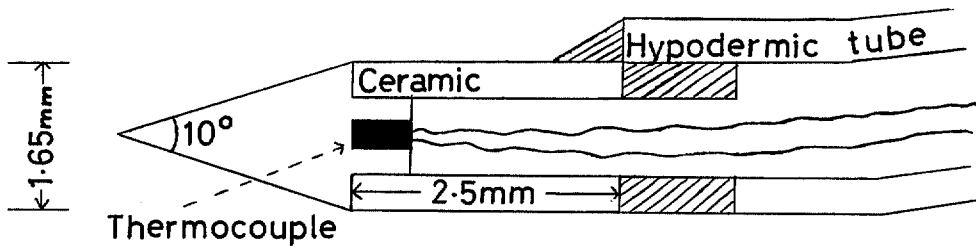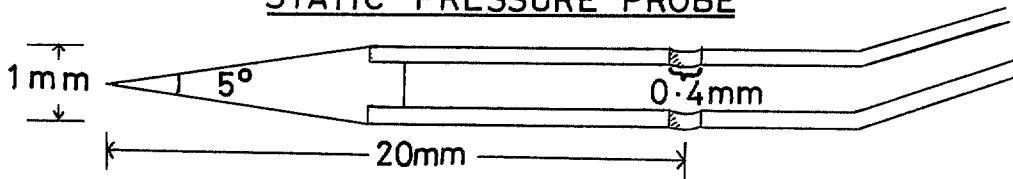
Fig. 3. Probes.
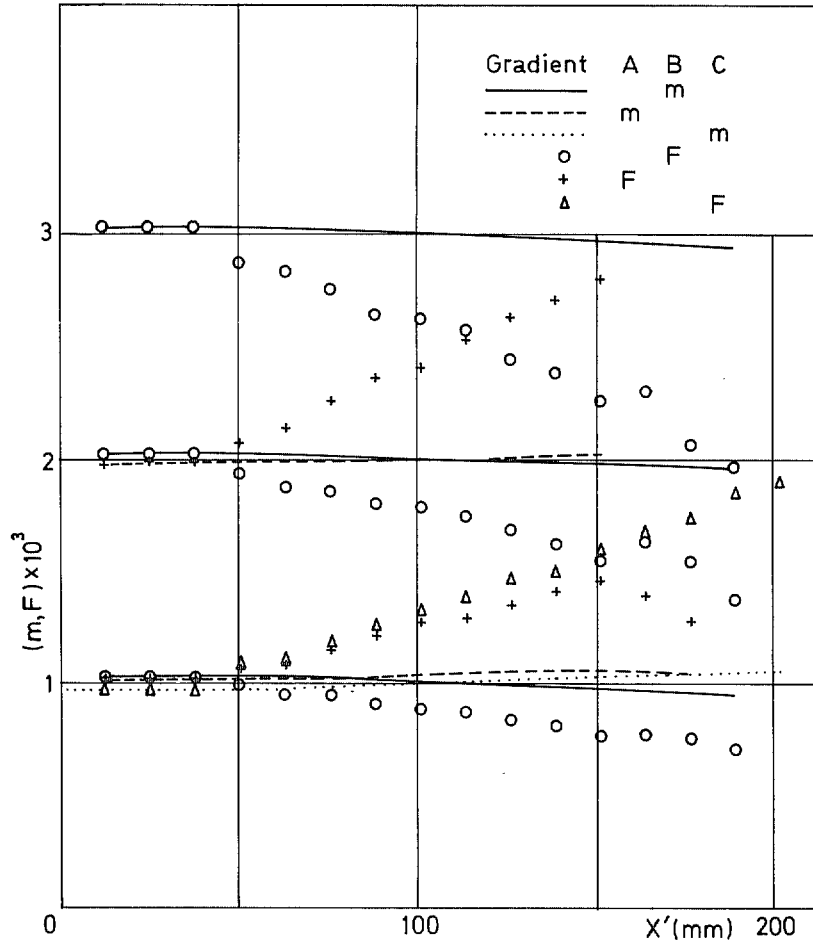
FIG. 4. Variation of m and F.
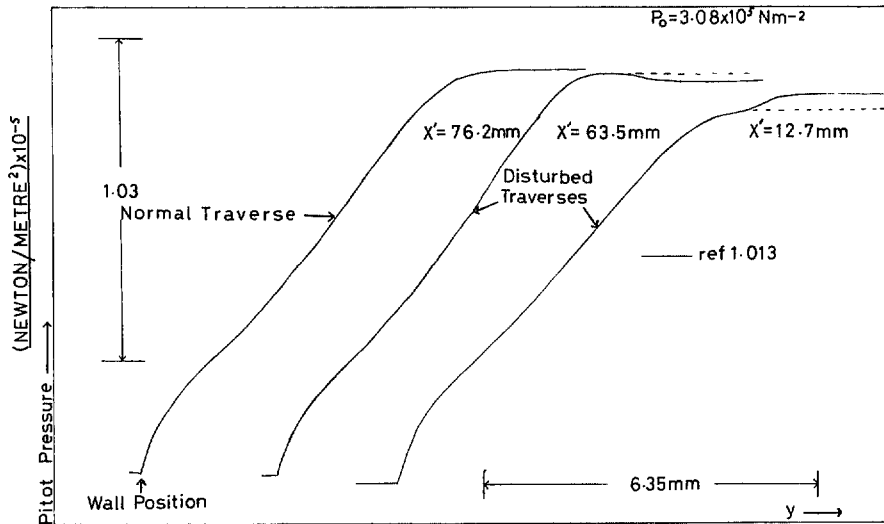
FIG. 5. Gradient B Disturbed Profiles.

razor blade

PRESENT CONFIGURATION

static pressure
hole

SMITH GAUDET
& WINTER
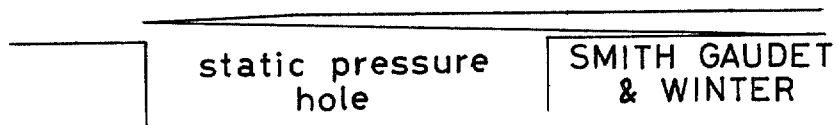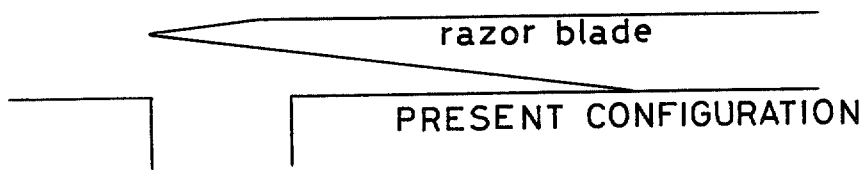
The scale of the above two is equal,
that below is ~ ¼th. of the above.

HOPKINS & KEENER
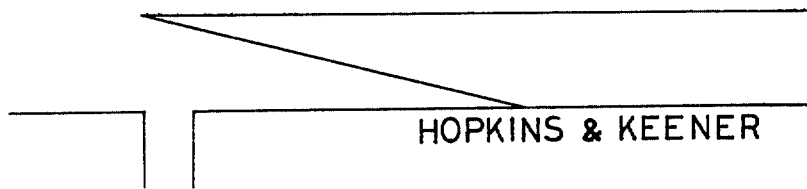
PRESENT STANTON TUBE DETAILS

~.9mm

=⟩~.03mm

0.14mm

} ~.025mm

.254mm

Cataloy Paste

3·8mm

6·35mm
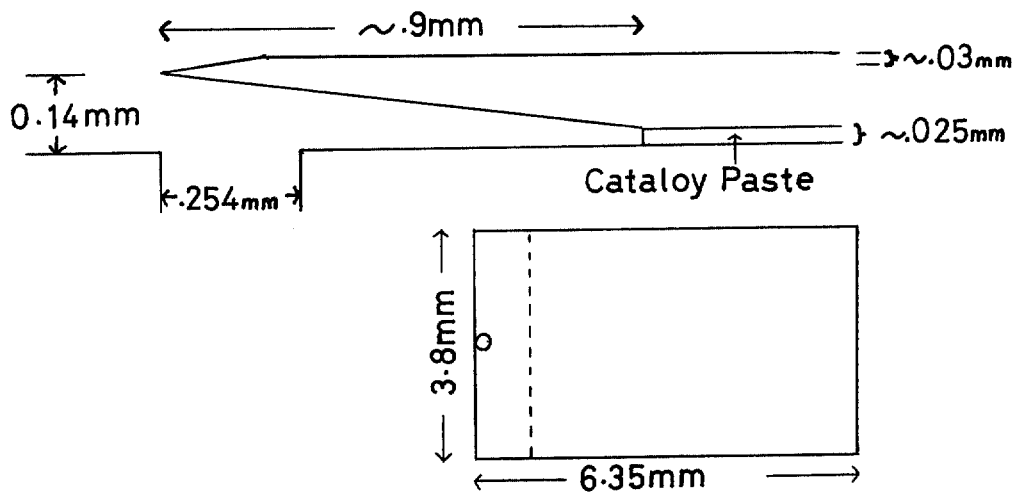
FIG. 6.   Stanton Tube Geometry.
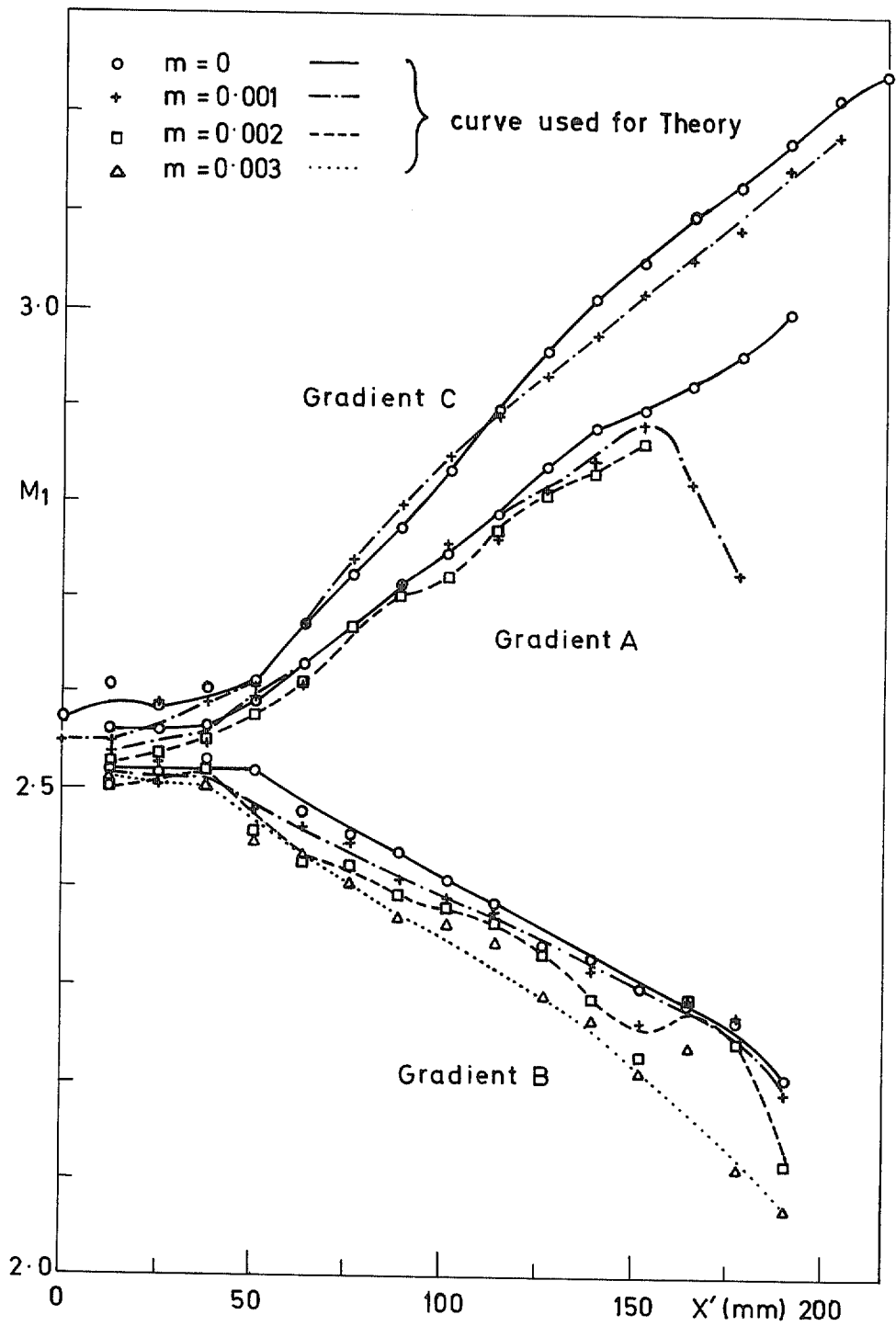
FIG. 7. Free-Stream Mach Number Variation.

52
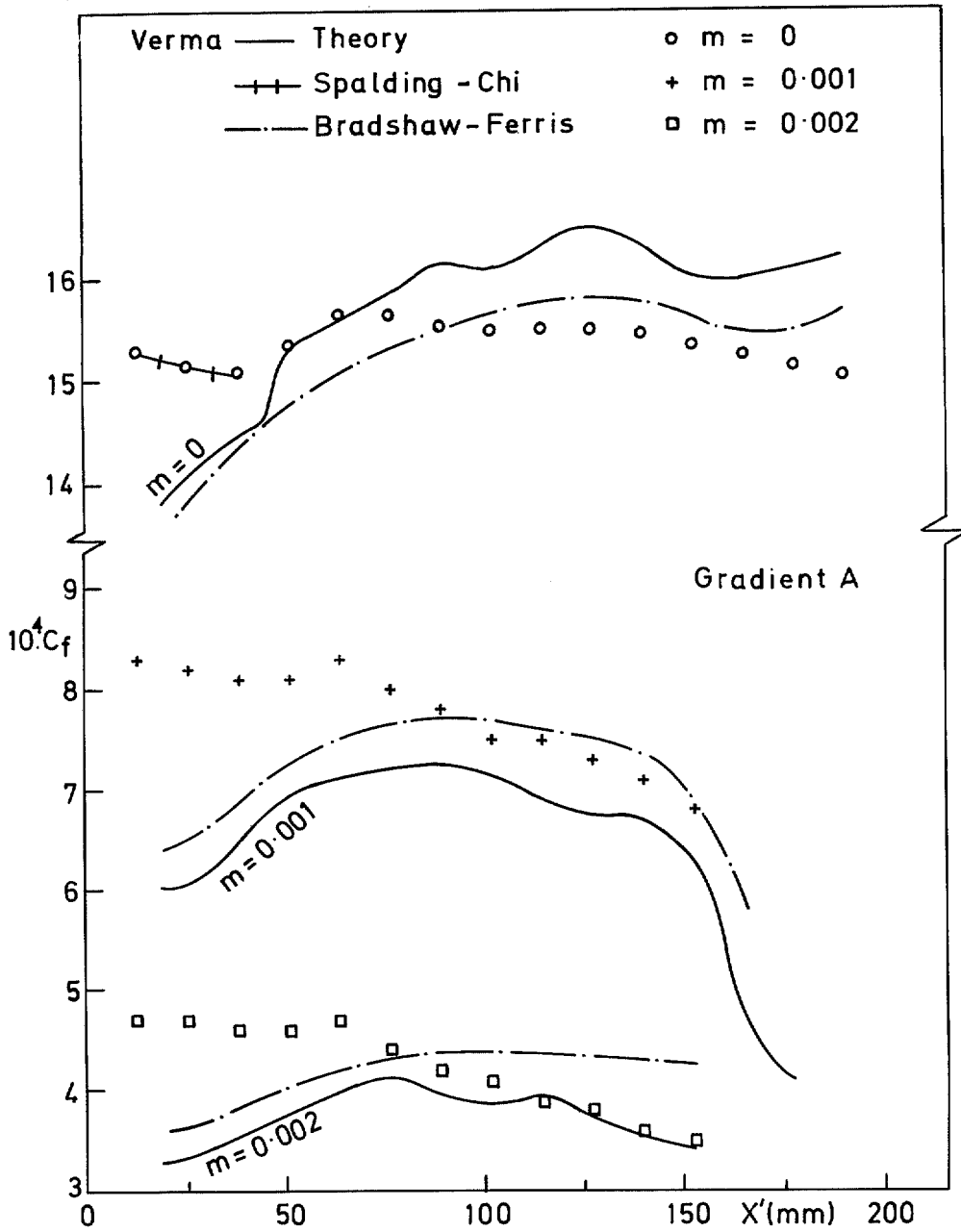
FIG. 8. Variation of Skin Friction.
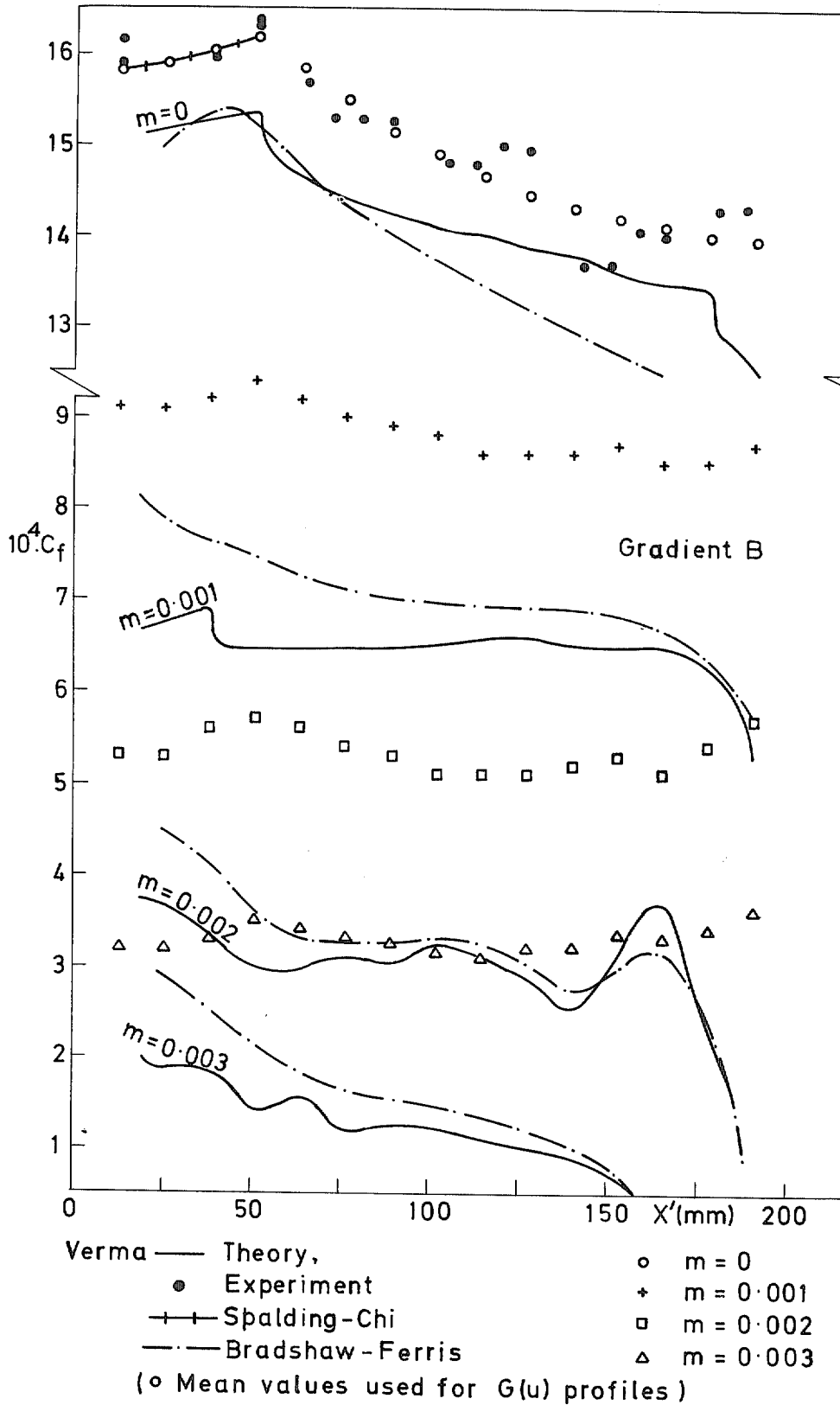
FIG. 9. Variation of Skin Friction.
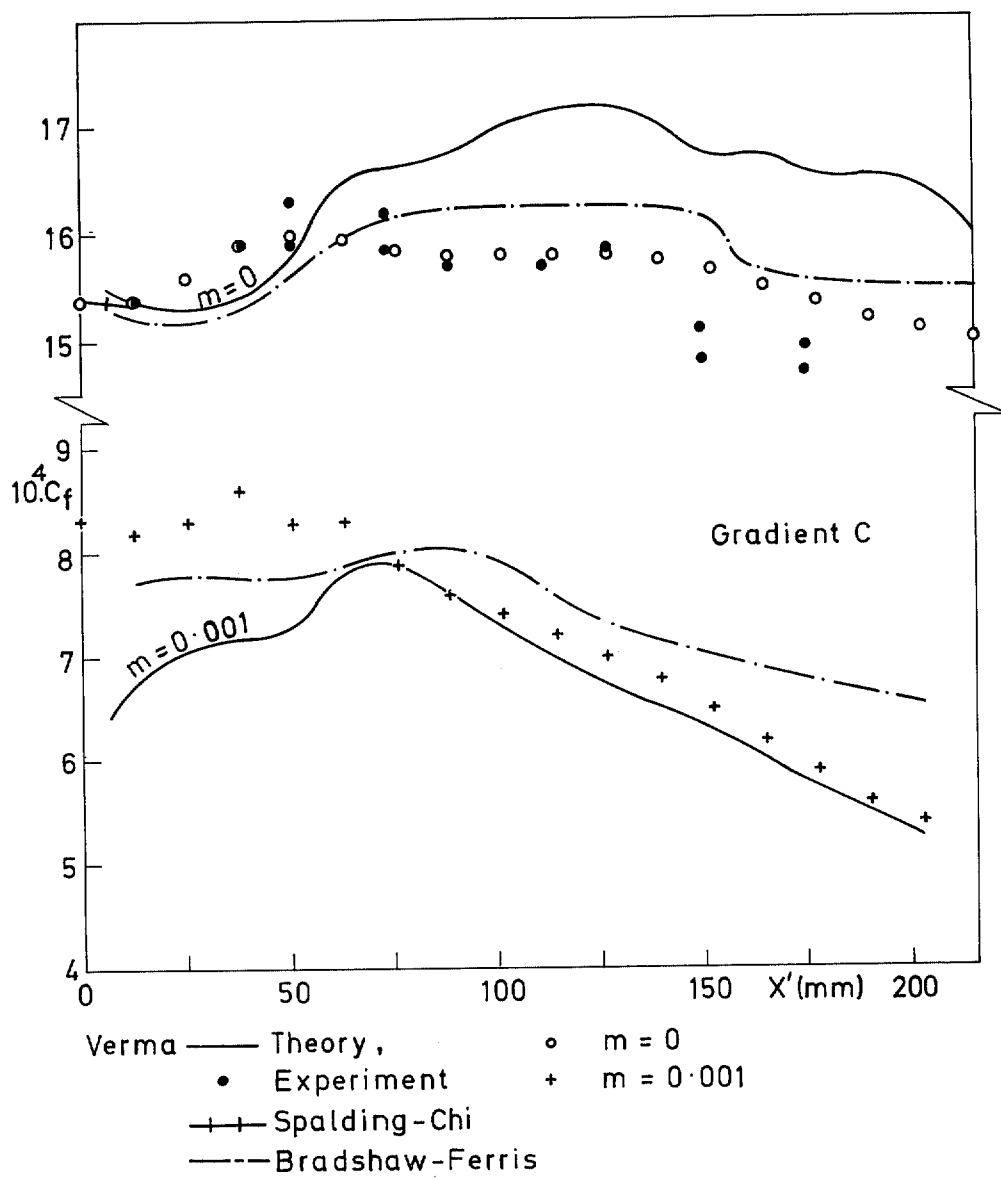
FIG. 10. Variation of Skin Friction.
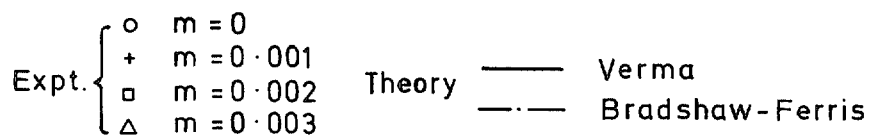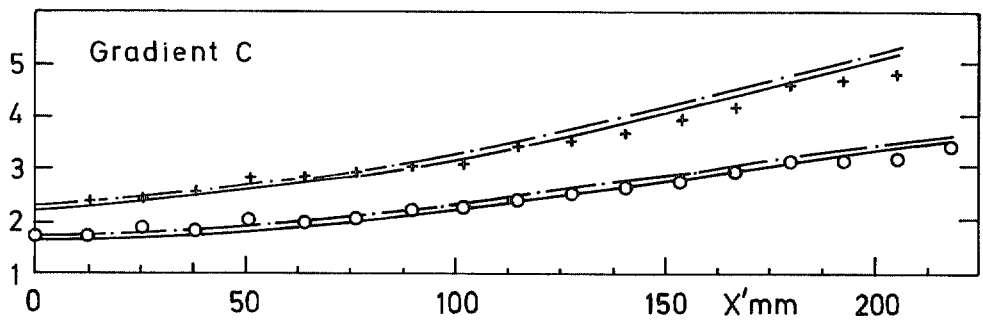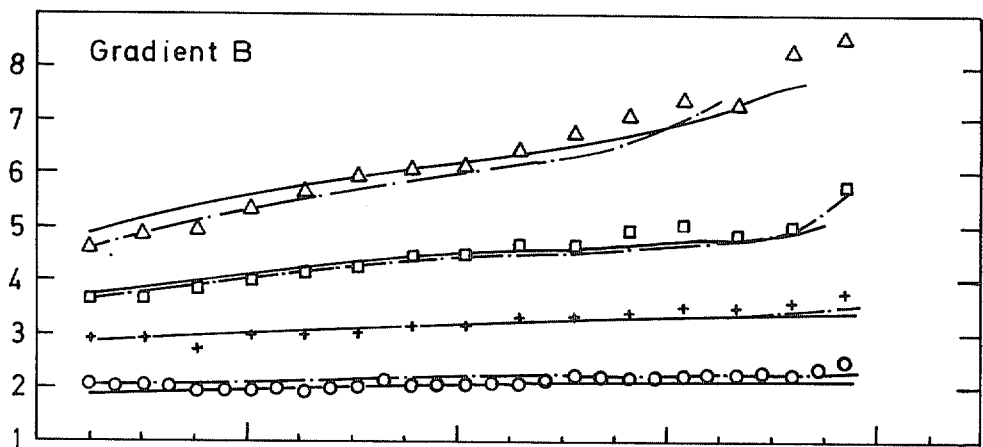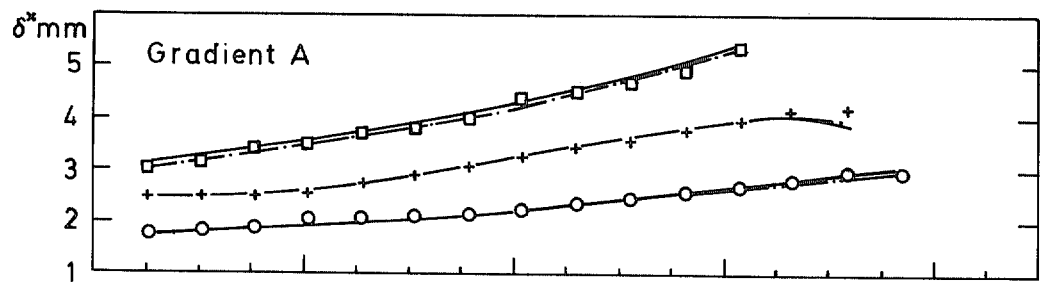
FIG. 11. Variation of Displacement Thickness.
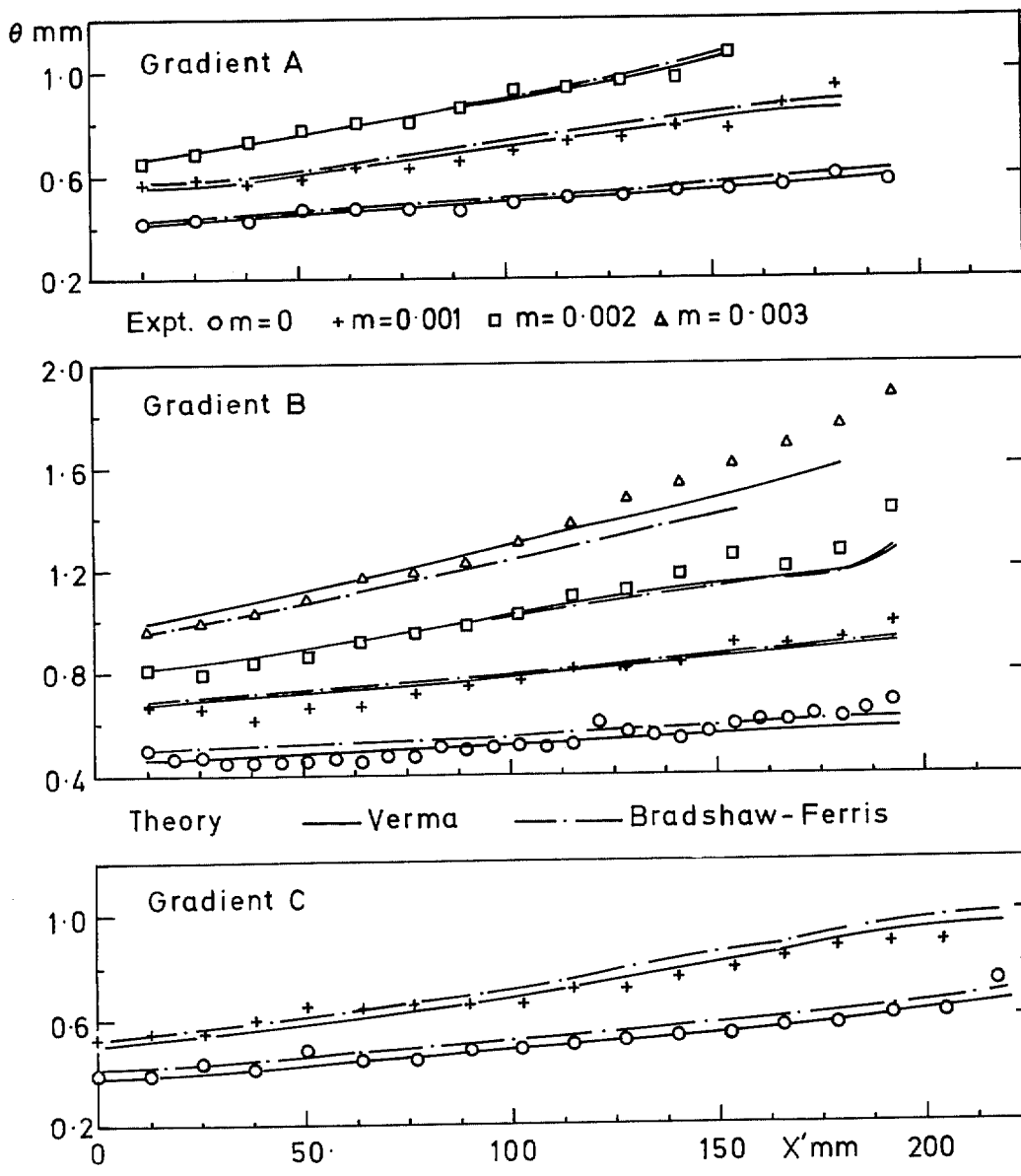
FIG. 12. Variation of Momentum Thickness.
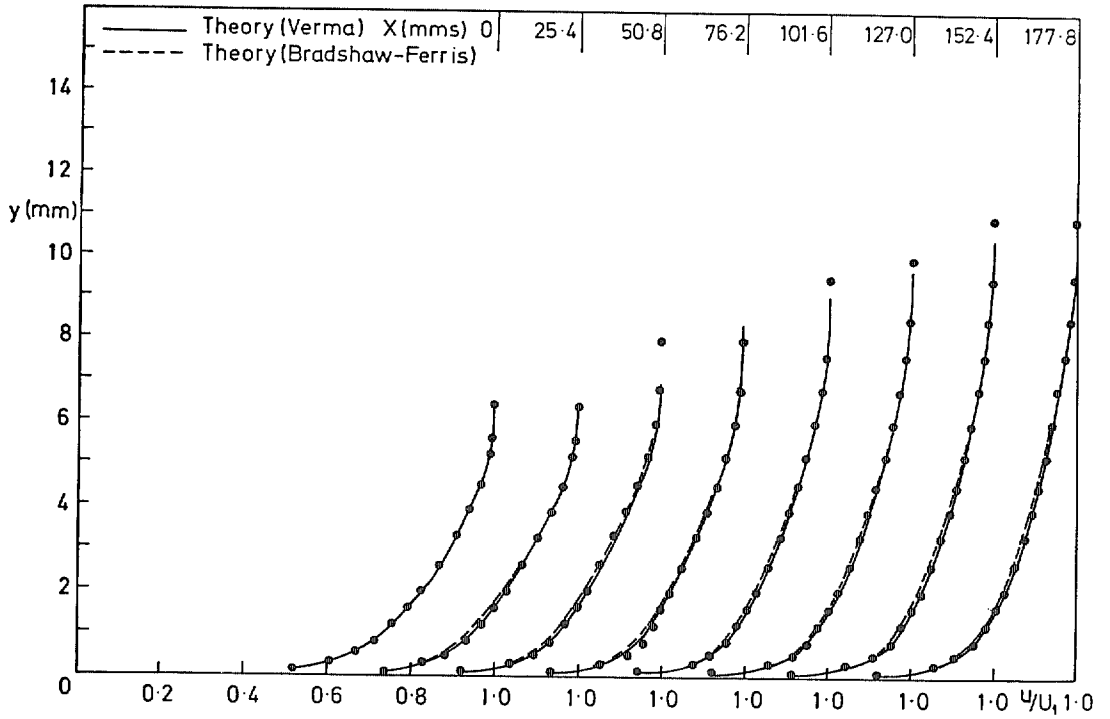
FIG. 13. Velocity Profiles Gradient A $m = 0$.
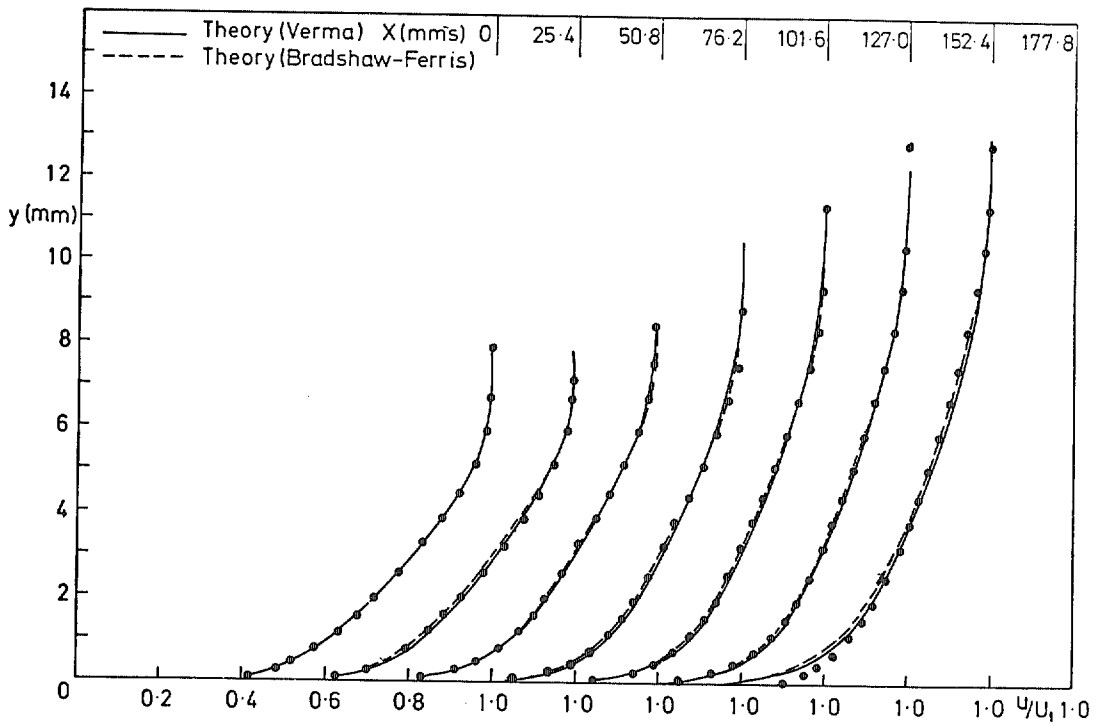
FIG. 14. Velocity Profiles Gradient A $m = 0.001$.

58
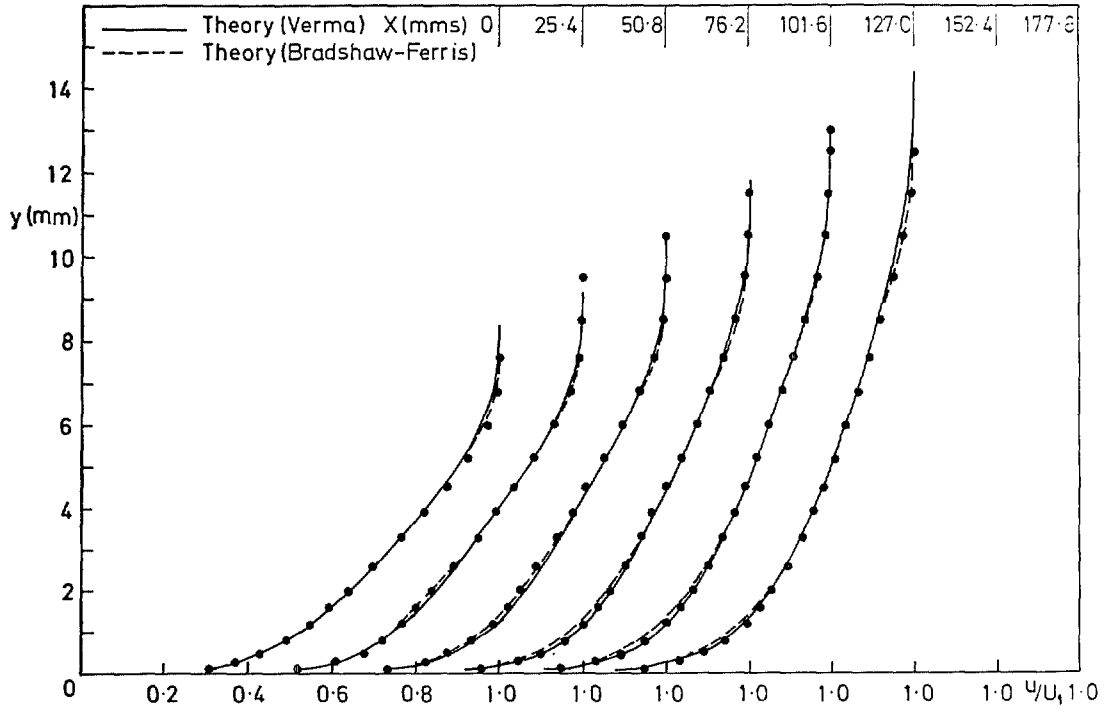
FIG. 15.   Velocity Profiles Gradient A $m = 0.002$.
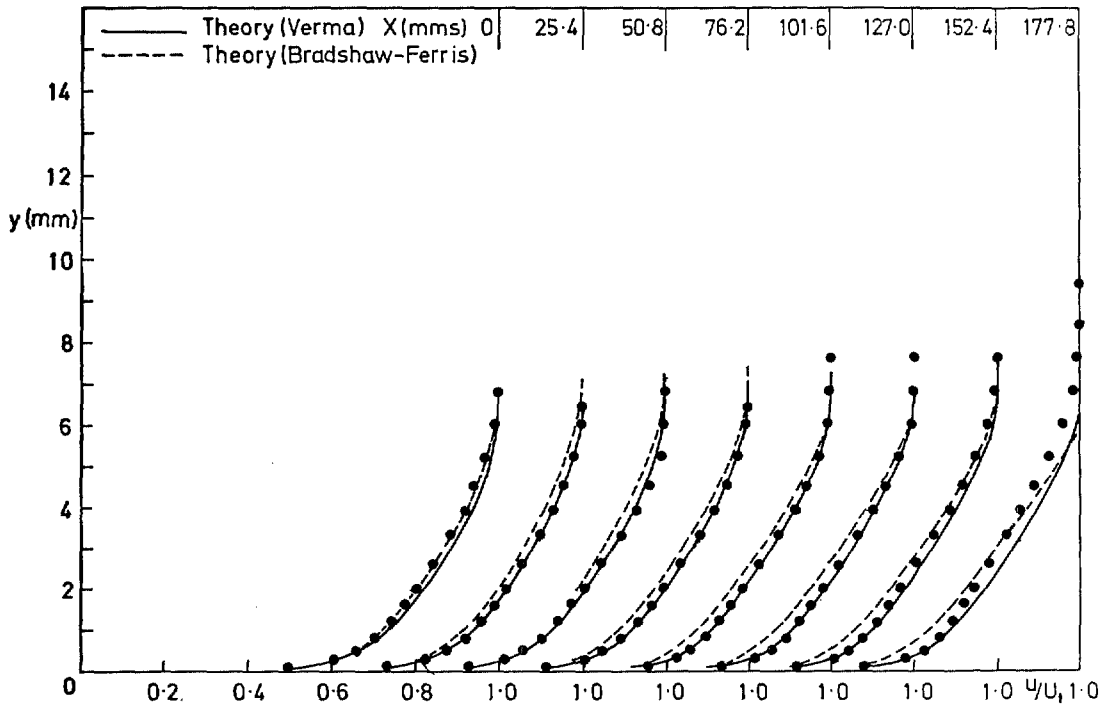
FIG. 16.   Velocity Profiles Gradient B $m = 0$.

59
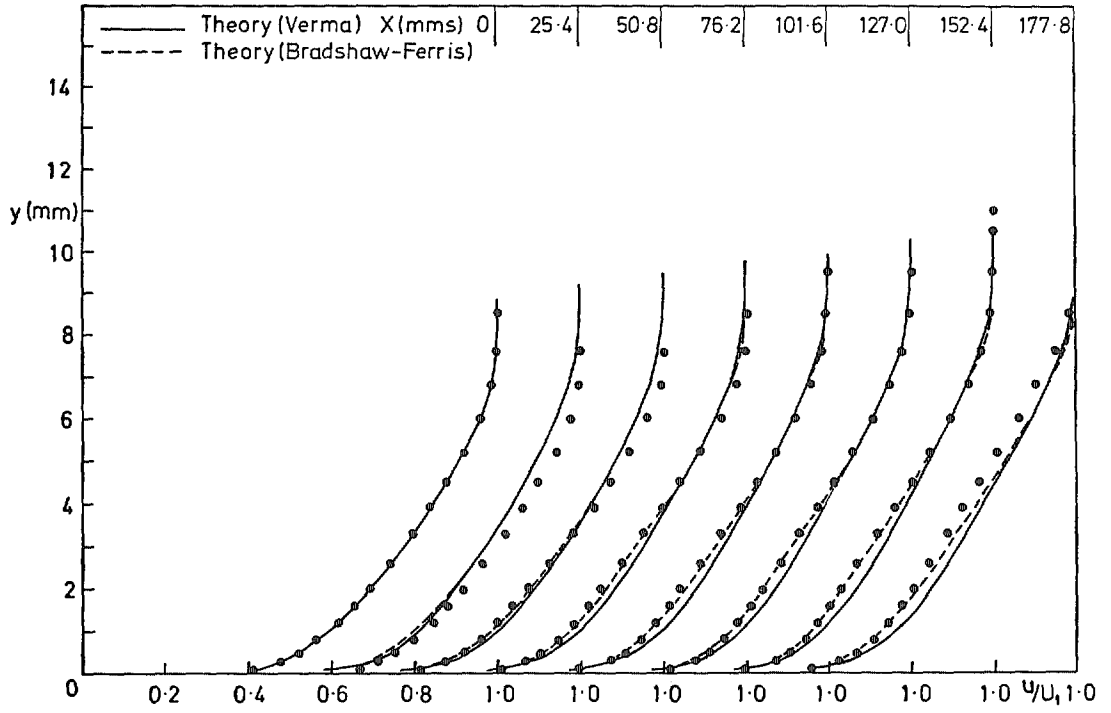
FIG. 17.   Velocity Profiles Gradient B $m = 0.001$.
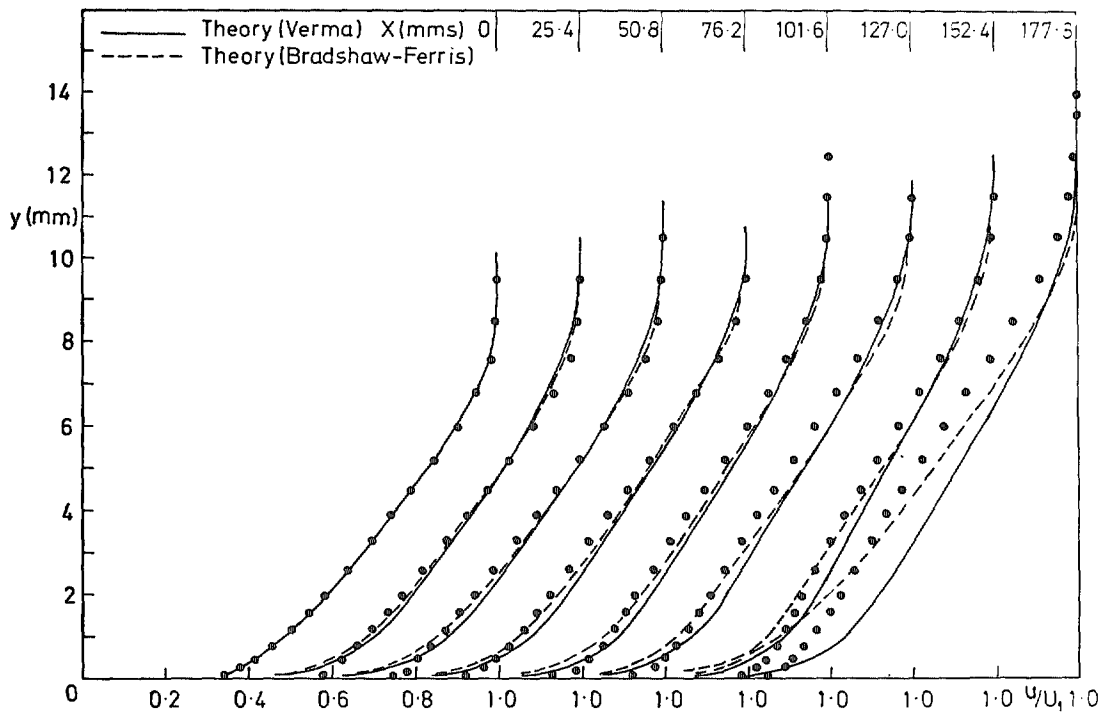
FIG. 18.   Velocity Profiles Gradient B $m = 0.002$.

60
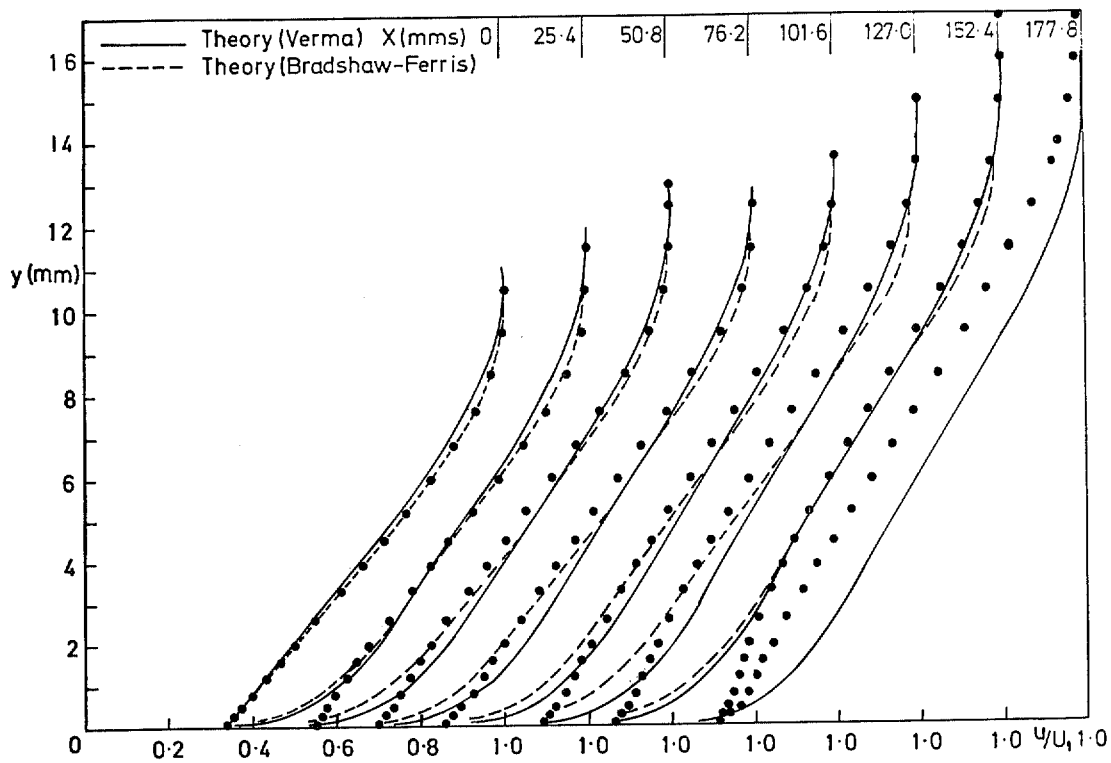
FIG. 19.   Velocity Profiles Gradient B $m = 0·003$.
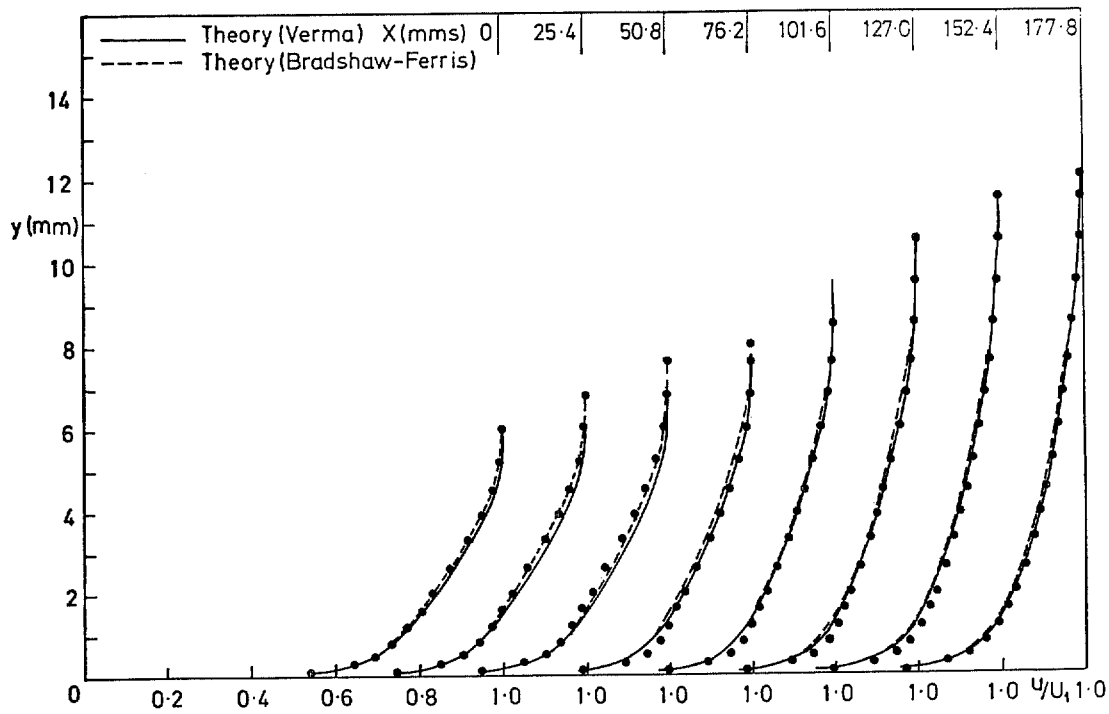
FIG. 20.   Velocity Profiles Gradient C $m = 0$.
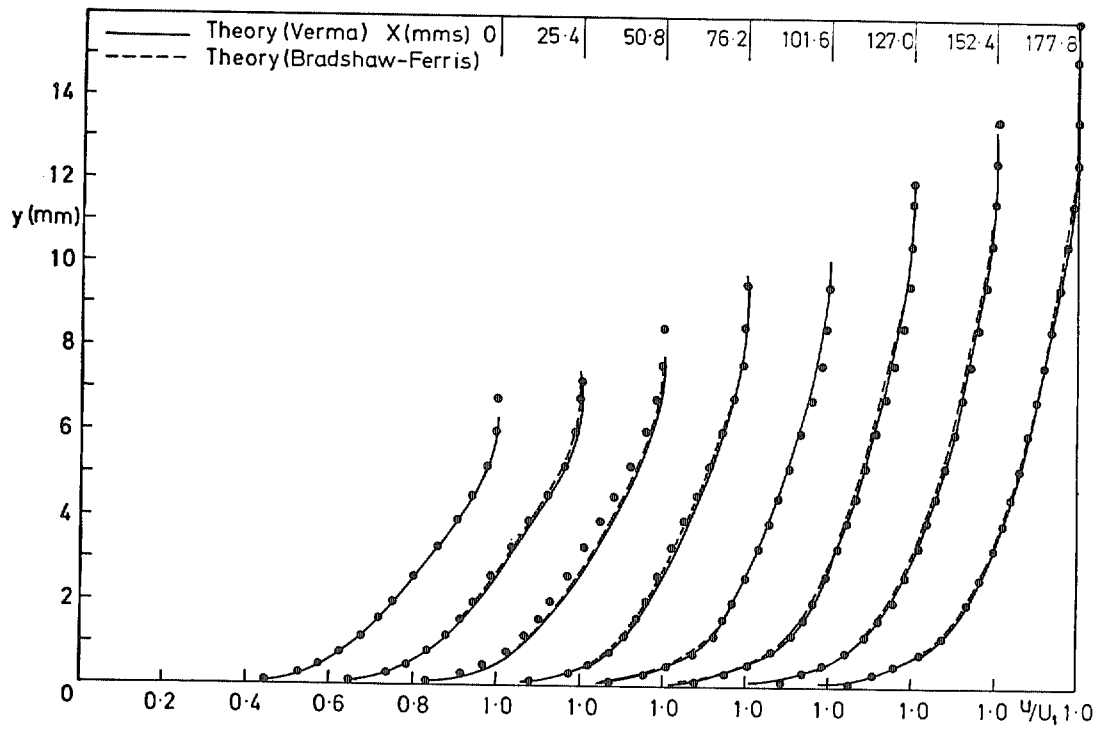
FIG. 21.   Velocity Profiles Gradient C $m = 0.001$.

	Author	M_1	β
o	Ludwieg-Tillman	0	0·58
+	"	0	0·48
△	"	0	1·92
x	Baker	0	0·98
□	"	0	1·18
◊	Schubauer Klebanoff	0	1·74
⊿	"	0	12·00
▽	Stratford	0	16·30
●	Peake et al	2·9	1·00
■	"	2·9	1·03
▲	"	3·19	1·33
◆	"	3·19	1·37
▼	"	2·08	1·40
◀	"	2·08	1·42
▶	"	2·08	1·60
◤	"	2·08	1·62
◣	Sivasegaram	2·37	0·235
◤	"	2·15	0·52
▽	Voisinet et al	4·17	2·00
◁	"	4·39	1·70
△	"	4·62	1·20
—	Thomas Gradient B		0·5-0·6

FIG. 22.   Velocity profiles $\beta > 0$, $\nu_\omega / U_1 = 0$.

	Author	Gas	v_w/U_1	β
o	Baker	Air	0·0027	0·98
+	,,	,,	0·0038	0·98
×	,,	,,	0·0062	0·98
□	,,	,,	0·0061	1·18
△	,,	,,	0·0032	1·18
▽	,,	Freon	0·0021	4·20
◇	,,	,,	0·0041	4·20
▥	,,	,,	0·0019	1·24
●	,,	,,	0·0037	1·24
▲	McQuaid	Air	0·0020	0·46
▼	,,	,,	0·0019	0·20
—·—	Thomas	,,	0·0021	0·5-0·6
—··—	,,	,,	0·0040	,,
—···—	,,	,,	0·0059	,,

y/θ_i

u/U_1

FIG. 23.   Velocity Profiles $\beta > 0$, $\nu_\omega/U_1 > 0$.

Author	M_1	$-\beta$
o Herring Norbury	0	0·62
+ Loyd	0	0·64
× "	0	0·93
□ Julien	0	0·61
△ Baker	0	0·47
▽ "	0	0·78
● Sivasegaram	2·38	0·16
■ "	2·60	0·33
▲ "	2·70	0·33
◄ Michel et al	2·25	0·40
▶ "	1·83	0·49
▼ "	2·57	0·54
▷ "	2·88	0·64
—— Thomas Gradient A	0·6 – 0·7	
– – " " C	0·7 – 0·85	

FIG. 24.   Velocity Profiles $\beta < 0$, $\nu_\omega / U_1 = 0$.

Author	Gas	v_w/U_1	$-\beta$
○ Julien	Air	0·001	0·61
+ "	"	0·002	0·61
◇ "	"	0·004	0·61
× Loyd	"	0·002	0·75
● "	"	0·004	0·82
□ Baker	"	0·0017	0·47
△ "	"	0·0033	0·47
▽ "	"	0·0036	0·78
▣ "	"	0·0068	0·47
▲ "	"	0·0071	0·78
◆ "	Freon	0·0031	0·46
▼ "	"	0·006	0·46
◁ "	"	0·002	1·01
◀ "	"	0·0043	1·01
▱ McQuaid	Air	0·0066	1·28
▱ "	"	0·0046	0·77
▱ "	"	0·0035	0·40
—--- Thomas	"	0·0025	0·6-0·7
—-- "	"	0·0051	0·6-0·7
—·— "	"	0·0026	0·7-0·85

FIG. 25.   Velocity Profiles $\beta < 0$, $v_\omega/U_1 > 0$.

66

FIG. 26.   Temperature Profiles Gradient A.
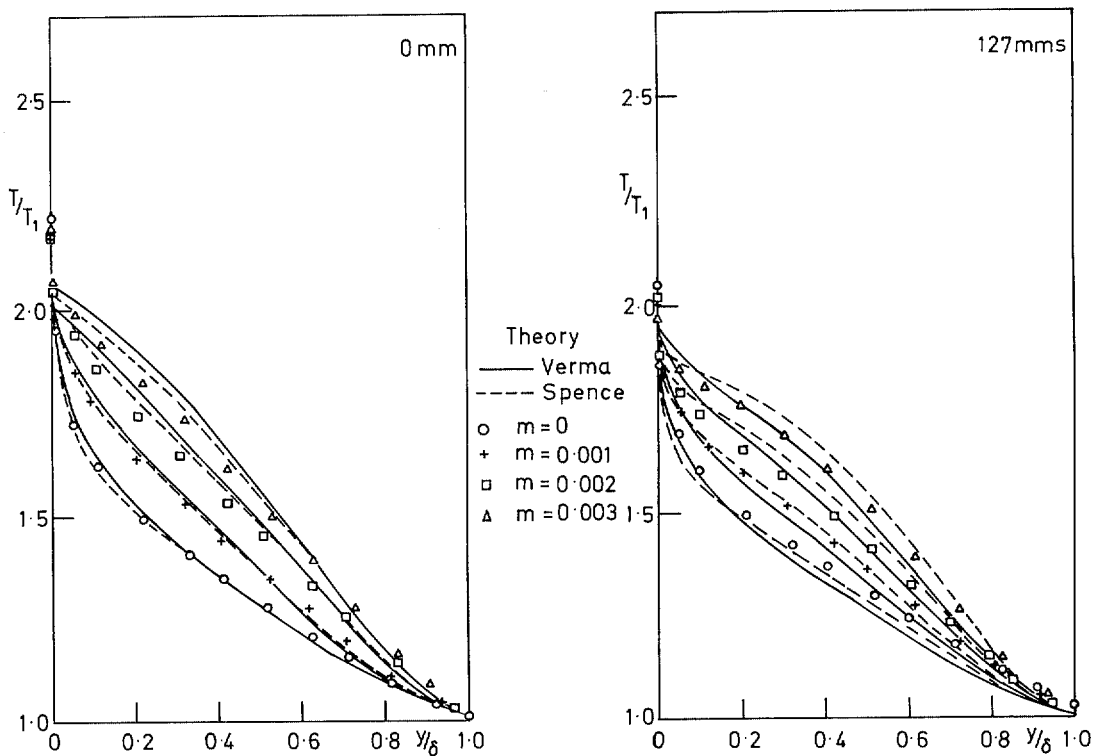
FIG. 27.   Temperature Profiles Gradient B.
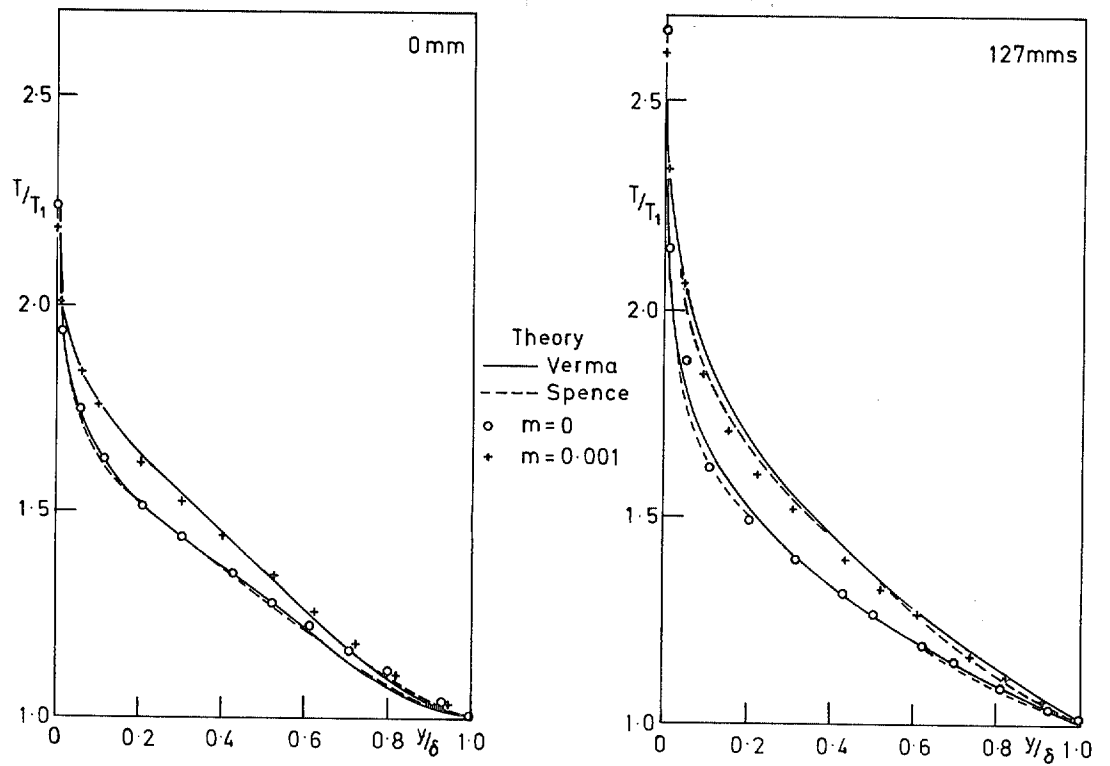
FIG. 28.   Temperature Profiles Gradient C.
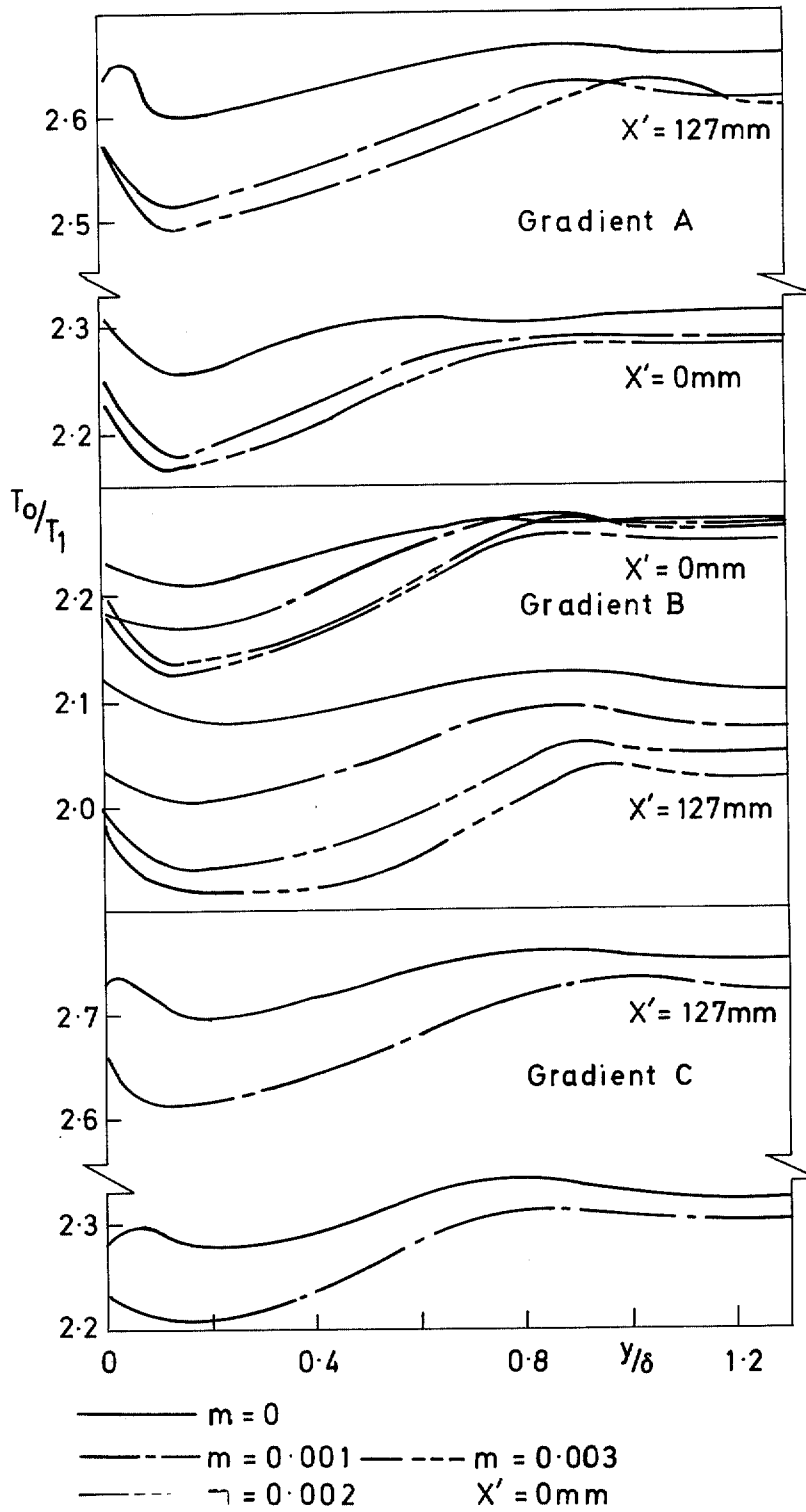
FIG. 29.   Variation of T_0 with y.
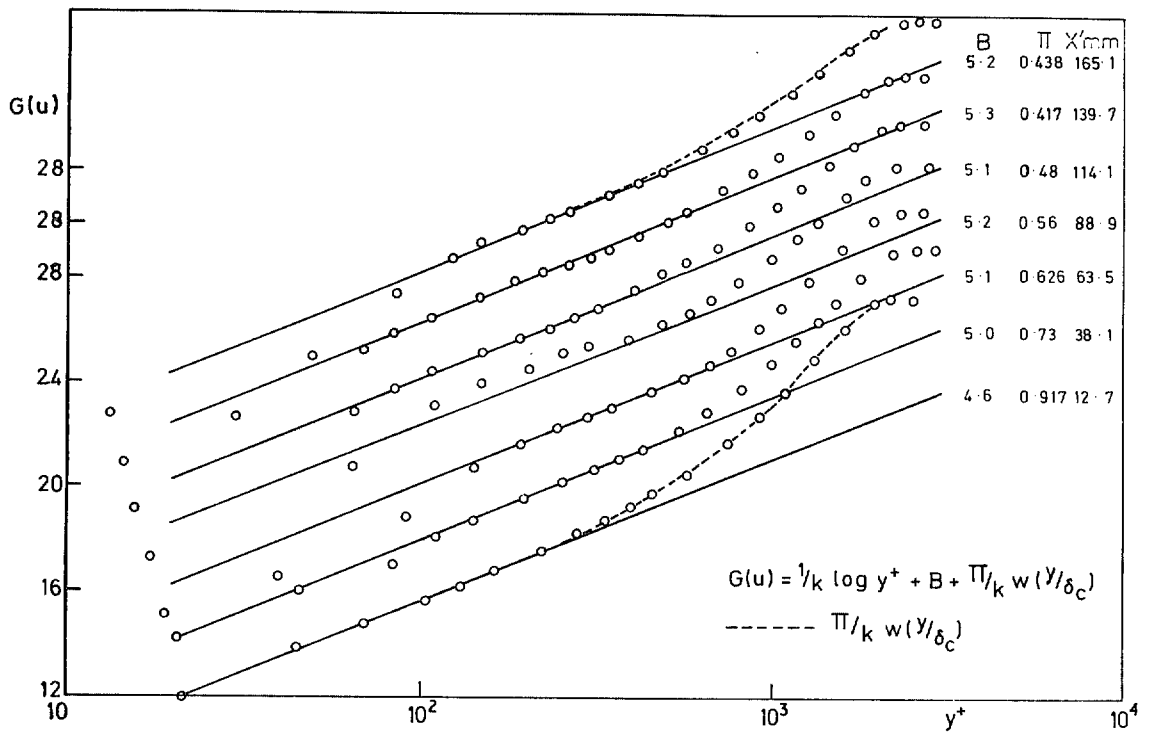
FIG. 30. $G(u)$ vs log y^+ Gradient A $m = 0$.

FIG. 31. $G(u)$ vs log y^+ Gradient A $m = 0.002$.

70

		B	Π	X'mm
		4·7	0·94	12·7
		4·9	0·81	38·1
		4·7	0·94	63·5
		4·9	1·0	88·9
		5·4	1·06	139·7
		5·5	1·2	165·1
		4·9	1·25	190·5

FIG. 32. $G(u)$ vs log y^+ Gradient B $m = 0$.

B	Π	X'mm
1·4	1·13	12·7
0·05	1·25	38·1
-0·6	1·37	63·5
0·1	1·46	88·9
-0·7	1·63	114·3
-2·2	1·96	139·7
-4·2	2·46	165·1
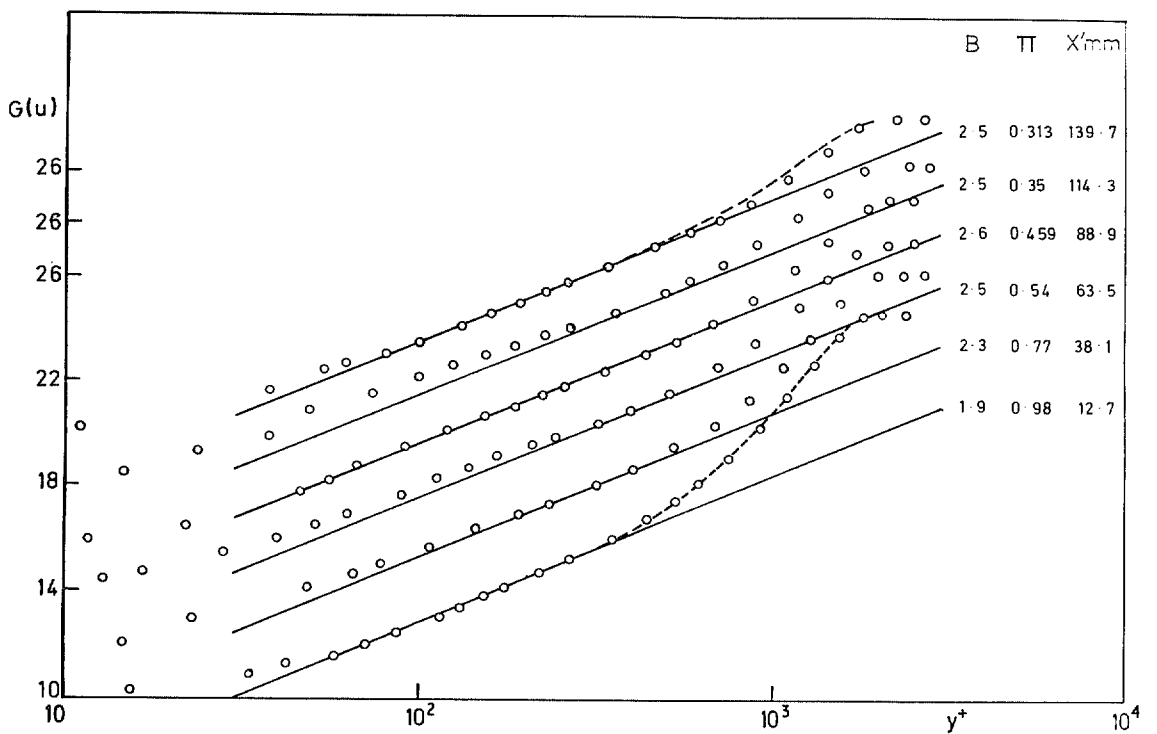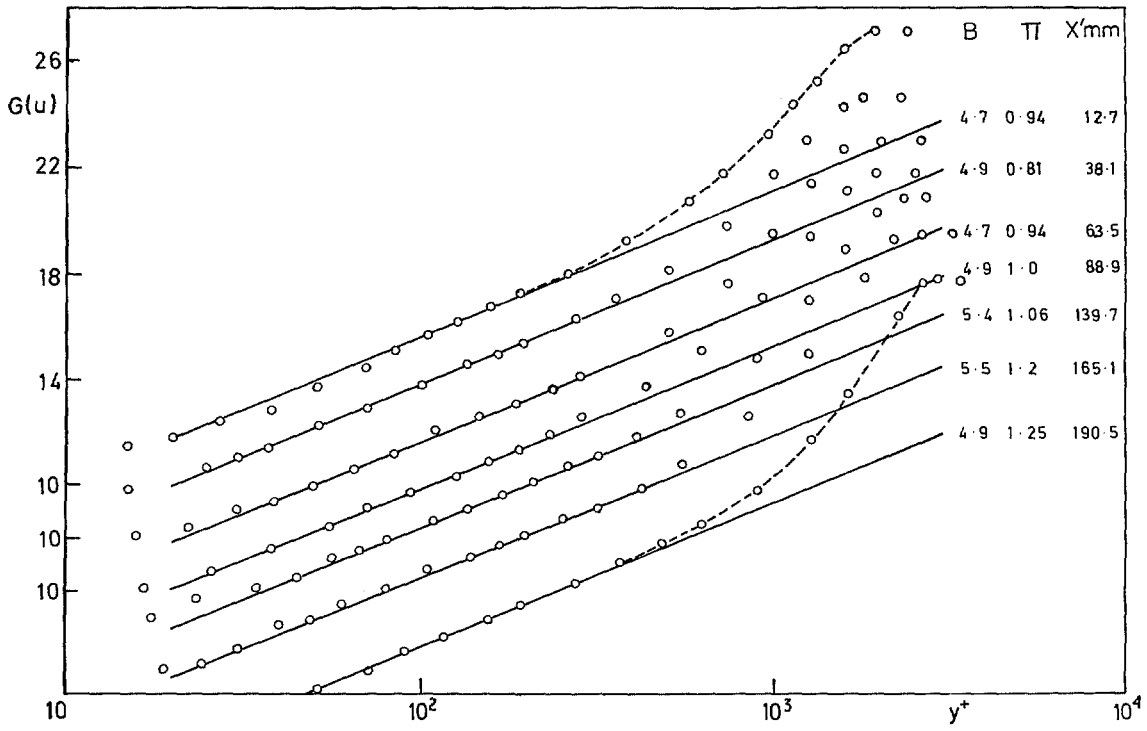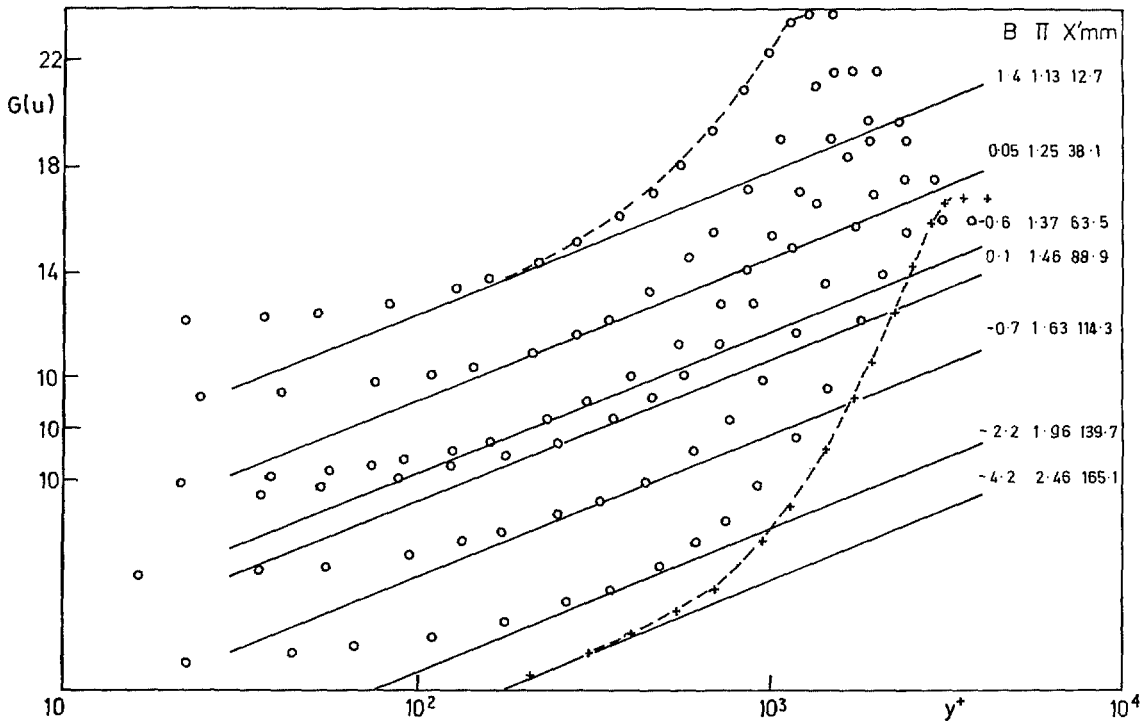
FIG. 33. $G(u)$ vs log y^+ Gradient B $m = 0·003$.
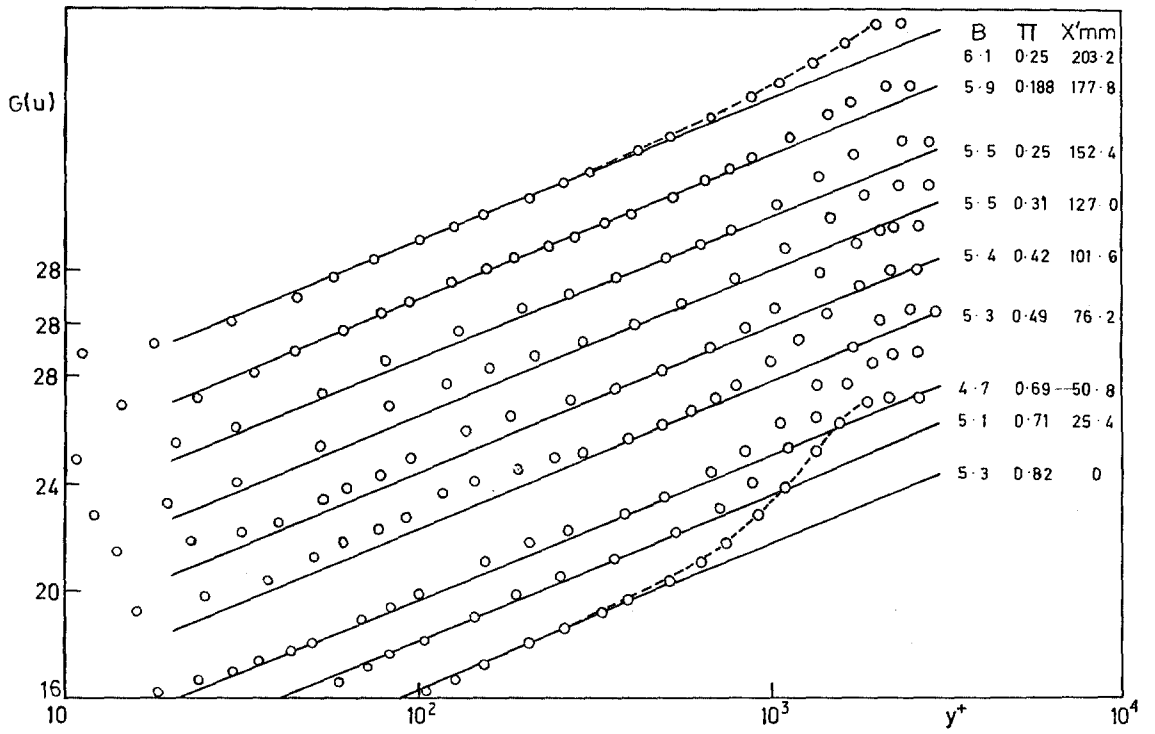
FIG. 34. $G(u)$ vs log y^+ Gradient C $m = 0$.

FIG. 35. $G(u)$ vs log y^+ Gradient C $m = 0{\cdot}001$.

72
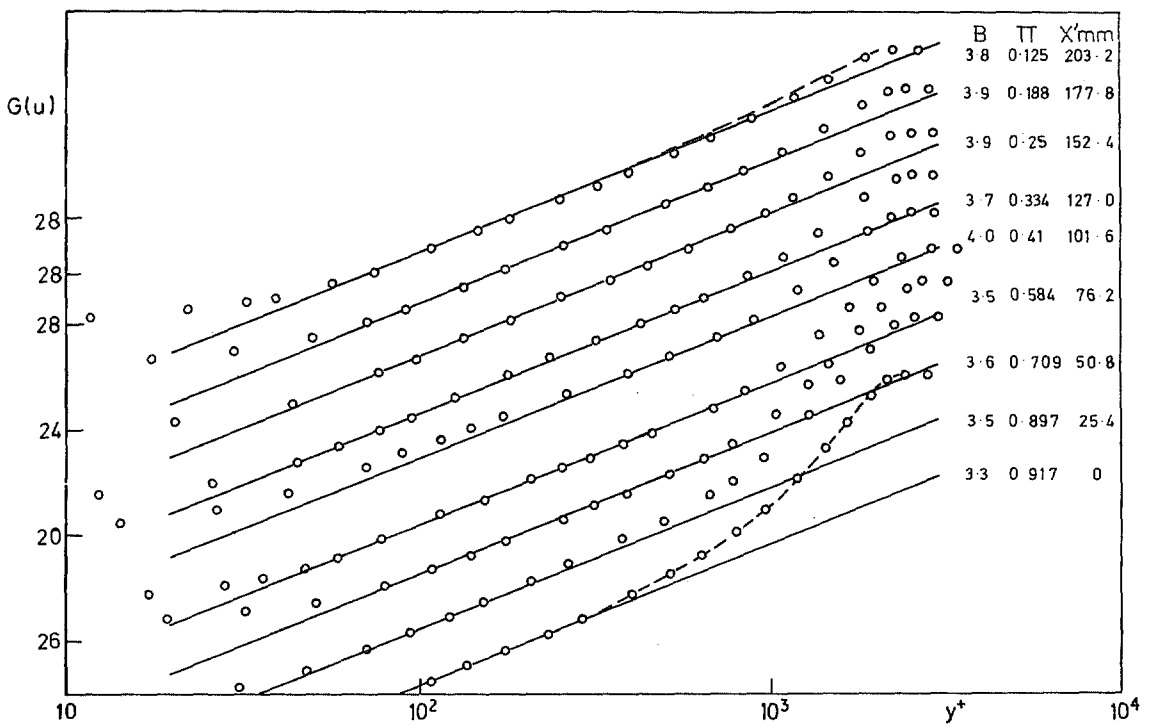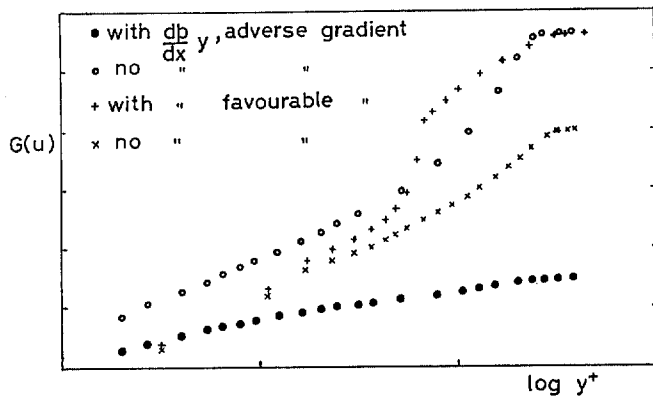
FIG. 36. The Effect of the Pressure Gradient Term on $G(u)$.

○ m = 0, + m = 0·001, □ m = 0·002, △ m = 0·003
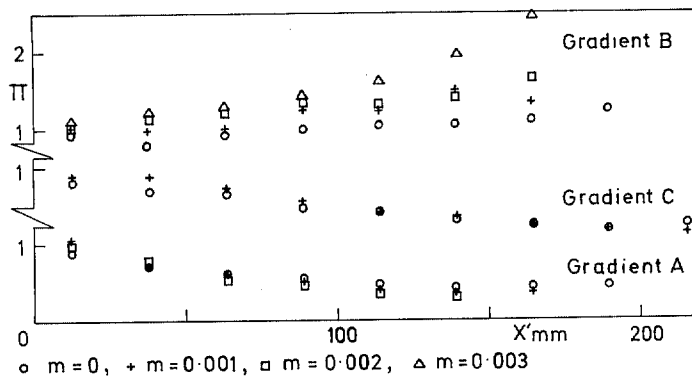
FIG. 37. Variation of π with F Along Plate.
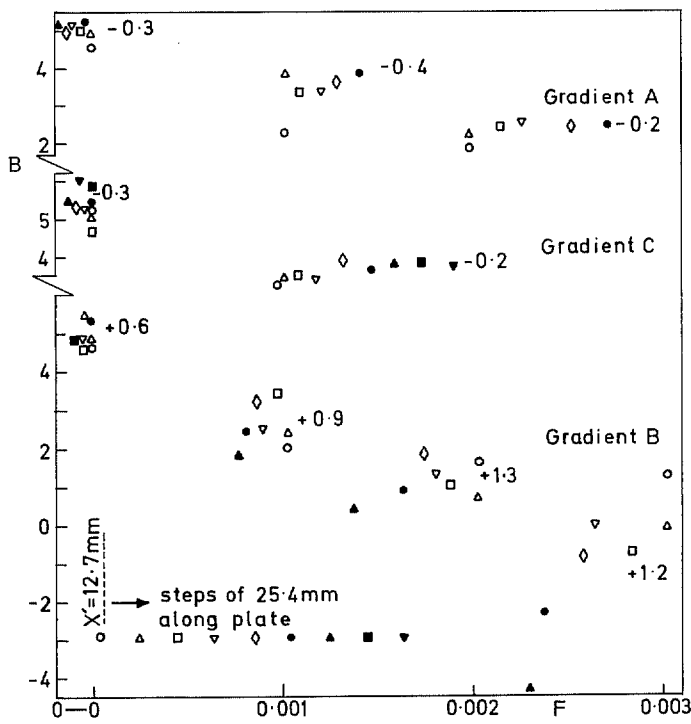
FIG. 38. Variation of B with F.

73
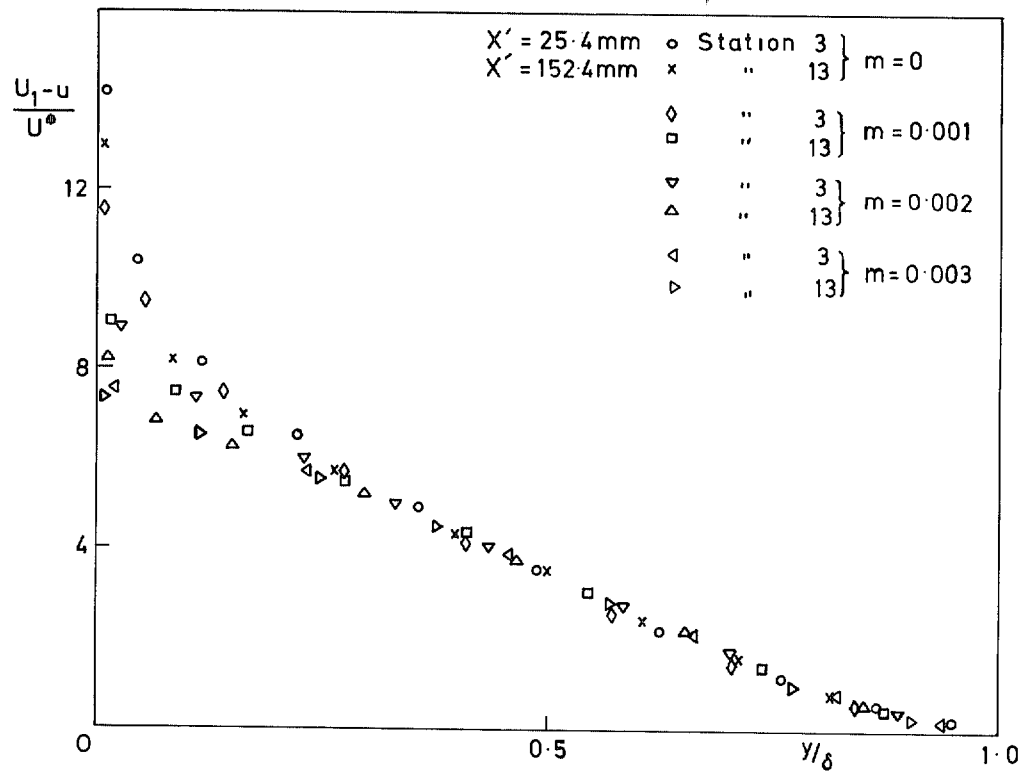
FIG. 39. Velocity Defects in Gradient B.
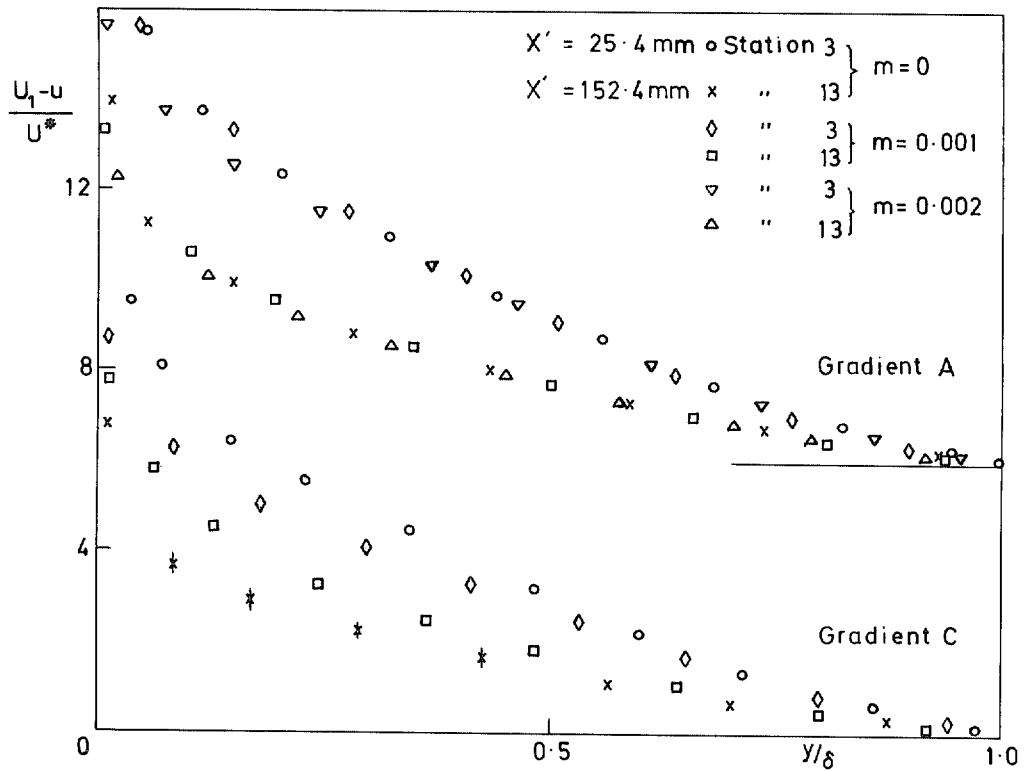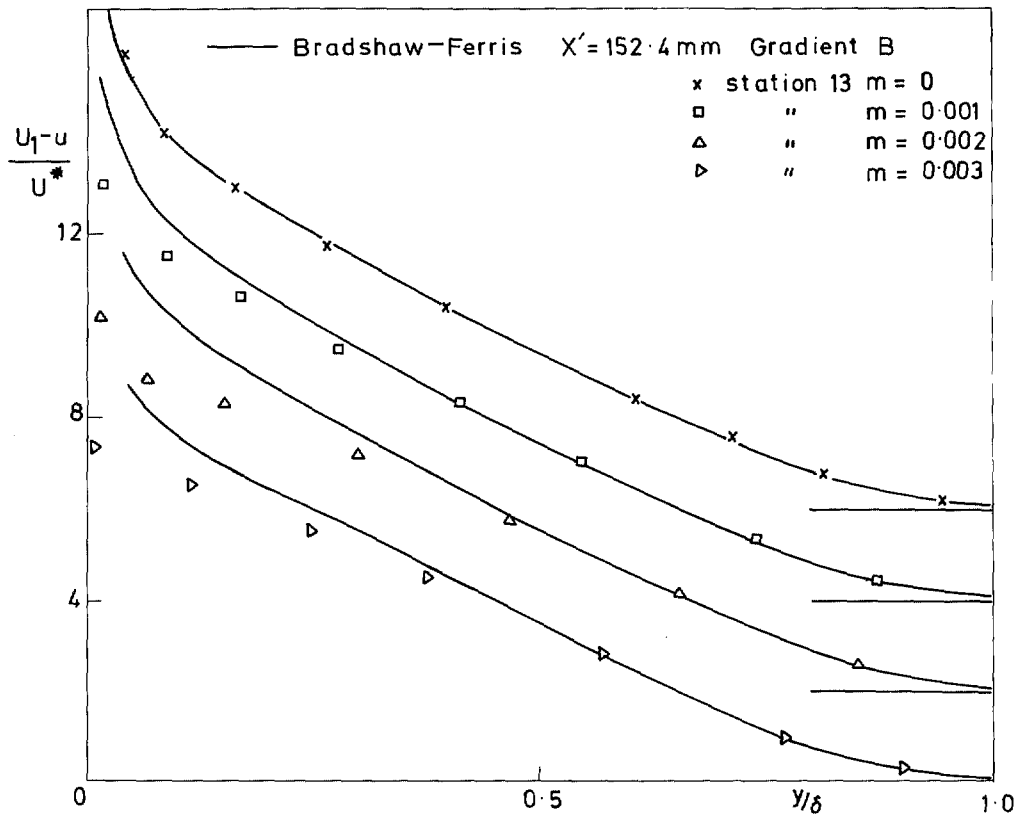

FIG. 40. Velocity Defects in Favourable Gradients.
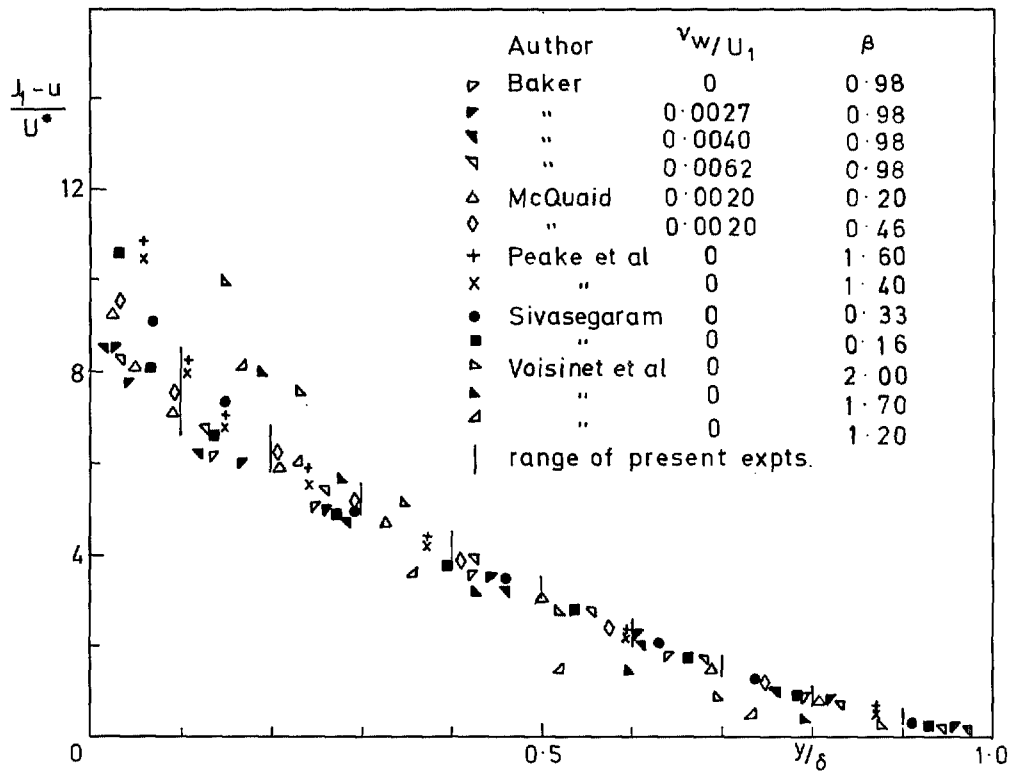
FIG. 41.   Experimental and Predicted Velocity Defects.

FIG. 42.   Velocity Defects for Positive β Flows.